27-Feb-2026

Doctoral Thesis

Development of methods to quantify secondary amino acids and iodine in complex matrices and their application to investigate effects of long-term excess iodine intake on major metabolism in mice

Supervisor Prof. Tetsuo Ishida

Applied Nutrition
Graduate School of Nutrition
Koshien University
812351・Bhisma Rai

Abstract

Iodine is a micronutrient essential for thyroid hormone synthesis, and its deficiency causes severe health problems both in children and adults. As most of iodine is stored in the ocean, the soil of regions far from the ocean such as Nepal lacks iodine and foods contain insufficient iodine. Therefore, in these regions, iodine-fortified salt has been used to prevent iodine deficiency disorders. Importantly, inappropriate usage of iodine-fortified salt can cause excess intake of iodine. In fact, recent survey in Nepal showed excess iodine intake at the population level. However, effects of long-term excess intake of iodine on human health remain to be unclear. In addition, recent studies have revealed that iodide is actively secreted into saliva and gastric juice, suggesting that iodine also plays physiological roles by mechanisms independent of thyroid hormone.

Therefore, it is essential to investigate effects of long-term excess intake of iodine on human health. To perform the investigation, the following two methods are absolutely necessary. (1) Some means to quantify changes in metabolites induced by excess iodine through thyroid hormone dependent and independent mechanisms. (2) On-site method to determine iodine content of various samples such as food, urine, and serum because it is essential to know in vivo kinetics of iodine and balance between intake and excretion of iodine in individuals.

In the present study, I successfully developed a method to quantify L-proline (L-Pro), D-proline (D-Pro), *trans*-4-hydroxy-L-proline (t-4-HP_L), *trans*-4-hydroxy-D-proline (t-4-HP_D), *cis*-4-hydroxy-L-proline (c-4-HP_L), and *cis*-4-hydroxy-D-proline (c-4-HP_D). $^{13}C_6$-dabsyl chloride and $^{13}C_6$-dabsyl-amino acids were synthesized for the first time. By using standard addition method and respective $^{13}C_6$-dabsyl amino acids as internal standards, high-quality linear calibration curves were obtained for Pro, t-4-HP, and c-4-HP, enabling to obtain the total amounts of these three secondary amino acids with high precision and accuracy. Using small

chiral columns, enantiomers of dabsylated Pro, t-4-HP, and c-4-HP were completely separated and thus the D- and L-enantiomer ratio ($r_{D/L}$) was successfully determined for various natural samples using liquid chromatography-mass spectrometry.

Next, a method to quantify iodine in various foods was developed by improving the Sandell-Kolthoff method, which is used worldwide to determine urine iodine content in population. To judge the disturbance to the Sandell-Kolthoff reaction by various substances contained in samples, the standard addition method was used, and sample calibration curve and water calibration curve were simultaneously obtained by measuring the pseudo-first order rate constant. Iodine-extraction method was optimized for each group of samples such as raw milk, seaweed, and some common food samples. Iodine content of various food samples was successfully determined for the first time.

Finally, a pilot mouse study was performed to design a mouse model which mirrors lifelong effects of moderate excess iodine intake on human health. Recently, in many countries including Chaina, excess iodine intake has becoming urgent health concerns and not only large-scale human cohort studies have been carried out but also studies using various mouse and rat models for excess iodine intake have been performed. However, these animal experiments have the following shortcomings. Iodine is given to animals through drinking water or by means of oral gavage, unnatural way of taking iodine. Breeding period is short, mostly 3 months, and samples were collected only on the first day and the end of experiment. Balance between intake and excretion of iodine is not followed. To overcome these problems, I performed a pilot study using 6 female mice (C57BL/6J) to establish methods to give feed, to collect 24-hour urine, to collect 10-μL amounts of blood through the tail vein, and to take out organs, including the thyroid gland.

Index

Chapter I

Introduction

1-1 Change from iodine deficiency to iodine excess in Nepal

Iodine is an element necessary for synthesizing thyroid hormones, and thyroid hormones are essential for normal development and growth of mammals including humans. In Napal, visible goiter, enlargement of thyroid gland, had long been prevalent (about 55% of the population) because both foods and drinking water contain insufficient amounts of iodine due to the lack of iodine in soils. To tackle the iodine deficiency problem, usage of iodized salt has been started from1973 in Nepal. As shown in Figure 1-1, at present, almost all households use iodized salt, and concomitantly visible goiter almost disappears (the prevalence of 0.4%). However, many people (29~39%) in Nepal have thyroid disorders, about 2~3-fold higher prevalence compared to European countries, USA, and Japan. The reason why the prevalence of thyroid disorder remains high after the spread of iodized salt in households is unclear. Recently, median urinary iodine content in Nepal, which is used as a measure of population level iodine status, was reported to be 314 μg/L, indicating the excess iodine intake.

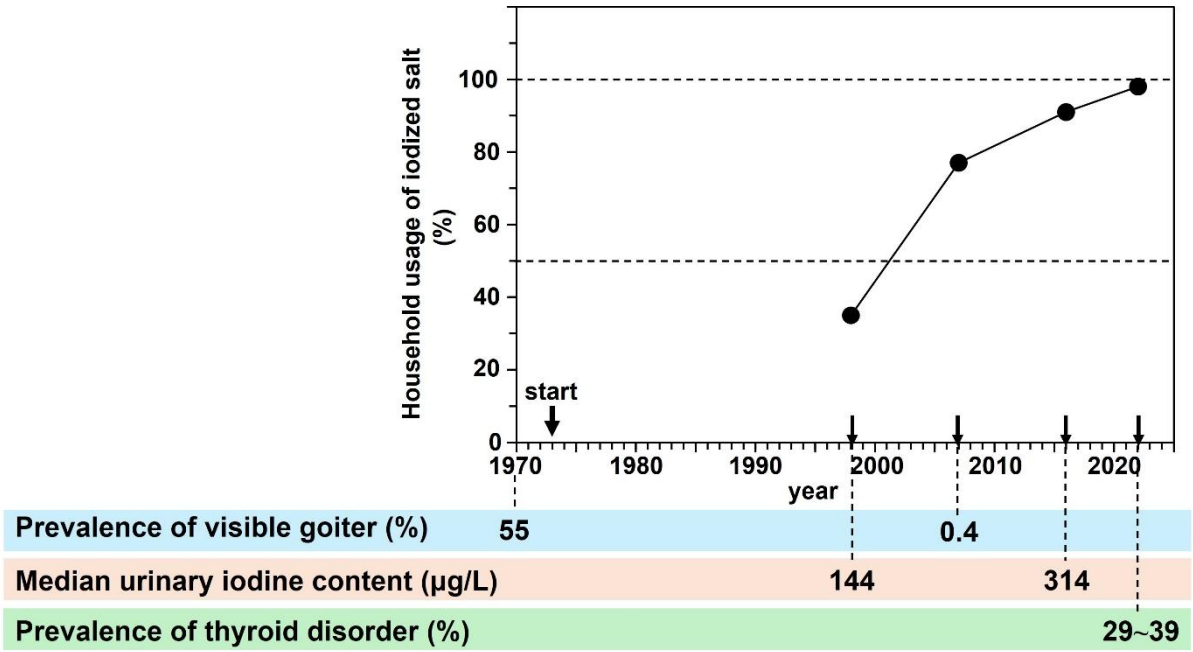

Figure 1-1. Household usage of iodized salt and change in population level iodine intake and the prevalence of thyroid disorders

As universal salt iodization is a global strategy recommended by World Health Organization (WHO), iodine-deficient countries like Napal have performed this strategy to prevent iodine-deficiency diseases. In this strategy, the amount of iodine added into salt, usually 20–40 mg iodine/kg salt, should be adjusted regularly based on the recent median urinary iodine content, otherwise excess iodine intake occurs. In fact, excess iodine intake in population levels was observed in 13 countries in 2020 (1). As for individual levels, excess iodine intake becomes a newly emerging health problem in most countries due to global distribution of foods and supplements containing large amounts of iodine such as brown seaweeds extracts, which have no labels displaying iodine contents. At present, chronic effects of excess iodine intake on human health are far from to be elucidated. Therefore, many research groups have now investigating possible risks of long-term intake of excess iodine from perspectives of not only authentic thyroid function but recent findings of extra-thyroid receptor roles of iodine and thyroid hormones (2–7).

1-2 High prevalence of metabolic and cardiovascular diseases in Nepali patients with hypothyroidism

To reveal the association between hypothyroidism and lifestyle-related diseases, in my master's thesis, I examined comorbidities of the patients with hypothyroidism: 85% of adults with hypothyroidism were obese and 69% of them had comorbidities such as hypertension, type 2 diabetes and dyslipidemia. In this study, although I performed diet survey, the daily iodine intake of each participant was not estimated because I had no means to assay the iodine contents of foods and urine. Therefore, effects of excess iodine intake on thyroid function and pathogenesis of lifestyle-related diseases in Napal remain to be completely unknown.

1-3 Necessity of biomarkers to detect metabolic changes induced by excess iodine intake

It is well known that excess iodine intake can cause subclinical hypothyroidism, which is diagnosed by the slight increase in thyroid stimulating hormone (TSH) and normal levels of free thyroxin (T_4) and free triiodothyronine (T_3). Excess iodine intake is also associated with appearance of antibodies to thyroglobulin and thyroid peroxidase (8–13). On the other hand, recent investigations have revealed various aspects of iodine that these traditional biomarkers cannot detect (14). For example, excess iodine exposure increases salivary concentrations of iodide (I^-) and hypoiodous acid (HOI), suggesting a role to inhibit oral microbial pathogens

(15). Excess iodine intake changes gut microbiota and disrupts T17/Treg balance by reducing butyric acid (16,17). In rats, chronic excess iodine intake damages the articular cartilage and epiphysial growth plate (18) and inhibits bone reconstruction (19). Excess iodine intake impairs reproductive functions in male rats due to oxidative stress on testis induced by testis-accumulated iodine (20−22). Long-term excess iodine impairs the learning and memory of rats via induction of mitochondrial apoptosis (23). These recent findings indicate that we need biomarkers to sensitively detect various kinds of metabolic changes occurring in our body due to excess iodine intake. As urine is obtained without invasive treatment and iodine content in the urine is needed to evaluate excess levels of iodine intake, it is worth trying to find the biomarkers in urine samples.

1-4 Aims of the present study

In Nepal, there are about 142 ethnic groups, and each group has own language and lifestyle including eating habits. Therefore, to elucidate long-term effects of excess iodine intake on the health of Nepalese people, it is essential to perform long-term follow up study of as many individuals as possible. In such study, first of all, we need a safe and easy to perform on-sight method to measure iodine in various samples including salts, foods, and urine. In the present study, I have improved the Sandell-Kolthoff method to be applicable to this purpose, which is described in Chapter III of this PhD thesis.

Iodine is inevitable for the synthesis of thyroid hormone, and all the cells in our body are the target of this hormone. Although iodine is essential for human health as a building block of thyroid hormone, recent studies strongly indicate that iodine plays various important roles through mechanisms independent of thyroid hormone synthesis. Therefore, it is insufficient to monitor only classical biomarkers of T3, T4, TSH, antibodies to thyroglobulin and thyroid peroxidase. In the present study, I focused on not cells but the extracellular matrix (ECM) surrounding cells because cellular metabolic changes are intimately coupled with remodeling of ECM. Collagen is the major component of ECM and thus the most abundant protein in animal body (24). Importantly, about 20% of the amino acids in collagen are L-proline (L-Pro) and *trans*-4-hydroxy-L-proline (t-4-HP_L), and t-4-HP_L is produced by post-translational modification of collagen catalyzed by prolyl hydroxylase. In fact, urine hydroxyproline has long been investigated as a possible biomarker for the metabolic turnover of collagen in various health and disease conditions including thyroid dysfunction (25−29). However, in all these previous studies, only the total amount of 4-hydroxyproline is measured despite the fact that 4-

hydroxyproline consists of 4 stereoisomers. Therefore, in the present research I aimed to develop a method to quantify all the stereoisomers of proline and 4-hydrosyproline, which is described in Chapter II of this PhD thesis.

Although a large-scale follow-up study on human cohorts is inevitable to elucidate possible good or bad effects of excess iodine intake on human health, it needs large amounts of money, manpower, and decades of time. Therefore, studies using appropriate mouse models are indispensable for screening possible effects of excess iodine intake and obtaining mechanistic hypotheses about the effects. Recently, various mouse models for excess iodine intake have been reported (30−36). Most of these studies, iodine is given to mice via drinking water containing sodium iodide or iodate because in China there are regions where groundwater contains more than 300 μg/L iodine (37). However, in Napal, drinking water contains very low levels of iodine and excess iodine intake is occurring through taking foods fortified with iodine by iodine-added salt. Therefore, in the present study, I performed a pilot mouse study to find a mouse model suitable for the excess iodine intake in Napal, which is described in Chapter IV of this PhD thesis.

Figure 1-2 shows the relationship between my future study plan in Nepal and the studies performed in the PhD thesis.

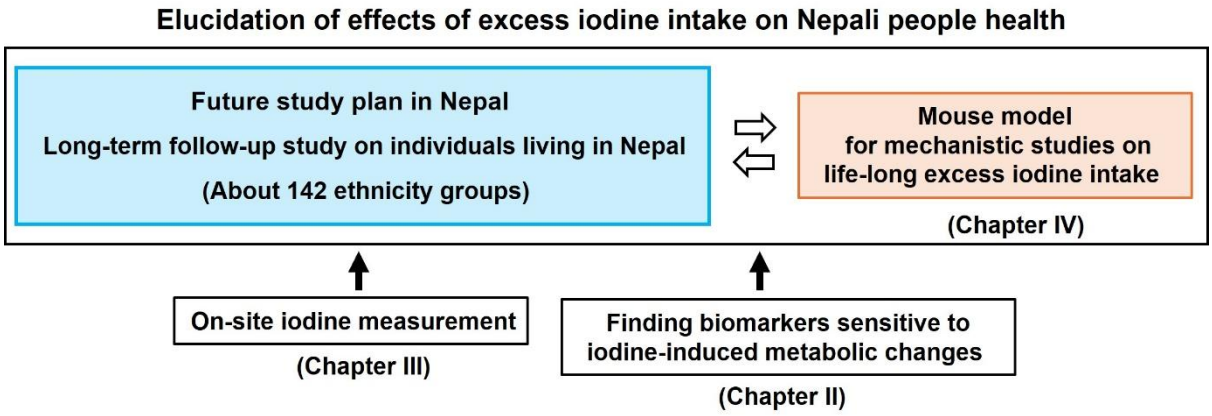

Figure 1-2. The relationship between future study plan in Nepal and the present PhD studies.

References

1. Zimmermann M. B., and Andersson M. (2021) Global perspectives in endocrinology: coverage of iodized salt programs and iodine status in 2020. *Eur. J. Endcrinol*. 185, R13–R21
2. Luo Y., Kawashima A., Ishido Y., Yoshihara A., Oda K., Hiroi N., Ito T., Ishii N., Ito T., Ishii N., and Suzuki K. (2014) Iodine excess as an environmental risk factor for autoimmune thyroid disease. *Int J. Mol. Sci.* 15, 12895–12912
3. Farebrother J., Zimmermann M. B., and Andersson M. (2019) Excess iodine intake: sources, assessment, and effects on thyroid function. *Ann. N.Y. Acad. Sci.* 1446, 44–65
4. Silva de Morais N., Saraiva D. A., Corcino C., Berbara T., Schischerbyna A., Moreira K., Vaisman M., Alexander E. K., and Teixeira P. (2020) Consequences of iodine deficiency and excess in pregnancy and neonatal outcomes: a prospective cohort study in Rio de Janeiro, Brazil. *Thyroid* 30, 1792–1801
5. Teti C., Panciroli M., Nazzan E., Pesce G., Mariotti S., Olivieri A., and Bagnasco M. (2021) Iodoprophylaxis and thyroid autoimmunity: an update. Immunol. Res. 69, 129–138
6. Sohn S. Y., Inoue K., Rhee C. M., and Leung A. M. (2024) Risks of iodine excess. *Endocrine Rev*. 45, 858–879
7. Khudair A., Khudair A., Niinuma S. A., Habib H., and Butler A. E. (2025) From deficiency to excess: the impact of iodine excess on reproductive health. *Front. Endocrinol.* 16:1568059
8. Rayman M. P. (2019) Multiple nutritional factors and thyroid disease, with particular reference to autoimmune thyroid disease. *Proc. Nutr. Soc.* 78, 34–44
9. Weetman A. P. (2021) An update on the pathogenesis of Hashimoto's thyroiditis. *J. Endocrinol. Invest*. 44, 883–890
10. Chen X., Wu C., Wang Z., Wu C., Guo Y., Zhu X., Hu Y. P., Shi Z., Song Q., Cui X., Su J., and Zang J. (2022) Iodine nutrition status and thyroid autoimmunity during pregnancy: a cross-sectional study of 4635 pregnant women. *Nutrition J*. 21:7
11. Du Y., Liu P., Zhang W., Yao J., Meng F., Fan L., Liu L., Li N., Lv C., Jiang W., and Sun D. (2023) Serum thyroglobulin as a biomarker of iodine excess and thyroid disease occurrence in adults. *J. Trace Elem. Med. Biol.* 78, 127172
12. Zhang L., Shang F., Liu C., and Zhai X. (2024) The correlation between iodine and metabolism: a review. *Front. Nutr.* 11:1346452

13. Vargas-Uricoechea H., Castellanos-Pinedo A., Meza-Cabrea I. A., Pinzón-Fernández M. V., Urrego-Noguera K., and Vargas-Sierra H. (2025) Iodine intake from universal salt iodization programs and Hashimoto's thyroiditis: a systematic review. *Diseases* 13, 166
14. Khudair A., Khudair A., Niinuma S. A., Habib H., and Butler A. E. (2025) Beyond thyroid dysfunction: the systemic impact of iodine excess. Front. Endocrinol. 16:1568807
15. Akiba Y., Leung A. M., Bashir M-T., Ebrahimi R., Currier J. M., Neverova N., and Kaunitz J. D. (2022) Excess iodine exposure acutely increases salivary iodide and antimicrobial hypoiodous acid concentrations in humans. *Sci. Reports* 12:20935
16. Gong B., Meng F., Wang X., Han Y., Yang W., and Wang C. (2024) Effects of iodine intake on gut microbiota and gut metabolites in Hashimoto thyroiditis-diseased humans and mice. *Commun. Biol.* 7:136
17. He H., Jiang Y., Qiu J., Shen F., Qian D., and Meng L. (2025) Role of interleukin 17 and T helper cells 17 cells as a new immune target and signaling in the pathogenesis and treatment of autoimmune thyroid diseases. Annal. Med. 57:2586216
18. Zhang Y., Zhao X., Shan L., Liu M., Zhang Z., Wang Z., Zhang X., Meng H., Song Y., Zhang W., and Sang Z. (2024) Chronic iodine intake excess damages the structure of articular cartilage and epiphysial growth plate. *Biol. Trace Element Res*. 202, 4078−4086
19. Zhang Y., Zhao X., Zhao N., Meng H., Zhang Z., Song Y., Shan L., Zhang X., Zhang W., and Sang Z. (2024) Chronic excess iodine intake inhibits bone reconstruction leading to osteoporosis in rats. *J. Nutr.* 154, 1209−1218
20. Chakraborty A., Mandai J., Mondal C., Sinha S., and Chandra A. K. (2016) Effects of excess iodine on oxidative stress markers, steroidogenic-enzyme activities, testicular morphology, and functions in adult male rats. *Biol. Trace Elem. Res.* 172, 380−394
21. Chandra A. K., and Chakraborty A. (2017) Influence of iodine in excess on seminiferous tubular structure and epididymal sperm character in male rats. Environ. Toxicol. 32, 1823−1835
22. Chakraborty A., Singh V., Singh K., and Rajender S. (2020) Excess iodine impairs spermatogenesis by inducing oxidative stress and perturbing the blood testis barrier. *Reproductive Toxicol*. 96, 128−140
23. Cui Y., Zhang B., Zhang Z., Nie J., and Liu H. (2021) Long-term repetitive exposure to excess iodine induces mitochondrial apoptosis, and alters monoamine neurotransmitters in hippocampus of rats of different genders. *Toxicol. Res.* 10, 975−982
24. Salo A. M., and Myllyharju J. (2021) Prolyl and lysyl hydroxylases in collagen synthesis.

Exp. Dermatol. 30, 38−49

25. Jasin H. E., Fink C. W., Wise W., and Ziff M. (1962) Relationship between urinary hydroxyproline and growth. *J. Clin. Invest.* 41, 1928−1935
26. Prockop D. J. (1964) Isotopic studies on collagen degradation and the urine excretion of hydroxyproline. *J. Clin. Invest.* 43, 453−460
27. Utitto J., Laitinen O., Lamberg B-A., and Kivirkko K. I. (1968) Further evaluation of the significance of urinary hydroxyproline determination in the diagnosis of thyroid disorders. *Clin. Chimi. Acta* 22, 583−591
28. Onwuka C. I., Uguru C. C., Onwuka C., and Obiechina A. E. (2021) Evaluation of urinary hydroxyproline and creatinine level in patients with benign mandibular odontogeneic tumor. *Clin. Exp. Dent. Rest. Res.* 7, 934−940
29. Paules E. M., Trulill-Gonzalez I., VerHague M., Albright J., Stewart D., Sumner S. J., McRitchie S. L., Kirchner D., Coleman M. F., Bennett B. J., Howard A. G., Gordon-Larsen P., French J. E., and Hursting S. D. (2025) Urinary signatures are associated with calorie restriction-mediated weight loss in obese diversity outbred mice. *PloS One* 20:e0329422
30. Chen X., Lin C., Yang L., Li W., Zhang J., Zheng W., Wang X., Qian J., Huang J., and Lei Y. (2016) The effect on sodium/iodine symporter and pendrin in thyroid colloid retention developed by excess iodide intake. *Biol. Trace Elem. Res.* 172, 193−200
31. Shen H., Han J., Li Y., Zhou J., Li Y., and Su X. (2019) Different host-specific responses in thyroid function and gut microbiota modulation between diet-induced obese and normal mice given the same dose of iodine. *Appl. Microbiol. Biotechnol*. 103, 3537−3547
32. Guo Y., Hu C., Xia B., Zhou X., Luo S., Gan R., Duan P., and Tan Y. (2022) Iodine excess induces hepatic, renal and pancreatic injury in female mice as determined by attenuated total reflection Fourier-transformed infrared spectrometry. *J. Appl. Toxicol*.42, 600−616
33. Nie G., Li S., Zhang W., Meng F., Ru Z., Li J., Sun D., and Li M. (2024) A new LNC89/LNC60-Col11a2 axis revealed by whole-transcriptome analysis may be associated with goiters related to excess iodine nutrition. *Front. Endocrinol.* 15:1407859
34. Gong B., Meng F., Wang X., Han Y., Yang W., Wang C., and Shan Z. (2024) Effects of iodine intake on gut microbiota and gut metabolites in Hashimoto thyroiditis-diseased humans and mice. *Commun. Biol*. 7:136
35. Wang D., Li P., Zhou Z., Jin M., Li B., Li F., and Shen H. (2024) The association between endothelial function and autoimmune thyroiditis induced by iodine excess. *J. Trace Elem.*

Med. Biol. 83:127413

36. Amano I., Ninomiya A., Yajima H., Suda-Yajima M., Kokubo M., Khairinisa M. A., Takatsuru Y., Kawabata-Iwakawa R., Kameo S., Haraguchi S., Haijima A., and Koibuchi N. (2025) Effects of excessive iodine intake during the perinatal period on thyroid function and higher brain functions in mouse offspring. *Endocrine J*. 72, 999−1010
37. Ma. R., Yan M., Han. P., Wang T., Li B., Zhou S., Zheng T., Hu Y., Borthwick A. G. L., Zheng C., and Ni J. (2022) Deficiency and excess of groundwater iodine and their health associations. *Nature Commun.* 13:7354

Chapter II

Development of a method to quantify proline and 4-hydroxyproline stereoisomers in complex matrices

2-1 Introduction

Figure 2-1 shows the chemical structures of proline (Pro) and 4-hydroxyproline (4-HP). Pro has a single chiral center at C_α atom and there exist L-proline (L-Pro) and D-proline (D-Pro). In the case of 4-HP, two chiral centers (C_α and C4 carbon atoms) exist to give four isomers: *trans*-4-hydroxy-L-proline (t-4-HP_L), *trans*-4-hydroxy-D-proline (t-4-HP_D), *cis*-4-hydroxy-L-proline (c-4-HP_L), and *cis*-4-hydroxy-D-proline (t-4-HP_D).

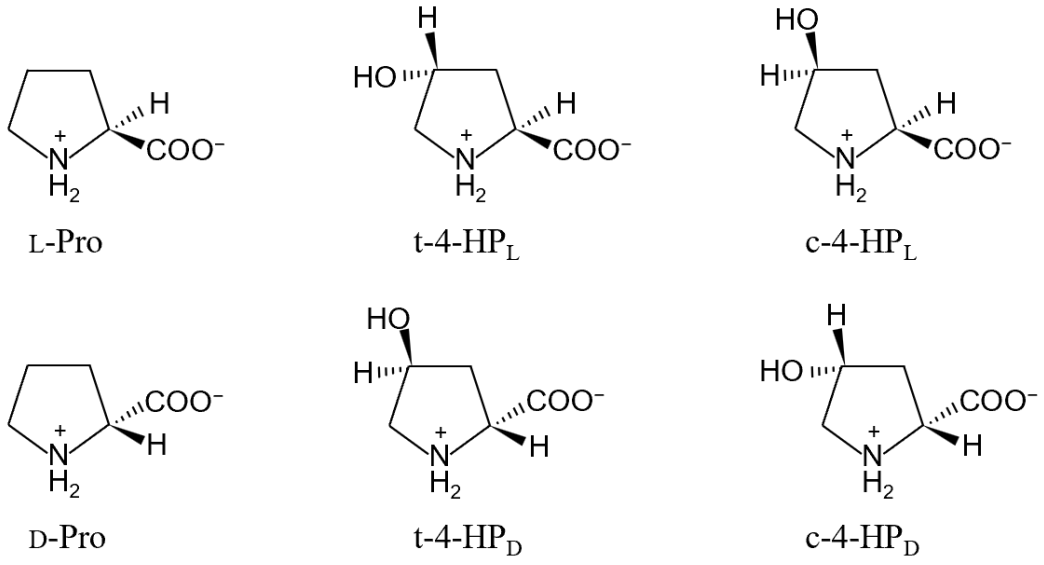

Figure 2-1. Chemical structure of L- and D-proline, and enantiomers of *trans*-4-hydroxyproline and *cis*-4-hydroxyproline.

L-Pro is the only proteinogenic amino acid that contains a secondary amino group in the pyrrolidine ring structure. A large amount of L-Pro is found in collagen, which is the most abundant protein in animals, distributed ubiquitously in the entire body (1). During the maturing process, nearly 40% of the Pro residues of collagen are post-translationally hydroxylated to t-4-HP_L by the enzyme prolyl-4-hydroxylase (2,3). t-4-HP_L is widely found not only in collagen but also in hydroxyproline-rich glycoprotein of the plant cell wall (4,5). Both Pro and 4-HP play vital roles in the strength, structure, and thermodynamic stability of

mature collagen (6,7). Hydroxyproline-rich glycoproteins are vital structural ingredients in the plant cell wall. They participate in the formation of cross-linked networks in the cell wall, which is significant for wall strengthening as well as disease resistance (8).

Free L-Pro plays various roles in cellular metabolism and physiology (9). Animal model studies suggest that dietary L-Pro supplementation improves fetal growth and survival (10–12). In plants, L-Pro accumulates in response to scavenging free radicals and protection from osmotic stress (13,14). On the other hand, substantial amounts of D-Pro are contained in bacterial fermented foodstuffs such as cheese, yogurt, sourdough, pickles, vinegar, seafoods (bivalves and crustaceans), and beverages like wine and beer (15). In recent years, D-Pro is gaining attention due to its role in disease biomarkers and physiologically active substances. For example, D-Pro levels are known to correlate with the progression of chronic kidney disease (9) and Alzheimer's disease (16,17). Some bacteria, such as *Sinorhizobium meliloti* have been shown to catabolize D-Pro as a carbon and nitrogen source for their growth and development (18).

Generally, it is insufficient to know the total amounts of amino acid of interest. Therefore, chiral separation of various amino acids has been intensively challenged by many research groups. However, it is still difficult to determine respective amounts of enantiomers in biological samples with complex matrices. As for 4-HP, t-4-HP_L is the major stereoisomer found in most biological samples (19,20). t-4-HP_L is mainly produced by the degradation of collagen and used as a marker of turnover of bone and muscle connective tissues (18,21). In addition, it is used as a nutritional supplement in the food industry and as an intermediate in the pharmaceutical industry (22,23). It is also reported that t-4-HP_L promotes collagen synthesis. On the other hand, animal studies have indicated that c-4-HP_L inhibits collagen synthesis (24,25). Mueller et al. showed that c-4-HP_L causes growth inhibition, loss of adherence, and apoptosis in the rat pancreatic carcinoma cell line DSL6A, which could be prevented by L-Pro supplementation (26). In the case of t-4-HP_D, it is rarely found in mammals, and some naturally occurring peptides contain t-4-HP_D (1). Small amounts of c-4-HP_D are found in nature (27). For example, certain bacterial species produce free c-4-HP_D from L-Pro and/or t-4-HP_L (29–30). Ishii et al. showed the presence of c-4-HP_D in human urine and tissues of bivalves (5).

As each isomer of Pro and 4-HP is expected to play various physiological functions, it is essential to determine all these six secondary amino acids in biological samples. To date, a few methods have been reported to quantify all six isomers (5,31). However, the reported

methods did not take matrix effects into sufficient consideration and thus are not suitable for application to biological samples with complex matrices. It is still challenging to quantify small amounts of one enantiomer in the coexistence of large amounts of another enantiomer.

In the present study, I selected 4-dimethylaminoazobenzene-4'-sulphonyl chloride (Dabs-Cl) as a pre-column labeling reagent because it is relatively easy to synthesize Dabs-Cl from aniline. Using $^{13}C_6$-aniline, $^{13}C_6$-Dabsyl-Cl was successfully synthesized. Then I prepared $^{13}C_6$-dabsyl derivatives of L- and D-Pro and all four stereoisomers of 4-HP in crystals. These stable isotopes labeled derivatives were used as internal standards to correct step by step recovery. To take matrix effects into quantification, I applied the standard addition method (32) and obtained a calibration curve under the matrix of the samples. Combined use of standard addition and 6-dalton heavy standard significantly enhanced the accuracy and precision. Using small chiral columns of OJ-H (Daicel Corporation, Osaka, Japan), each pair of the enantiomers (D-Pro and L-Pro, t-4-HP_D and t-4-HP_L, and c-4-HP_D and c-4-HP_L) was completely separated.

2-2 Materials and Methods

2-2-1 Reagents

D-Pro, DL-Pro, t-4-HP_L, c-4-HP_L, c-4-HP_D, and Dabs-Cl were purchased from Tokyo Chemical Industry (Tokyo, Japan). L-Pro, t-4-HP_D, methanol (LC-MS grade), ethanol (LC-MS grade), acetonitrile (LC-MS grade), and trifluoroacetic acid (TFA, LC-MS grade) were obtained from FUJIFILM Wako Pure Chemical Corporation (Osaka, Japan). Ultrapure Milli-Q water was used in all experiments.

2-2-2 Synthesis of $^{13}C_6$-Dabs-Cl

$^{13}C_6$-Dabs-Cl was synthesized from $^{13}C_6$-methyl orange ($^{13}C_6$-MO) according to the protocol of Lin et al. (33). Figure 2-2 shows the reaction scheme for the synthesis. $^{13}C_6$-MO (1 g), which was synthesized from $^{13}C_6$-aniline, was taken into an agate mortar and ground into fine powder using an agate pestle. Then, 1.5g of phosphorus pentachloride was added to the mortar and the mixture was ground for 8−10 min using the pestle. After the reaction, the mixture was poured into 500 mL of water with cracked ice. The precipitates were collected onto a filter paper by suction filtration, and the collected precipitates were washed with water (200 mL) twice. The washed precipitates were completely dried and then Dabs-Cl was

extracted from the precipitates with acetone (300 mL) using a Soxhlet apparatus. The acetone solution was concentrated to about 50 mL using a rotary evaporator and the concentrated solution was left at 4°C overnight. Shiny, deep red crystals of Dabs-Cl appeared. After removing the acetone, the crystals were completely dried at 60°C. The dried $^{13}C_6$-Dabs-Cl crystals (Fig. 2-3) were stored at room temperature in a polypropylene container with large amounts of silica gel. It is of note that Dabs-Cl is unstable under moisture.

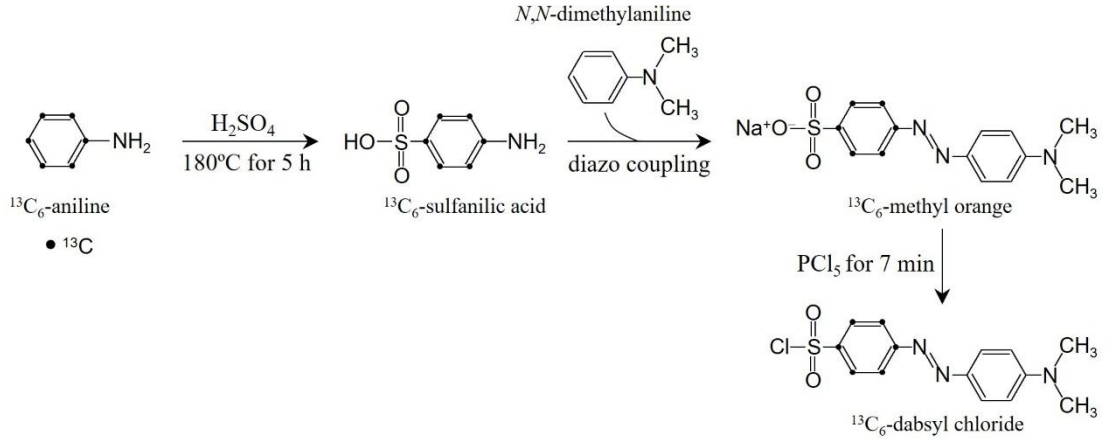

Figure 2-2 Reaction scheme for synthesis of $^{13}C_6$-dabsyl chloride.

Figure 2-3 Crystals of $^{13}C_6$-dabsyl chloride.

2-2-3 Synthesis of $^{13}C_6$-dabsyl derivatives of proline and 4-hydroxyproline stereoisomers

$^{13}C_6$-Dabsyl labeled L-Pro, D-Pro, racemic Pro ($_{DL}$-Pro), t-4-HP_L, t-4-HP_D, c-4-HP_L, and c-4-HP_D were prepared as follows. Each amino acid (150 μmol) was dissolved in 5 mL of 0.2M $NaHCO_3$ (pH 9.0), and the solution was pre-incubated at 60°C for 2 min. Then, 5 mL aliquot of $^{13}C_6$-Dabs-Cl solution (2mg/mL acetone, prepared just before use) was added to the solution. The mixture was incubated for 6 minutes at 60°C under constant shaking. After cooling the

reaction mixture to room temperature, acetone was removed using a centrifugal evaporator (CVE-1000, EYELA, Tokyo, Japan) equipped with a trap cooled with liquid nitrogen under reduced pressure for about 30 min. An equal volume (1:1) of water containing 0.1% TFA (solvent A) was added to the acetone-removed solution and then the mixtures were applied to a Wako gel 50C18 column (1.5 cm × 1 cm), which was first primed with methanol and then pre-equilibrated with solvent A. The column was washed with solvent A and then washed with 10% acetonitrile:90% water (v/v) containing 0.1% TFA until the eluate became nearly colorless. $^{13}C_6$-Dabsyl labeled amino acid was eluted with a minimum amount of 90% acetonitrile:10% water (v/v) containing 0.1% TFA (solvent B). The eluted sample was evaporated to dryness using the centrifugal evaporator under reduced pressure. The dried sample was completely redissolved with a minimum amount of solvent B (or ethanol), and then water was added to the solution until turbidity appeared. The resultant solution was kept at 4°C overnight to crystallize the $^{13}C_6$-Dabsyl amino acid. The crystals were collected by centrifugation at 13200 × g for 10 min. After removing the supernatant, the crystals were completely dried at 65ºC. The purity of each $^{13}C_6$-dabsyl derivatives was confirmed by HPLC analysis on an ODS-3 column (3 μm, 1.5 mm × 150 mm, GL Sciences Inc.), and the chemical structure was confirmed by measuring mass spectrum using LC-MS. Stock $^{13}C_6$ dabsyl-amino acid standards were prepared as follows. Each $^{13}C_6$ dabsyl-amino acids crystals were dissolved in 1 mL of solvent B to give 2.5 mmol/L solution. The solution was aliquoted into 0.5-mL Eppendorf tubes (20 μL/tube), and the aliquoted samples were evaporated to dryness using the centrifugal evaporator under reduced pressure. The resultant tubes containing 50 nmol $^{13}C_6$ dabsyl-AA were stored at −18°C until use. Figure 2-4 shows the crystals of $^{13}C_6$-dabsyl c-4-HP_L.

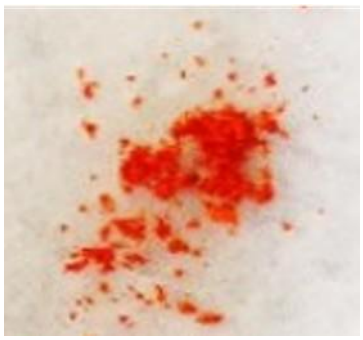

Figure 2-4 Crystals of $^{13}C_6$-dabsyl c-4-HP_L.

2-2-4 Preparation of amino acid stock solutions

Stock solutions of L-Pro, t-4-HP_L, and c-4-HP_D were prepared as follows. Each amino acid (approximately 250 μmol) was weighed using a Shimazu balance (AP125WD) and transferred into a 100-mL volumetric flask. One hundred grams of 0.1 mol/L HCl was added to the flask, and the amino acid was dissolved completely. The concentration of the resultant solution was calculated by assuming the specific gravity of the solution of 1.00 g/mL. The solution (approximately 2.50 mmol/L) was aliquoted into 1 mL in a 1.5-mL Eppendorf tube, and the tubes were stored at −18°C until use.

Five working solutions were prepared from the respective stock solutions by stepwise diluted with water at the concentrations of 50, 25, 12.5, 6.25, and 3.1 μmol/L for L-Pro and 25, 12.5, 6.25, 3.1, and 1.6 μmol/L for t-4-HP_L and c-4-HP_D. Stepwise dilution was performed as follows. First, a stock solution containing 50 μmol/L of L-Pro, 25 μmol/L of t-4-HP_L and 25 μmol/L of c-4-HP_D (St-5) was prepared and this solution was stepwise diluted with water to obtain St-4, St-3, St-2, and St-1, where St-i contains $50/(2^{5-i})$ μmol/L L-Pro and $25/(2^{5-i})$ μmol/L t-4-HP_L and c-4-HP_D. Working solutions were prepared just before use.

2-2-5 Sample preparation

Serum from female mice (8-9 weeks old) was obtained from Kiwa Laboratory Animals Co., Ltd. (Wakayama, Japan). The serum was aliquoted to 100 μL in 0.5-mL Eppendorf tubes and stored at −80°C until use. Just before analysis, one of the tubes was kept at room temperature to thaw the serum, vortexed for a few seconds, and centrifuged at 13,200 × g for 20 min. The supernatant was used for analysis.

Snails (*Achatina fulica*, giant land snail invaded into Okinawa) were captured near the University of the Ryukyus and hemolymph was collected from 10 snails under cold anesthesia. The collected hemolymph was combined, and the combined hemolymph was aliquoted to 500 μL in 1.5-mL Eppendorf tubes and stored at −80°C until use. Just before analysis, one of the tubes was thawed at room temperature, vortexed for a few seconds, and then the hemolymph was centrifuged at 13,200 × g for 20 min. The resultant supernatant was used for analysis.

Frozen (−80ºC) aronia berries harvested at Ueno (Hokkaido, Japan) from 2017 to 2021 were obtained from Hokuren (Sapporo, Hokkaido). Frozen aronia berries harvested each year (25–34g) were wrapped with gauze, partially thawed, and then the juice was collected into a 50-mL tube by squeezing the berries through gauze by hand. The resultant raw juice was centrifuged at 13,200 × g for 20 minutes at 4°C. The supernatant (about 6 mL) was aliquoted

into 1.5-mL Eppendorf tubes and immediately stored at −80°C until use.

After juice collection, aronia seeds were collected from the pulp and stored in a 1.5-mL Eppendorf tube at −80°C until use. Just before analysis, six-aronia seeds (3−3.5g) were weighed into 2-mL Eppendorf tubes (2 seeds per tube). The seeds were then crushed into powder using SK-200 Mill (Tokken, Chiba) under liquid nitrogen. Crushed seeds were collected in one tube by suspending them in 1−1.5 mL of 80% methanol. The suspension was homogenized using a disposable homogenizer BioMasher (Nippi, Tokyo). The regulating homogenate was centrifuged at 13,200 × g at 4°C for 20 min. The supernatant was aliquoted into 1.5-mL Eppendorf tubes (100 μL/tube).

Persimmon, apple, and pear were purchased from a local supermarket (Takarazuka, Japan). Each fruit was crushed using a grinder and the crushed fruit was wrapped with gauze. Then, the juice was collected into a 50-mL tube by squeezing the crushed fruit through gauze by hand. The collected juice was aliquoted into 1.5-mL Eppendorf tubes (1 mL/tube) and stored at −80°C until use. Just before analysis, one of the tubes was thawed and the juice was centrifuged at 13,200 × g at 4°C for 10 min. The resultant supernatant was used for the analysis.

Santalum album L (*S. album*) wood powder was obtained from the local market of Kathmandu (Nepal). The wood powder (about 3.3 mg) was weighed into a 15-mL tube and 600 μL of water was added to the tube. The tube was vortexed vigorously for about 10 min. Subsequently, four volumes of methanol were added to the tube, and the mixture was vortexed vigorously for 5 min. The mixture was centrifuged at 13,200 × g at 4°C for 10 min. The resultant supernatant was aliquoted into 1.5-mL Eppendorf tubes (100 μL/tube) and stored at −80°C until use.

2-2-6 Standard addition and extraction of free amino acids

One tube containing frozen sample prepared as described above was thawed. The thawed sample was centrifuged at 13,200 × g at 4°C for 10 min, and the supernatant was transferred into a new Eppendorf tube. When it was necessary, the supernatant was appropriately diluted with water. For example, mouse serum, aronia juice, and pear juice were 10-fold diluted with water. In the case of determination of total amounts of Pro, t-4-HP, and c-4-HP, the sample was aliquoted into six 1.5-mL Eppendorf tubes (10 μL/tube or 100 μL/tube for aronia seeds and *S. album*). Then tubes labeled as S0~S5, 10 μL of water was added to tube (S0). To the remaining 5 tubes (S1~S5), the respective working solution (10 μL) containing known amounts of L-Pro, t-4-HP_L and c-4-HP_D prepared above (St-1~St-5) was added to the corresponding tube. After

the standard addition, four volumes of methanol (80 μL or 400 μL) were added to each tube. The tubes were vortexed for 5 min and kept on ice for 20 min. Then the mixtures were centrifuged at 13,200 × g at 4°C for 10 min. Each resultant supernatant was transferred into a new 1.5-mL Eppendorf tube and evaporated to dryness using the centrifugal evaporator under reduced pressure (standard-added samples).

In the case of determination of the ratio of D- and L-enantiomers, working solution was not added to the samples. Other procedures were similar as described for total Pro, t-4-HP, and c-4-HP determination.

2-2-7 Dabsylation of samples with commercial dabsyl chloride(^{12}C-Dabs-Cl)

Figure 2-5 shows reaction scheme for dabsylation of Pro and 4-HP.

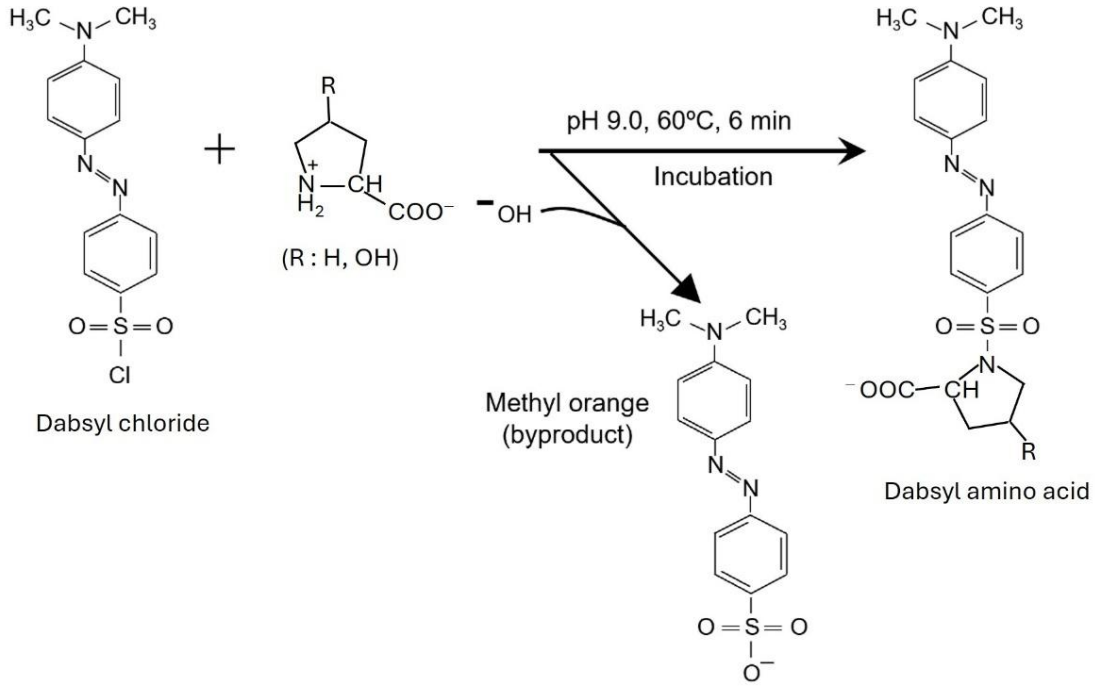

Figure 2-5 Reaction scheme for dabsylation of secondary amino acids.

A set of six standard-added samples (S0~S5) as described above were subjected to dabsylation. One hundred μL of 0.2 mol/L $NaHCO_3$ buffer (pH 9.0) was added to each tube and the tubes were vortexed for 5 min. These solutions were then pre-incubated at 60°C. During this incubation, Dabs-Cl solution was prepared as follows. Commercial Dabs-Cl (2~2.5 mg) was weighed into a 1.5-mL Eppendorf tube and 1.0 mL of acetone was added to the tube. The tube was vigorously vortexed for 1 min and then centrifuged for 1 min using a desk-top

centrifuge to remove insoluble substances. The resultant supernatant was transferred into a new 1.5-mL Eppendorf tube. The concentration of this Dabs-Cl solution was about 6 mM. After pre-incubation, 100 µL of the Dabs-Cl solution was added to each tube and the tubes were immediately vortexed for 1~2 seconds, and reaction mixtures were incubated at 60°C for 6 min. Two minutes after the start of the incubation, the tubes were vortexed for 1–2 seconds. After 6 min incubation, the reaction mixtures were cooled on ice (^{12}C-dabsylated samples). When the mixture of Dabs-Cl and amino acids was incubated at 60ºC in a water bath for 6 min at pH 9.0, the color of the mixture changed from red orange to orange. During this reaction, a significant amount of methyl orange (MO) was generated as an unavoidable byproduct. The MO was subsequently removed by solid phase extraction (see Sample cleanup step).

2-2-8 Addition of $^{13}C_6$-dabsyl secondary amino acids as internal standards

To correct the recovery of ^{12}C-dabsyl amino acids for each step (Fig. 2-6), solutions of $^{13}C_6$-dabsyl-DL-Pro, $^{13}C_6$-dabsyl-t-4-HP$_L$ and $^{13}C_6$-dabsyl-c-4-HP$_D$ (20 µL, 200 pmol each) were added as internal standards to each ^{12}C-dabsylated sample. After vortex, the mixtures were centrifuged at 13,200 × g for 5 min and each of the supernatants was transferred to a new Eppendorf tube, and then the acetone was removed by centrifugal evaporation for 30 min under reduced pressure (acetone-removed samples).

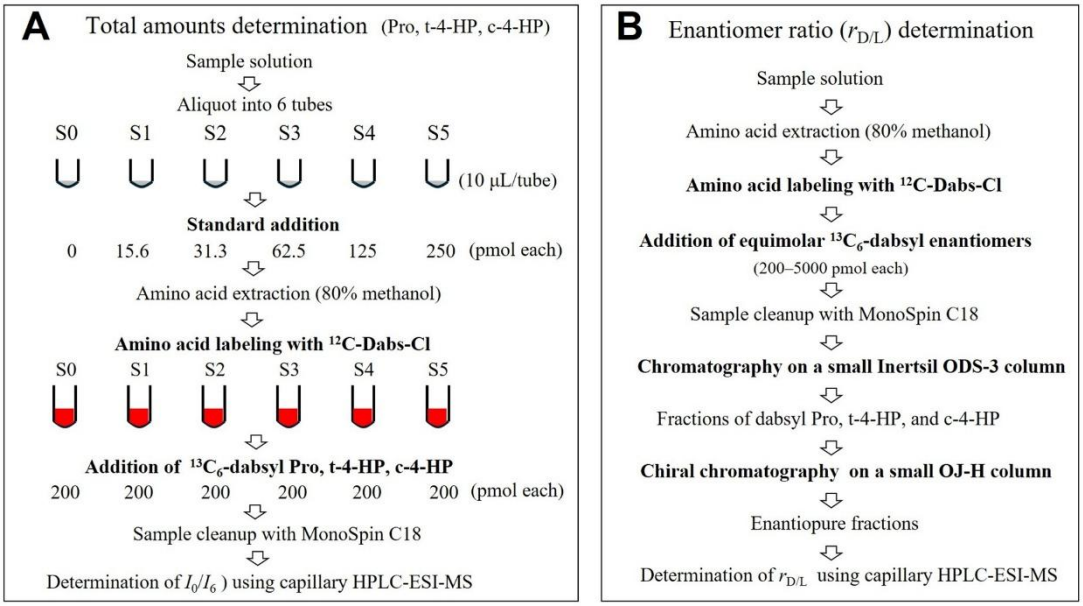

Figure 2-6 Procedures for determination of total amounts (A) and enantiomer ratio (B) of proline, *trans*-4-hydroxyproline and *cis*-4-hydroxyproline.

In the case of determination of the ratio of D- and L-enantiomers, equal amounts of $^{13}C_6$-dabsyl D-enantiomer and $^{13}C_6$-dabsyl L-enantiomer (200~1000 pmol each) were added to each ^{12}C-dabsylated sample and after the addition of each sample was treated as same way as described above.

2-2-9 Sample cleanup

To remove salts, unlabeled materials, and MO (major byproduct) from the acetone-removed samples, MonoSpin C18 columns (S type, GL Sciences, Tokyo, Japan) were used. Each column was first primed with 300 μL of methanol and then equilibrated with 300 μL of solvent A. Each acetone-removed sample was applied to the column. The column was washed with 300 μL of solvent A and then washed with 600 μL of 10% solvent B:90% solvent A (v/v) repeatedly until the eluate became nearly colorless. The dabsyl amino acids were eluted with 50 μL of solvent B into a new 1.5-mL Eppendorf tube. The eluted sample was evaporated to dryness using the centrifugal evaporator under reduced pressure and the dried samples were stored at 4°C until use (cleanup samples).

2-2-10 Liquid chromatography-electrospray ionization-mass spectrometry

Each cleanup sample was dissolved with 20 μL of 35% solvent B:65% solvent A (v/v) and the solution was filtered using a pre-column microfilter (0.4 μm, Upchurch) and a gas-tight syringe. A 2.5-μL aliquot of the filtrate was injected into an InertSustain C18 column (3 μm, 0.2 mm × 150 mm) pre-equilibrated with 35% solvent B. The flow rate was 1.3 μL/min, and a micro-flow pump (MP711V, GL Science) was used. The column temperature was controlled at 19°C with a column thermostat (IGLOO-CIL, OSTJ Co., Ltd., Osaka). Separation of dabsyl amino acids was performed according to the following time program: 0–5 min, 35% solvent B; 5–10 min, from 35% to 40% solvent B; 10–50 min, from 40% to 80% solvent B; 50–51 min, from 80% to 90% solvent B; 51–61 min, 90% solvent B; 61–62 min, from 90% to 35% solvent B. The eluent was subjected to electrospray ionization (ESI) using a tapered fused silica capillary (outer diameter 150 μm, ID 20 μm), whose position was controlled with a XYZ stage (AMR Inc., Tokyo). The spray voltage was 3.5 kV. The positive ions were introduced into an ion-trap mass spectrometer (LCQ Fleet, Thermo Fisher Scientific) through a capillary heated to 200°C. The control of the mass spectrometer and data processing was performed using Xcalibur (ver. 4.2 SP1, Thermo Fisher Scientific).

Chromatograms of respective dabsyl amino acids were extracted from the raw data using the following mass range: ^{12}C-dabsyl-Pro, 402.74–403.54; $^{13}C_6$-dabsyl-Pro, 408.74–409.54; ^{12}C-dabsyl-4-HP, 418.74–419.54;$^{13}C_6$-dabsyl-4-HP, 424.74–425.54. All the extracted data were transferred into Excel files and further analyzed using in-house programs written in Visual Basic for Applications (Microsoft).

2-2-11 Preparative separation of dabsyl derivatives of Pro, t-4-HP, and c-4-HP

In the case of the determination of the ratio of D- and L-enantiomers (Fig. 2-6B), dabsyl derivatives of Pro, t-4-HP, and c-4-HP were first purified from the cleanup samples as follows. Each cleanup sample was dissolved in 40 μL of 30% solvent B:70% solvent A (v/v) and the solution was filtered using the pre-column microfilter. All the filtrates were injected into an Inertsil ODS-3 column (3 μm, 1.5 mm × 150 mm, GL Sciences Inc.). The column was developed at a flow rate of 100 μL/min under the following time program: 0–10 min, 30% solvent B; 10–40 min, from 30% to 60% solvent B; 40–41 min, from 60% to 90% solvent B; 41–51 min, 90% solvent B; and 51–52 min, from 90% to 30% solvent B. The elution of dabsyl derivatives was monitored at the absorption at 430 nm using a photodiode array detector (1100 series, Agilent) and the respective peak corresponding to dabsyl t-4-HP, dabsyl c-4-HP, and dabsyl Pro was manually collected into a 1.5-mL Eppendorf tube. The collected fractions were evaporated to dryness using the centrifugal evaporator under reduced pressure. The dried samples were stored at 4°C until chiral separation.

2-2-12 Chiral separation of dabsyl secondary amino acids

In the present study, a chiral stationary phase of OJ-H (Daicel Corporation, Osaka, Japan) was found to have excellent separation ability for dabsyl Pro, t-4-HP, and c-4-HP. The dried dabsyl Pro fraction obtained by the preparative chromatography was dissolved in 20 μL of 50% methanol:50% ethanol (v/v) containing 0.1% acetic acid (solvent C). The solution was injected into a small OJ-H column (1.5 mm × 40 mm, in-house packed) pre-equilibrated with solvent C. The column was developed with solvent C at a flow rate of 150 μL/min and the absorbance at 430 nm of the eluate was monitored. The column temperature was at room temperature (about 20°C). Dabsyl L-Pro eluted much faster than dabsyl D-Pro, resulting in base-line separation. Each elution peak was manually collected into a 1.5-mL Eppendorf tube. The collected sample was evaporated to dryness using the centrifugal evaporator under reduced pressure.

The dried dabsyl c-4-HP fraction was dissolved in 20 μL of solvent C. The solution was injected into the small OJ-H column (1.5 mm × 40 mm), and the column was developed in the same conditions as used for dabsyl Pro. Dabsyl c-4-HP_L eluted faster than dabsyl c-4-HP_D to give baseline separation. Each elution peak was manually collected into a 1.5-mL Eppendorf tube and dried. In the case of dabsyl t-4-HP, a long OJ-H column (1.5 mm × 150 mm) was needed to attain the baseline separation of dabsyl t-4-HP_L and dabsyl t-4-HP_D. Dabsyl t-4-HP_L eluted faster than dabsyl t-4-HP_D.

2-3 Results

2-3-1 Determination of total amounts of Pro, t-4-HP, and c-4-HP

In LC-MS analysis using an InertSustain C18 column (3 μm, 0.2 mm × 150 mm), dabsyl t-4-HP, dabsyl c-4-HP and dabsyl Pro eluted in this order as observed in the semi-preparative HPLC on an Inertsil ODS-3 column (3 μm, 1.5 mm × 150 mm) (Fig. S2-2).

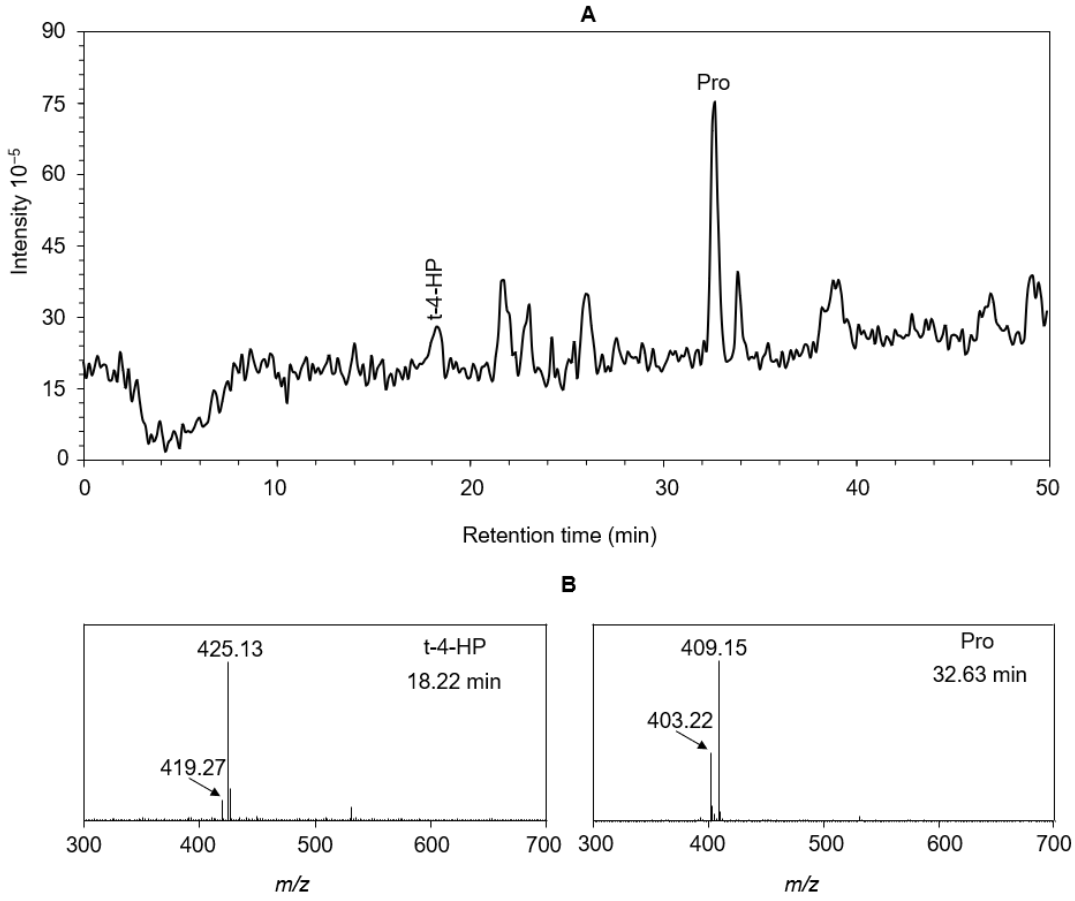

Figure 2-7 A typical total ion chromatogram (A) and mass spectra with doublet peak (B) obtained for mouse serum (S0 sample). *m*/*z* 419.27, [^{12}C-dabsyl t-4-HP + H]$^+$; *m*/*z* 425.13, [$^{13}C_6$-dabsyl t-4-HP + H]$^+$. *m*/*z* 403.22, [^{12}C-dabsyl Pro + H]$^+$; *m*/*z* 409.15, [$^{13}C_6$-Pro + H]$^+$.

Although it was difficult to attain reproducible retention time using a non-high grade syringe pump for gradient elution at the flow rate of 1.3 μL/min, it was easy to assign each peak on the basis of the elution of the corresponding $^{13}C_6$-dabsyl derivative. Figure 2-7A shows a typical total ion chromatogram obtained for mouse serum. There was a peak at 18.22 min and the left mass spectrum of Figure 2-7B was a typical mass spectrum observed at this peak. The ion with *m*/*z* 425.13 is protonated $^{13}C_6$-dabsyl t-4-HP$_L$, which was added to the sample as an internal standard, and the ion with *m*/*z* 419.27 is protonated ^{12}C-dabsyl t-4-HP derived from t-4-HP contained in the mouse serum because nothing added to S0 sample, indicating clearly that the mouse serum contains t-4-HP. The left mass spectrum of Figure 2-7B was obtained at 32.63 min, corresponding to the large peak in Figure 2-7A. The ion with *m*/*z* 409.15 is protonated $^{13}C_6$-dabsyl-L-Pro, internal standard, and the ion with *m*/*z* 403.22 is ^{12}C-dabsyl Pro from the mouse serum. These results demonstrate that the presence of Pro, t-4-HP, and c-4-HP can be easily judged by the appearance of doublet ion peaks with difference in *m*/*z* by 6 in mass spectrum. All the total ion chromatograms obtained for S0 sample analyzed are listed in Supporting Figures S2-3–7.

Figure 2-8 show extracted ion chromatograms for *m*/*z* 419.14 ([^{12}C-dabsyl-t-4-HP + H]$^+$ ion) and *m*/*z* 425.16 ([$^{13}C_6$-dabsyl-t-4-HP + H]$^+$ ion) obtained for S0–S5 samples of 10-fold diluted mouse serum. Unexpectedly, $^{13}C_6$-dabsyl-t-4-HP eluted faster by 1.4–2.6 seconds compared to ^{12}C-dabsyl-t-4-HP (Δ*t* and enlarged chromatograms in Figs. 2-8A–F). Therefore, the ratio between the intensity of *m*/*z* 419.14 ion (I_0) and that of *m*/*z* 425.16 ion (I_6) was calculated by adjusting appropriately this elution time lag, resulting in the horizontal distribution of the I_0/I_6 value across the peak (black dots in Figs. 2-8A–F). The mean value and standard deviation (SD) were obtained using these I_0/I_6 values, and they were plotted against the amounts of t-4-HP$_L$ added to the serum sample (Fig. 2-8G). The calibration curve showed excellent linearity (the correlation coefficient R^2 was 0.998) and the total t-4-HP content was obtained to be 53.4 ± 2.6 pmol from the intersection between the calibration curve and the horizontal axis. Using the same chromatographic raw data, *m*/*z* 403.14 ion ([^{12}C-dabsyl-Pro + H]$^+$ ion) and that of *m*/*z* 409.16 ion ([$^{13}C_6$-dabsyl-Pro + H]$^+$ ion) were extracted and the calibration curve of Pro obtained as the same method as described for t-4-HP (Fig. 2-8H). As for c-4-HP, no peak was detected for S0 sample as shown in the inset to Fig. 2-8A and thus c-4-HP was not added to the mouse serum sample.

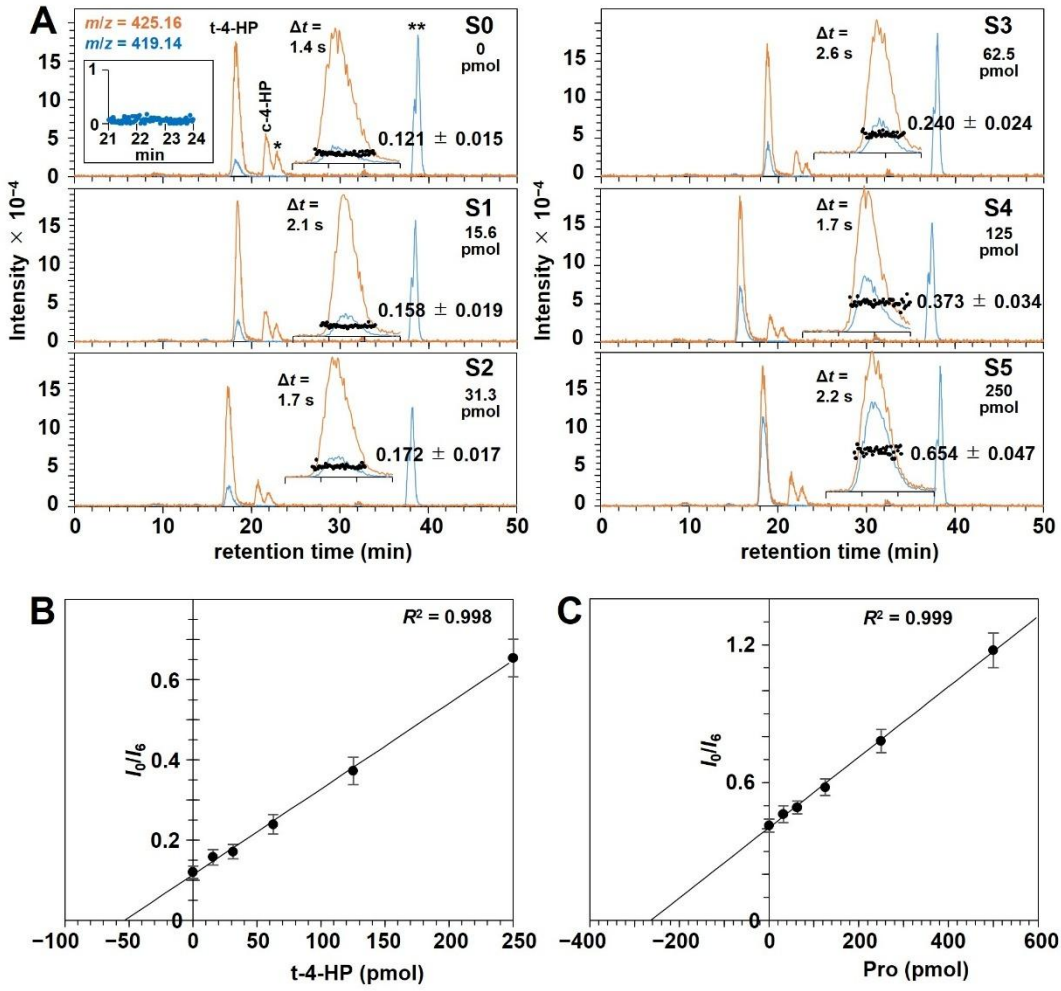

Figure 2-8. The extracted ion chromatograms for m/z 419.14 and m/z 425.16 from LC-MS analysis of S0–S5 samples of 10-fold diluted mouse serum (A) and the calibration curves for t-4-HP (B) and Pro (C). The t-4-HP peaks are enlarged in each figure. $^{13}C_6$-Dabsyl t-4-HP eluted slightly faster than ^{12}C-Dabsyl t-4-HP by 1.4–2.6 s (Δt in the figure). The peak intensity ratio between m/z 419.14 and m/z 425.16 was calculated for each retention-time adjusted ion pair and the obtained values are shown as black dots on the enlarged peaks. The mean value of these intensity ratio values and the SD are shown in black numbers, mean ± SD. The peak marked with **, the isotope peak of leucine. The peak marked with *, unknown peak.

The total amounts of Pro, t-4-HP, and c-4-HP in various samples were successfully determined and are summarized in Table 2-1. All the samples examined contained Pro and t-4-HP. In the case of *A. fulica* hemolymph, t-4-HP was clearly detected but at levels below the limit of quantification.

Table 2-1. Total amounts of Pro, t-4-HP, and c-4-HP contained in various samples

Samples	Pro (μmol/L)		t-4-HP (μmol/L)		c-4-HP (μmol/L)	
	mean	CV (%)	mean	CV (%)	mean	CV (%)
Mouse serum (n = 6)*	243 ± 16	6.6	51 ± 10	19.6	ND**	
A. fulica hemolymph (n =7)	35.4 ± 7.3	20.6	NQ***		ND	
Aronia juice (n = 5)	192 ± 9	4.7	70 ± 3	4.3	ND	
Aronia seed (n = 5)	163 ± 11	6.7	24.0 ± 1.9	7.9	ND	
Persimmon (n = 5)	4.8 ± 0.7	14.6	1.5 ± 0.3	20	ND	
Apple (n = 5)	10.9 ± 1.1	10.1	1.2 ± 0.2	16.7	ND	
Pear (n = 3)	508 ± 25	4.9	9.2 ± 1.6	17.4	ND	
	nmol/g		μmol/g		μmol/g	
S. album L. (n = 4)	337 ± 51	15	1.39 ± 0.08	5.7	11.3 ± 0.6	5

Values are mean ± standard deviation (SD). *n, the number of independent analyses. **ND, not determined. ***NQ, detected but less than quantifiable levels. CV (%), (SD/mean) × 100.

As for c-4-HP, it was detected only in the wood powder of *S. album*. The powder contained exceptionally high amounts of c-4-HP (11.3 mmol/kg). Except in bacteria and microorganisms, the presence of c-4-HP is uncommon in animals and plants. The reason why high levels of c-4-HP exits in *S. album* remains unclear. Further studies are needed to elucidate the biochemical pathways responsible for the production of c-4-HP and to better understand the physiological in Table 2-1 are the mean values of samples harvested from 2017 to 2021 and the dependence of the contents on harvest year is summarized in Table S2-1.

2-3-2 Determination of the enantiomer ratio (rD/L) of Pro, t-4-HP, and c-4-HP

Usually, natural samples contain predominantly only one of the enantiomers of chiral substances, and another enantiomer is less than 1% of the total amount, making it difficult to accurately quantify small amounts of rare enantiomer under the background of large amounts of predominant one. As schematically explained in the method section (Fig. 2-6B), equal amounts of $^{13}C_6$-dabsyl-D- and L-enantiomers ($Q_{6,D}$ and $Q_{6,L}$, respectively) were added in sufficient amounts (200–5000 pmol) to ^{12}C-dabsylated sample. The enantiomer ratio ($r_{D/L}$) of Pro, t-4-HP, or c-4-HP in the sample is expressed as

$$r_{D/L} = Q_{0,D}/Q_{0,L} \quad \text{(Eq 1)}$$

where $Q_{0,D}$ and $Q_{0,L}$ are the amount of ^{12}C-dabsylated D- and L-enantiomers, respectively. As $Q_{6,D} = Q_{6,L}$, the following equation is obtained.

$$r_{D/L} = (Q_{0,D}/Q_{6,D})/(Q_{0,L}/Q_{6,L}) \quad \text{(Eq 2)}$$

Therefore, if we can determine the ratio of $Q_{0,D}/Q_{6,D}$ and $Q_{0,L}/Q_{6,L}$, then the enantiomer ratio ($r_{D/L}$) is obtained according to Equation 2.

Figure 2-9A shows a typical chromatogram on an Inertsil ODS-3 column (3 μm, 1.5 mm × 150 mm) to isolate dabsyl t-4-HP, dabsyl c-4-HP, and dabsyl Pro from a ^{12}C-dabsylated *S. album* sample spiked with $^{13}C_6$-dabsyl enantiomers. As 1 nmol of each enantiomer of $^{13}C_6$-dabsyl Pro and t-4-HP and 5 nmol of each enantiomer of $^{13}C_6$-dabsyl c-4-HP were added to the ^{12}C-dabsylated sample, each dabsyl secondary amino acid eluted as a distinct peak, making it easy to collect it manually. Then, the isolated dabsyl t-4-HP, dabsyl c-4-HP, and dabsyl Pro were subjected to chiral chromatography on OJ-H columns. As shown in Figures 2-9B–D, L-enantiomer migrated much faster than D-enantiomer through the chiral column, resulting in complete separation of L- and D-enantiomers. Importantly, as equal amounts of authentic $^{13}C_6$-dabsyl enantiomers in nmol levels were added, both L- and D-enantiomers eluted as a distinct peak, enabling the collection of each enantiomer without mutual contamination.

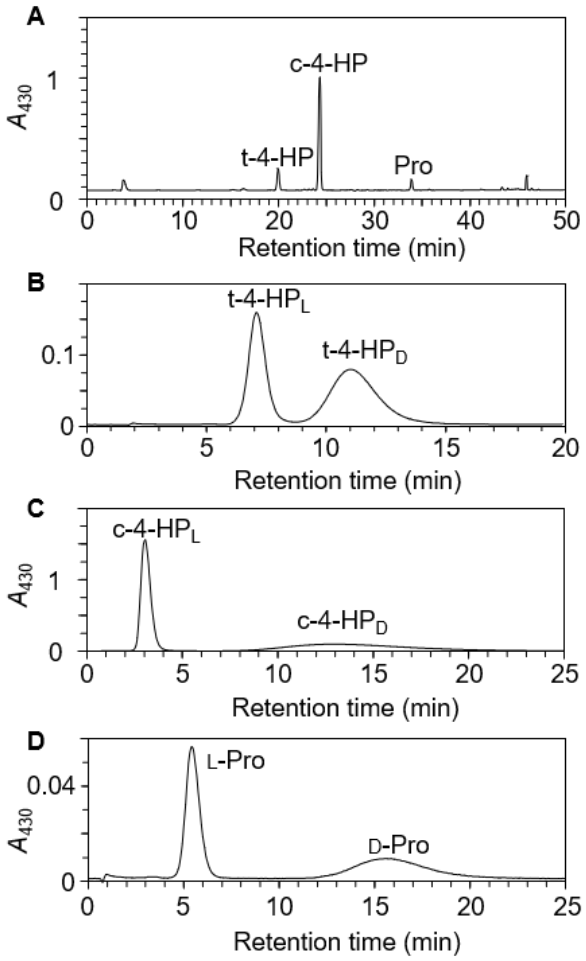

Figure 2-9. Partial purification of dabsyl t-4-HP, dabsyl c-4-HP, and dabsyl Pro by semi-preparative HPLC on an Inertsil ODS-3 column (A) and complete separation of L- and D-enantiomers of dabsyl t-4-HP (B), dabsyl c-4-HP (C), and dabsyl Pro (D) by chiral chromatography on an OJ-H column. Amino acid extracts from *S. album* powder were labelled with ^{12}C-Dabs-Cl, and then to this reaction mixture equal amounts of $^{13}C_6$-dabsyl-L-Pro and $^{13}C_6$-dabsyl-D-Pro (1 nmol each), $^{13}C_6$-dabsyl-t-4-HP$_L$ and $^{13}C_6$-dabsyl-t-4-HP$_D$ (1 nmol each), $^{13}C_6$-dabsyl-c-4-HP$_L$ and $^{13}C_6$-dabsyl-c-4-HP$_D$ (5 nmol each) were added. The mixture was cleaned up and then applied to the ODS column. Each peak was manually collected, and then the resultant enantiopure fraction subjected to chiral chromatography.

Each isolated enantiomer fraction was analyzed by LC-MS as described for total amounts determination to obtain the ratio of $Q_{0,D}/Q_{6,D}$ and $Q_{0,L}/Q_{6,L}$ as the intensity ratio between doublet peaks in mass spectra, $I_{0,D}/I_{6,D}$ and $I_{0,L}/I_{6,L}$, respectively. Figures 2-10A and B show typical extracted ion chromatograms obtained for dabsyl t-4-HP$_L$ and dabsyl t-4-HP$_D$ fractions

from *S. album* wood powder, respectively.

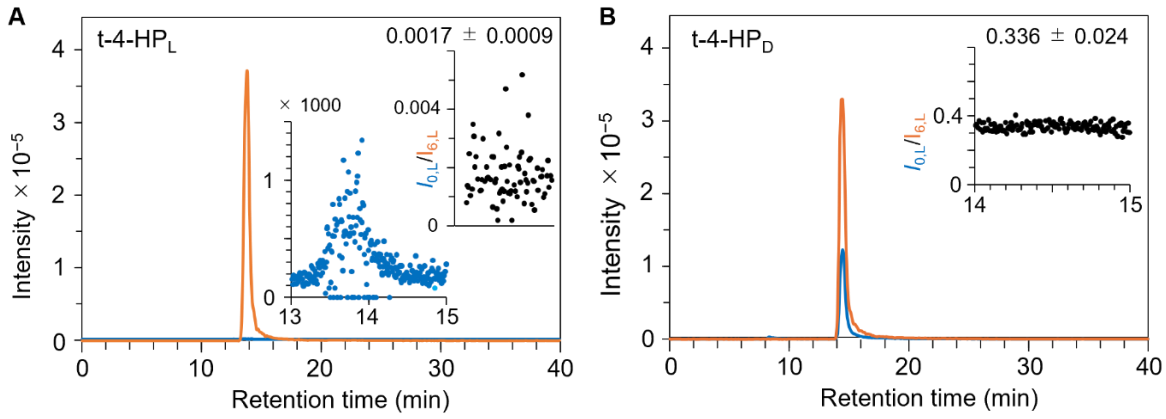

Figure 2-10. The extracted ion chromatograms for m/z 419.14 and m/z 425.16 obtained for the L-enantiomer fraction of dabsyl-t-4-HP$_L$ (A) and the D-enantiomer fraction of dabsyl-t-4-HP$_D$ (B). The L-and D-enantiomer fractions of dabsyl-t-4-HP obtained by complete chiral separation of isolated dabsyl t-4-HP from *S. album* wood powder (Fig. 2-9B) were analyzed by LC-MS. $I_{0,L}/I_{6,L}$ is the ratio between intensity of *m/z* 419.14 ion and that of *m/z* 425.16 ion. (A) The *m/z* 419.14 peak is 1000-fold enlarged (blue dots).

^{12}C-Dabsyl t-4-HP$_L$ showed a weak but significant peak, about 3-fold higher levels than noise levels (1000-fold enlarged figure in Fig. 2-10A), and the $I_{0,L}/I_{6,L}$ ratio was obtained to be 0.0017 ± 0.0009 by calculating the mean and standard deviation of the values shown in the inset to Figure 2-10A, which were obtained after correction of the base line noise and isotope effect on the elution time as described for the total amounts determination. As for t-4-HP$_D$, the $I_{0,D}/I_{6,D}$ ratio was obtained to be 0.336 ± 0.024 (Fig. 2-10B). According to Equation 2, the enantiomer ratio of t-4-HP of *S. album* wood powder, $r_{D/L}$, was obtained to be 217 ± 64 because $Q_{0,D}/Q_{6,D} = I_{0,D}/I_{6,D}$ and $Q_{0,L}/Q_{6,L} = I_{0,L}/I_{6,L}$. To the best of our knowledge, this is the first report on experimental determination of the enantiomer ratio of t-4-HP of *S. album*, indicating the dominance of t-4-HP$_D$.

Table 2-2 summarizes the enantiomer ratio ($r_{D/L}$) for Pro, t-4-HP, and c-4-HP obtained for various samples. In mouse serum, L-enantiomer was confirmed to be dominant both for Pro and t-4-HP, $r_{D/L}$ of 0.0068 ± 0.0004 and 0.0040 ± 0.0008, respectively. As for *A. fulica* hemolymph, we could not determine $r_{D/L}$ value for Pro with satisfactory levels of precision, but the presence of D-Pro was unambiguously confirmed. In the case of *S. album* wood powder,

all 6 enantiomers were detected.

Table 2-2 The molar ratio of D-enantiomer to L-enantiomer ($r_{D/L}$) for Pro, t-4-HP, and c-4-HP

Samples	Pro ($r_{D/L}$)	t-4-HP ($r_{D/L}$)	c-4-HP ($r_{D/L}$)
	$\times 10^{-3}$	$\times 10^{-3}$	$\times 10^{-3}$
Mouse serum	6.78 ± 0.39 (n = 4)*	4.04 ± 0.76	ND
A. fulica hemolymph	2.99 ± 0.92 (n = 3)	ND**	ND
Aronia juice	60.2 ± 13. 2 (n = 5)	ND	ND
Aronia seed	1.43 ± 0.58 (n = 6)	ND	ND
Persimmon	3.11 ± 0.32 (n = 3)	ND	ND
Apple	2.16 ± 0.15 (n = 3)	ND	ND
Pear	1.03 ± 0.98 (n = 3)	ND	ND
S. album L.	0.21 ± 0.13 (n = 3)	0.193 ± 0.056 (n = 3)	1.82 ± 0.57 (n = 4)

*n is the number of independent analyses performed in different days.

**ND: not detected.

2-3-3 Contents of L-Pro, D-Pro, t-4-HP$_L$, t-4-HP$_D$, c-4-HP$_L$, and c-4-HP$_D$

Using the total amounts (C_t) and the $r_{D/L}$ ratio, the content of each enantiomer (C_L and C_D, respectively) was obtained based on the following equations.

$$C_L = C_t/(1 + r_{D/L}) \quad \text{(Eq 3)}$$

$$C_D = C_t\, r_{D/L}/(1 + r_{D/L}) \quad \text{(Eq 4)}$$

The standard deviation of C_L and C_D (σ_L and σ_D, respectively) was calculated according to the following equations.

$$\sigma_L = (\sigma_t^2/(1 + r_{D/L})^2 + C_t^2\sigma_r^2/(1 + r_{D/L})^4)^{1/2} \quad \text{(Eq 5)}$$

$$\sigma_D = (r_{D/L}^2\sigma_t^2/(1 + r_{D/L})^2 + C_t^2\sigma_r^2/(1 + r_{D/L})^2 + r_{D/L}^2C_t^2\sigma_r^2/(1 + r_{D/L})^4)^{1/2} \quad \text{(Eq 6)}$$

where σ_t and σ_r are the standard deviation of C_t and $r_{D/L}$, respectively. The results are summarized in Table 2-3.

Table 2-3. Contents of D-Pro, L-Pro, t-4-HP_D, t-4-HP_L, c-4-HP_D, and c-4-HP_L in various samples.

Samples	D-Pro	L-Pro	t-4-HP_D	t-4-HP_L	c-4-HP_D	c-4-HP_L
	μmol/L	μmol/L	μmol/L	μmol/L		
Mouse serum	1.64 ± 0.14	241 ± 16	0.20 ± 0.06	50.4 ± 10.1	ND*	ND
A. fulica	0.11 ± 0.03	35.29 ± 0.14	ND	NQ**	ND	ND
Aronia juice	9.2 ± 2.4	183.0 ± 64.7	ND	70 ± 3	ND	ND
Aronia seed	0.27 ± 0.13	162.8 ± 92.8	ND	24 ± 1.9	ND	ND
Persimmon	0.017 ± 0.005	4.783 ± 0.005	ND	1.5 ± 0.3	ND	ND
Apple	0.023 ± 0.005	10.877 ± 0.005	ND	ND	ND	ND
Pear	0.52 ± 0.05	507.47 ± 0.05	ND	NQ	ND	ND
	nmol/g	nmol/g	μmol/g	μmol/g	μmol/g	μmol/g
S. album L.	7.1 ± 4.4	330 ± 50	1.38 ± 0.57	0.0072 ± 0.0021	0.021 ± 0.007	11.3 ± 0.6

The data is shown as mean ± SD. *ND: not detected. **NQ: detected but less than quantifiable levels.

Surprisingly, relatively high amounts of D-Pro were detected in plant samples, such as in aronia juice and *S. album* wood powder. In these samples, the D-Pro levels were higher compared to mouse serum and *A. fulica* hemolymph (Table 2-3). *S. album* wood powder contained D-enantiomer of Pro, t-4-HP and c-4-HP. Although there are no recent studies on this *S. album* species, Kuttan et al. reported the presence of t-4-HP_L in the bound state and c-4-HP_L in free form in the leaves and pericarp of *S. album* (34–37). Physiological roles of the D-enantiomer of Pro and 4-HP in plants are not yet known, and it also remains unclear how the D-enantiomers are produced. One study reported that AtProT2 (*Arabidopsis* Proline Transporter 2) in *Arabidopsis thaliana* can transport both L- and D-Pro, and that excess external D-Pro inhibits the growth of *Arabidopsis* roots and can be detrimental to plant growth (38).

2-4 Discussion

Biological samples contain large amounts of Dabs-Cl-reactive substances such as amines and phenols, and the secondary amino acids are only small portions of them. Therefore, the high reactivity of Dabs-Cl with secondary amino acids is important for quantification of Pro,

t-4-HP, and c-4-HP. To obtain reliable calibration curves, the standard addition method was applied to the present study. Although I used a conventional nano-HPLC system and low-resolution ion-trap mass spectrometer to perform capillary LC-MS at the flow rate of 1.3 μL/min, chromatographic peak of target dabsyl amino acid could be easily identified using $^{13}C_6$-dabsyl derivatives of Pro, t-4-HP, and c-4-HP as internal standards. As amino acids extracted from a sample were labeled with commercial Dabs-Cl (^{12}C-Dabs-Cl), characteristic doublet ion peaks with difference in *m*/*z* by 6 were observed in mass spectra when sample contained the target secondary amino acids. Linear calibration curves were obtained by plotting the peak intensity ratio between the ^{12}C-dabsyl amino acid and the corresponding $^{13}C_6$-dabysl amino acids (I_0/I_6) against the known amounts of the amino acid added (the standard addition method), resulting in accurate and reproducible determination of the total amounts of Pro, t-4-HP, and c-4-HP.

In the present study, complete separation of L- and D-enantiomers of Pro, t-4-HP, and c-4-HP was successfully attained using small OJ-H columns. To determine the enantiomer ratio ($r_{D/L}$), equal amounts of $^{13}C_6$-dabsyl D- and L-enantiomers were added to the sample amino acids treated with ^{12}C-dabsyl chloride before sample cleanup step. The $r_{D/L}$ ratio was determined by obtaining the I_0/I_6 peak intensity ratio using LC-MS analysis of each enantiopure fractions prepared by semipreparative reverse-phase chromatography and following chiral separation of enantiomers. In the case of *S. album* wood powder, very small $r_{D/L}$ ratio of 0.00021 was determined.

Recently, Ishii et al. developed their two-dimensional LC-MS/MS system for the determination of Pro and 4-HP enantiomers in biological food samples using 4-fluoro-7-nitro-2,1,3-benzoxadiazole as labeling reagent (5). Although they examined various samples including bivalves and beverages, they could not detect c-4-HPL and t-4-HPD in all the samples examined. In the present study, to validate the method, various samples were analyzed and *S. album* L wood powder was focused on because this medicinal plant is known to have a large amount of c-4-HP and a substantial amount of t-4-HP (34–37). In these studies, the evaluation of the enantiomer dominance of c-4-HP and t-4-HP in *S. album* was performed by paper chromatography of the copper salts. Therefore, it is worth reexamining the enantiomer ratio using the present method. In fact, all the 6 secondary amino acids (Figure 2-1) were detected and quantified in *S. album* L wood powders, and unexpectedly the D-enantiomer of t-4-HP was found to be dominant (Table 2-2). The present results indicate that this plant sample is very useful for validation of methods to analyze the enantiomers of secondary amino acids.

The amounts of each enantiomer can be calculated using the total amounts and the $r_{D/L}$ ratio (Equations 3–6). In the present study, I determined independently the total amount of a target analyte (C_t) and the molar ratio of D- and L-enantiomers of the analyte ($r_{D/L}$). This strategy allowed us to show the presence of 0.2 μmol/L levels of t-4-HP_D in mouse serum (Table 2-3). It is of note that the present method can be performed in high-throughput and much higher sensitivity just only using modern sophisticated nano-HPLC system and high-resolution mass spectrometer. Furthermore, it is easy to synthesize $^{13}C_2$-, $^{13}C_8$-, $^{13}C_{12}$-, and $^{13}C_{14}$-Dabs-Cl using *N*,*N*-dimethylaniline-$^{13}C_2$ in combination with sulfanilic acid-$^{13}C_6$. Therefore, it is possible to analyze 6 samples by one LC-MS analysis.

References

1. Ishikawa Y. (2025) Collagen biosynthesis and its molecular ensemble: what remains unexplored. *Biochemistry*. 64, 3149-3155.
2. Li P, and Wu G. (2018) Roles of dietary glycine, proline, and hydroxyproline in collagen synthesis and animal growth. *Amino Acids*. 50, 29-38.
3. Tojo Y., Hamase K., Nakata M., Morikawa A., Mita M., Ashida Y., Lindner W., and Zaitsu. (2008) Automated and simultaneous two-dimensional micro-high-performance liquid chromatographic determination of proline and hydroxyproline enantiomers in mammals. J. Chromatogr. B 875, 174–179
4. Kieliszewski M. J., O'Neill M., Leykam J., and Orlando R. (1995) Tandem mass spectrometry and structural elucidation of glycopeptides from a hydroxyproline-rich plant cell wall glycoprotein indicate that contiguous hydroxyproline residues are the major sites of hydroxyproline O-arabinosylation. *J. Biol. Chem*. 270, 2541–2549
5. Ishii C., Tojo Y., Iwasaki K., Fujii A., Akita T., Nagano M., Mita M., Ide T., and Hamase K. (2024) Development of a two-dimensional LC-MS/MS system for the determination of proline and 4-hydroxyproline enantiomers in biological and food samples. *Anal. Sci.* 40, 881–889
6. Shoulders M. D., and Raines R. T. (2009) Collagen structure and stability. *Annu. Rev. Biochem.* 78, 929–958
7. Albaugh V. L., Mukherjee K., and Barbul A. (2017) Proline precursors and collagen synthesis: biochemical challenges of nutrient supplementation and wound healing. *J.Nutr.* 147, 2011–2017
8. Mishra U. K., and Ramesh N. G. (2020) A carbohydrate based straightforward approach

to trans-4-hydroxy-D-proline and trans-4-hydroxy-D-prolinol. *Tetrahedron Lett.* 61:152081

9. Ishii C., Akita T., Mita M., Konno R., and Hamase K. (2023) Chiral Amino Acid Analysis in the Plasma of B6DAO-/- Mice Lacking D-Amino Acid Oxidase Activity. Chromatography 44, 39–43
10. Wang J., Tan B., Li J., Kong X., Tan M., and Wu G. (2020) Regulatory role of l-proline in fetal pig growth and intestinal epithelial cell proliferation. *Anim. Nutr.* 6, 438–446
11. Liu N., Dai Z., Zhang Y., Chen J., Yang Y., Wu G., Tso P., and Wu Z. (2019) Maternal L-proline supplementation enhances fetal survival, placental development, and nutrient transport in micedagger. *Biol. Reprod.* 100, 1073–1081
12. Wu G., Bazer F. W., Burghardt R. C., Johnson G. A., Kim S. W., Knabe D. A., Li X., McKnight J. R., Satterfield M. C., and Spencer T. E. (2011) Proline and hydroxyproline metabolism: implications for animal and human nutrition. *Amino Acids* 40, 1053–1063
13. Patriarca E. J., Cermola F., D'Aniello C., Fico A., Guardiola O., De Cesare D., and Minchiotti G. (2021) The Multifaceted Roles of Proline in Cell Behavior. *Front. Cell Dev. Biol*. 9:728576
14. Meena M., Divyanshu K., Kumar S., Swapnil P., Zehra A., Shukla V., Yadav M., and Upadhyay R. S. (2019) Regulation of L-proline biosynthesis, signal transduction, transport, accumulation and its vital role in plants during variable environmental conditions. *Heliyon* 5:e02952
15. Sasabe J., and Suzuki M. (2019) Distinctive Roles of D-amino acids in the homochiral world: chirality of amino acids modulates mammalian physiology and pathology. *Keio J. Med.* 68, 1–16.
16. Liu M., Li M., He J., He Y., Yang J., and Sun Z. (2023) Chiral Amino Acid Profiling in Serum Reveals Potential Biomarkers for Alzheimer's Disease. *J Alzheime's Dis.* 94, 291–301
17. Kimura T., Hesaka A., and Isaka Y. (2020) D-Amino acids and kidney diseases. *Clin Exp Nephrol*. 24, 404–410
18. Chen S., White C. E., diCenzo G. C., Zhang Y., Stogios P. J., Savchenko A., and Finan T. M. (2016) L-Hydroxyproline and D-Proline Catabolism in *Sinorhizobium meliloti*. *J. Bacteriol.* 198, 1171–1181
19. Hu S., He W., and Wu G. (2022) Hydroxyproline in animal metabolism, nutrition, and cell signaling. *Amino Acids* 54, 513–528

20. Deng W-H., Lu Y., and Liao R-Z. (2024) Computational insights into chemoselectivity of *trans*-4-hydroxy-L-proline dehydratase HypD. *J. Catalysis* 439:115736
21. Opekar S., Zahradnickova H., Vodrazka P., Rimnacova L., Simek P., and Moos M. (2021) A chiral GC-MS method for analysis of secondary amino acids after heptafluorobutyl chloroformate & methylamine derivatization. *Amino Acids* 53, 347–358
22. Wu F., Wu X., Xu F., Han J., Tian H., and Ding C. F. (2022) Recognition of cis-trans and chiral proline and its derivatives by ion mobility measurement of their complexes with natamycin and metal Ion. *Anal. Chem*. 94, 3553–3564
23. Chen X., Yi J., Liu J., Luo Q., and Liu L. (2021) Enzymatic production of *trans*-4-hydroxy-L-proline by proline 4-hydroxylase. *Microbial Biotechnol.* 14, 479–487
24. Rosenbloom J., and Prockop D. J. (1971) Incorporation of *cis*-hydroxyproline into protocollagen and collagen: collagen containing *cis*-hydroxyproline in place of proline and *trans*-hydroxyproline is not extruded at a normal rate. *J. Biol. Chem*. 246, 1549–1555
25. Ciardiello F., Sanfilippo B., Yanagihara K., Kim N., Tortora G., Bassin R. H., Kidwell W. R., and Salomon D. S. (1988) Differential growth sensitivity to 4-*cis*-hydroxy-L-proline of transformed rodent cell lines. *Cancer Res.* 48, 2483–2491
26. Mueller C., Emmrich J., Jaster R, Braun D., Liebe S., and Sparmann G. (2006) Cis-hydroxyproline-induced inhibition of pancreatic cancer cell growth is mediated by endoplasmic reticulum stress. *World J. Gastroentero*l. 12, 1569–1576
27. Kuttan R., and Radhakrishnan A. N. (1973) Biochemistry of the hydroxyprolines. *Adv. Enzymol.* 37, 273–347
28. Watanabe S., Morimoto D., Fukumori F., and Watanabe Y. (2018) Characterization of *cis*-4-hydroxy-D-proline dehydrogenase from *Sinorhizobium meliloti*. *Biosci. Biotechnol. Biochem*. 82, 110–113
29. Adams E., and Frank L. (1980) Metabolism of proline and the hydroxyprolines. *Ann. Rev. Biochem*. 49, 1005–1061
30. Okumura Y., Ohnishi M., Okamoto R., and Ishikura T. (1982) Some effectors on the biosynthesis of *cis*-4-hydroxy-d-proline in viridogrisein. *Agric Biol Chem.* 46, 3063–3068
31. Vodova M., Babini E., Soglia F., Bordini M., Lioi M., Tengattini S., Temporini C., and Gotti R. (2025) Cyclodextrin-modified capillary zone electrophoresis for the chiral analysis of proline and hydroxyproline stereoisomers in chicken collagen hydrolysates. *Int. J. Mol. Sci.* 26:5832
32. Hasegawa K., Minakata K., and Suzuki M. (2021) The standard addition method and its

validation in forensic toxicology. *Forensic. Toxicology* 39, 311–333

33. Lin J. K., and Chang J. Y. (1975) Chromophoric labeling of amino acids with 4-dimethylaminoazobenzene-4'-sulfonyl chloride. *Anal. Chem.* 47, 1634–1638
34. Radhakrishnan, A. N., Gopalkrishnan, K. S., and Giri, K. V. (1961) Distribution and seasonal variation of allohydroxy-L-proline in *Santalum album* L. *Biochem. J.* 80, 378–384
35. Kuttan, R., and Radhakrishnan, A. N. (1970) The biosynthesis of *cis*-4-hydroxy-L-proline in Sandal (*Santalum album* L.). B*iochem. J.* 117, 1015–1017
36. Kuttan, R., and Radhakrishnan, A. N. (1970) Studies on bound *trans*-4-hydroxy-L-proline in Sandal (*Santalum album* L.). *Biochem. J.* 119, 651–657
37. Kuttan, R., Panikkar, B., and Binitha, P. P. (2015) Amino acids in sandal *(Santalum album* L) with special reference to *cis*-4-hydroxy-L-proline and sym. homospermidine. *SpringerPlus*. 4, 546
38. Lehmann S., Gumy C., Blatter E., Boeffel S., Fricke W., and Rentsch D. (2011) In planta function of compatible solute transporters of the AtProT family. *J. Exp. Botany.* 62, 787–796

Chapter III

Application of the Sandell-Kolthoff method to the determination of the iodine content of foods with complex matrices

3-1 Introduction

Iodine is a trace element required for the thyroid gland to synthesize thyroid hormones, triiodothyronine (T_3) and thyroxine (T_4) (1). The chemical structure of T3 and T4 are shown in Figure 3-1.

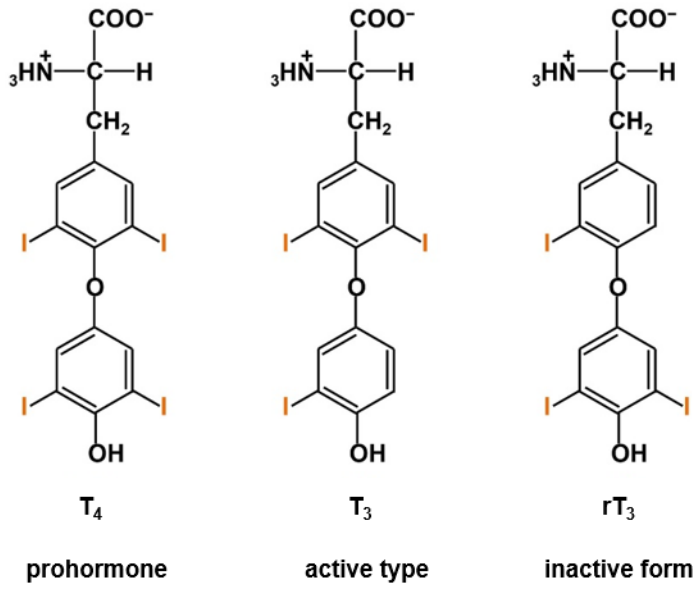

Figure 3-1. Chemical structure of thyroxine (T_4), triiodothyronine (T_3), and reverse triiodothyronine (rT_3).

Thyroid hormones are essential for normal growth and development, neuronal differentiation, metabolic regulation, and thermoregulation in mammals (2,3). They regulate many key biochemical reactions, especially protein synthesis and enzymatic activity. The major target organs are the developing brain, muscle, kidney, heart, and pituitary (4). A healthy adult body contains 15–20 mg of iodine, 70–80% of which is in the thyroid glands (5). Iodine content in food is highly variable and is low in the majority of foods (6,7). It is mostly found in oceans and coastal regions as iodide (I^-), highly water-soluble ion (2). As a result, approximately one-third of the world's population lives in areas where natural sources of iodine are low (8). Iodine deficiency is responsible for irreversible brain damage, cretinism, delayed psychomotor development, goiter (enlargement of the thyroid gland), and hypothyroidism. Iodine deficiency

disorder (IDD) is the most common cause of preventable brain damage during fetal development (8,9).

The World Health Organization (WHO) recommends a daily iodine intake of 90 μg for 0–59 months infants, 120 μg for school-age children, 150 μg for adolescents and adults, 250 μg for pregnant and lactating women (8,10), which is difficult to fulfill only by taking natural foods in iodine-deficient areas. Therefore, iodine fortification, such as universal salt iodization (USI) programs, has been implemented in iodine-deficient areas to prevent IDD. According to the UNICEF Global Database (2022), 89 % of the global population uses iodized salt (9). After the introduction of USI, the number of countries with insufficient iodine intake decreased from 113 in 1993 to 21 in 2021 (11). This indicates remarkable success in reducing the global prevalence of iodine deficiency. However, recurrence of iodine deficiency has been observed in countries where USI is not mandatory (5,11). Pregnant and lactating women, who have higher iodine requirements, are at higher risk of insufficient iodine intakes. Adequate iodine (neither excessive nor deficient) is crucial for pregnant and postpartum women and their offspring, as they are the most sensitive to the effects of iodine deficiency or excess. A meta-analysis reported a high prevalence (53%) of inadequate iodine intake among pregnant women globally (12). Iodine deficiency during pregnancy can cause miscarriage, stillbirth, and irreversible intellectual disability in the fetus (5). Therefore, the iodine status of pregnant women and women of reproductive age is crucial to monitor.

Importantly, after the introduction of USI, the number of countries with excessive iodine intake is increasing. According to the Iodine Global Network (2025), 11 countries have reported to be in excessive iodine intake (11). The WHO/UNICEF categorizes the median urine iodine concentration (mUIC) for school-age children as follows: < 100 μg/L, insufficient; 100–299 μg/L, adequate; > 300 μg/L, excessive (10,13). Chronic exposure to excess iodine has been shown to cause autoimmune thyroiditis, such as Hashimoto thyroiditis, Graves' disease, goiter, and thyroid nodules (14).

3-1-1 Iodine status in Nepal

Geographically, Nepal lies in an iodine-deficient zone of the world. Its mountainous terrain and high annual rainfall lead to low environmental iodine content. Nepal has achieved substantial progress in improving iodine status through the successful implementation of the USI. As a result, the prevalence of visible goiter declined dramatically from 55% in 1965 to 0.4% in 2007 (15). Household consumption of iodized salt increased from 10% in 1998 to 98%

in 2022 (15,16,17).

In Nepal, the recommended level of iodine content in iodized salt is at least 50 mg/kg salt at the production level, 30 mg/kg salt at the retail level, and 15 mg/kg salt at the household level (18). However, the mean iodine content of household salt samples was found much higher (> 40 mg/kg salt) than the recommended level. Similarly, the Nepal National Micronutrient Survey and various cross-sectional studies reported that the mUIC in school-age children exceeds 300 μg/L (17,19,20). In addition, the consumption of processed and packaged foods has increased in Nepal. Although data on the iodine content of such foods is lacking, it is suggested that salted packaged foods may contribute to additional iodine intake (18,21). Compared with populations in iodine-sufficient areas with normal thyroid function, previously iodine-deficient populations are more susceptible to thyroid dysfunction, even with a slight increase in iodine intake (22,23). That might be the reason for the increasing prevalence of thyroid disorders, particularly autoimmune thyroid disease (AITD) in Nepal (24,25). To address the problem of excessive iodine intake, proper monitoring of salt iodization is urgently needed in Nepal. Because of the diverse geography, ranging from lowland plains to high Himalayan regions, some communities still do not use iodized salt, the primary dietary iodine source in Nepal. Therefore, systematic assessment of iodine content in foods such as salted processed foods and packaged soups is essential in Nepal.

3-1-2 Iodine status in Japan

Japan is an iodine-sufficient country without need of iodine fortification (11,26). The iodine intake of the Japanese population is among the highest in the world (approximately 1–3 mg/day) (27). Seaweed is a major source of iodine in the Japanese diet, with an average daily consumption of 9.9 g (28). The Ministry of Health, Labor and Welfare of Japan recommends a daily iodine intake of 130 μg for adults, 240 μg for pregnant women, and 270 μg for lactating women. On the other hand, the tolerable upper limit (UL) of iodine intake for healthy Japanese adults is 3 mg/day, which is 3-fold higher than the WHO recommended UL of 1.1 mg/day (4,29). Healthy Japanese individuals have been shown to tolerate excess dietary iodine without exhibiting thyroid dysfunction (26). Although there is no recent nationwide study in Japan on the effects of long-term exposure to excessive iodine (>3 mg/day), only few studies have reported about iodine intake and thyroid dysfunction (30–32).

In recent years, deficiency in iodine intake has been observed in many industrialized and developed countries where sufficient iodine intake was previously established (5,33). In Japan,

the growing popularity of Westernized diets, especially among the younger generation (34,35), means that these foods may not provide sufficient iodine or may contain iodized salt, potentially leading to either inadequate or excessive iodine intake. Recent studies also reported lower dietary iodine intake among the younger age group compared to the older age group (26,34). In addition, low urinary iodine levels were detected in pregnant Japanese women (36). This might be due to changes in dietary habits among the younger generation. Therefore, population-based iodine monitoring is crucial, especially for vulnerable groups and those who tend to consume less seaweed and more Westernized foods, to control excessive and inadequate iodine intake.

3-1-3 Purpose of this study

Seafoods such as seaweed, fish, and crustaceans are the richest sources of dietary iodine. However, in countries where seafood is either unavailable or not regularly consumed, dairy products are the primary sources of iodine (37). In iodine-deficient countries like Nepal, salt iodization or iodine fortification is the only practical way to ensure adequate iodine intake.

Due to worldwide availability, milk and milk products are the major contributors of iodine globally (38). Naturally, cow's milk has a low iodine concentration, but various farming practices, such as providing cattle with iodine-enriched feed, mineral supplements, and using iodine-based disinfectants (iodophors), and sterilizing milking equipment, contribute to iodine content in milk as a result of carry-over (22,39).

As iodine content in foods varies widely, depending on soil iodine concentrations, agricultural practices, processing, and storage conditions. Even foods of the same species may show considerable differences in iodine content, and individual dietary iodine intake may fluctuate daily. To obtain a reliable iodine intake from dietary records or food diaries, the iodine content of the respective foods is necessary. It is important to know the iodine content of each food. For iodine determination, especially in food samples, a simple and inexpensive method is needed. Therefore, in the present study, I attempted to measure the iodine content of two mostly consumed foods (milk and seaweed) in Japan, which are considered good natural sources of iodine.

Additionally, although Nepal is an iodine-deficient country, there are no studies or national data about the iodine content of Nepalese foods partly because instruments to measure iodine such as ICP-MS are expensive and rarely available. Therefore, in the present method, I attempted to modify the Sandell and Kolthoff method (the S-K method) to measure iodine in

foods using inexpensive instruments and simple procedures. This approach can be performed in Nepal to help my future research in Nepal.

3-1-4 Sandell-Kolthoff method

Several analytical methods are used for iodine determination, including inductively coupled plasma-mass spectrometry (ICP-MS) (40), HPLC (41), and ion chromatography (42). All these methods use a chromatographic system and a special detector, and to obtain reliable data, sophisticated procedures are necessary (43).

The Sandell and Kolthoff (S-K) method, pioneered by Sandell and Kolthoff (44), is an inexpensive and simple colorimetric method for iodine determination. This method is based on the catalytic effect of iodide (I^-) on the reduction reaction of Ce^{4+} by As^{3+}. The S-K method is well-established for the determination of urine iodine, and it is used worldwide to monitor iodine status in population levels (45). However, this reaction is very sensitive to various kinds of compounds present in the sample matrix. In addition, non-negligible levels of iodine-independent reduction of Ce^{4+} occur. To prevent matrix effects on the S-K reaction, degradation of compounds that disturb the iodine-catalytic reaction is essential for obtaining reliable results.

To measure the iodine content in foods using the S-K method, it is crucial to find suitable procedures for each sample type not only to remove or destroy interfering substances but also to estimate the background level of iodine-independent reactions. Ammonium peroxodisulfate (APS) is non-explosive, low cost, and easy-to-use compound, and APS treatment has been shown to give similar results obtained by hazardous chloric acid treatment (45). Therefore, chloric acid digestion has been replaced by APS digestion (46). APS treatment is considered suitable for food samples with complex matrices. However, APS treatment produces a non-negligible amount of toxic waste (47). To minimize this problem and speed up the procedure, Ohashi et al. performed APS treatment using a microplate as a reaction vessel and a special sealing cassette (47). In the present study, commercial 0.5-mL safe-lock polypropylene tubes were used as the reaction vessel for APS treatment, and a sealing cassette was hand-made using cheap parts, which are on sale at local DIY shops.

3-1-5 Principle of the Sandell-Kolthoff method

In acidic aqueous solution of H_2SO_4, Ce^{4+} ion is very slowly reduced to Ce^{3+} ion by As^{3+} ion.

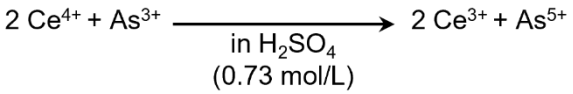

When I^- ion is present in this reaction mixture, the following catalytic cycle proceeds.

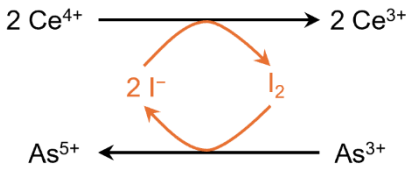

In this cycle, the reduction of I_2 molecules by As^{3+} ions to I^- ions (lower reaction in the above scheme) is very rapid. Therefore, if a large amounts of As^{3+} ions compared to iodine exist, almost all iodine is in I^- state. The reduction of Ce^{4+} ion to Ce^{3+} ion by I^- ion (upper reaction in the above scheme) is one-electron reduction process and proceeds much rapidly compared to the direct reduction of Ce^{4+} ion by As^{3+} ions.

Under the reaction conditions of $[As^{3+}] >> [Ce^{4+}] >>$ total iodine concentration, the reduction reaction of Ce^{4+} follows pseudo-first order reaction and the time-dependent change in Ce^{4+} concentration ($[Ce^{4+}]$) can be approximately expressed as the following equation.

$$\frac{d[Ce^{4+}]}{dt} = -k\,[I]_0[Ce^{4+}] \qquad (1)$$

where k is rate constant and $[I]_0$ is the total iodine concentration. By solving equation 1, the concentration of Ce^{4+} ions at time t is given by

$$[Ce^{4+}](t) = C_0\, e^{-k[I]_0 t} \qquad (2)$$

where C_0 is the initial concentration of Ce^{4+} ion. Figure 3-2 show the UV-vis absorption spectrum of Ce^{4+} ion in sulfuric acid solution (blue line in Fog. 3-2). Ce^{4+} ion exhibits broad absorption with peak at 317 nm, and the absorption band extends to longer wavelength over 450 nm, resulting in yellow color (inset in Fig. 3-2). On the other hand, Ce^{4+} ion exhibits no absorption at wavelength from 300 nm to 600 nm. In addition, both As^{3+} and As^{5+} ions also show no absorption in the same wavelength region. Therefore, Reduction reaction of Ce^{4+} ion can be continuously monitored by measuring absorbance in visible wavelength region.

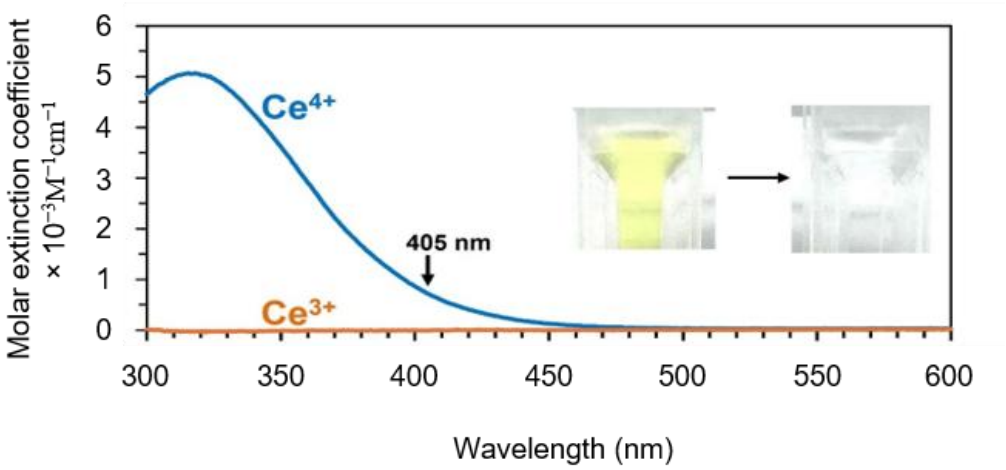

Figure 3-2. Absorption spectra of tetravalent and trivalent cerium ions in sulfuric acid solution. The inset shows the color change occurring upon the reduction of Ce^{4+} ion to Ce^{3+} ion.

In the present study, absorbance at 405 nm (A_{405}) was used to monitor the S-K reaction. Because A_{405} is proportional to [Ce^{4+}], the following relation is obtained using Equation 2.

$$A_{405}(t) = A_{405}(0)\, e^{-k[\mathrm{I}]_0 t} \tag{3}$$

By taking the logarithm of both sides of Equation 3, the following equation is obtained.

$$\ln A_{405}(t) = \ln A_{405}(0) - k[\mathrm{I}]_0 t \tag{4}$$

Using Equation 4, the pseudo-first order rate constant, $k[\mathrm{I}]_0$ was determined from the law data of $A_{405}(t)$ and used for obtaining calibration curves.

3-2 Materials and Methods

3-2-1 Reagents

Potassium iodate, ammonium cerium(IV) sulfate dihydrate, arsenic trioxide, sodium chloride, sodium hydroxide, sulfuric acid, and ammonium peroxodisulfate were purchased from Fujifilm Wako Pure Chemical Corporation (Osaka, Japan). Distilled water made from milli-Q-grade pure water was purchased from Hayashi Pure Chemical Industries (Osaka, Japan) and used as iodine-free water.

3-2-2 Materials

A total of 21 raw milk products from various regions in Japan were purchased from local supermarkets in Hyogo, Osaka, and Kyoto prefectures. Seaweeds (fresh, dried, and processed) were purchased from local supermarkets.

3-2-3 Stock solutions

(1) Arsenic acid solution (**AS solution**, 50 mmol/L As^{3+}, 428 mmol/L NaCl, 0.58 mol/L H_2SO_4)

Arsenic trioxide (2.5 g) was dissolved in 50 mL of 0.4375 mol/L sodium hydroxide solution using a magnetic stirrer. Then, in an ice bath, 8 mL of concentrated sulfuric acid was added slowly to this solution under continuous stirring. After addition of 6.25 g of sodium chloride, the mixture was diluted to 250 mL with distilled water. The diluted mixture was incubated at 60ºC under continuous stirring until the solution became clear. The clear solution was filtered using a Millex-GV filter (0.22 μm), and the filtrate was stored in a brown bottle in a dark place at room temperature.

(2) Ceric ammonium sulfate solution (**CE solution**, 19 mmol/L Ce^{4+}, 1.75 mol/L H_2SO_4)

Ammonium cerium(IV) sulfate dihydrate (3 g) was dissolved in 250 mL of 1.75 mol/L sulfuric acid. The solution was stored in a brown bottle in a dark place at room temperature.

(3) Sulfuric acid solution (1.75 mol/L)

Concentrated sulfuric acid (24.25mL) was added very slowly to about 200 mL of water in the ice bath under continuous stirring. After cooling, the solution was diluted to the final volume of 250 mL by adding distilled water.

(4) Iodine stock solution (100 mg/L iodine, 0.788 mmol/L IO_3^-)

In a 100-mL volumetric flask, 16.86 mg of potassium iodate was dissolved with about 80 mL of distilled water, and then the solution was diluted to100 mL with distilled water. The resultant solution was stored at −4°C in a brown bottle. Working iodine standard solutions were prepared by serial dilution of this stock solution just before use.

(5) Ammonium peroxodisulfate solution (APS solution, 300 mg/mL)

Ammonium peroxodisulfate (300 mg) was dissolved in 1.0 mL of distilled water. This solution was freshly prepared just before use.

3-2-4 Iodine extraction from samples

(1) Raw milk

In 1.5-mL Eppendorf tube, four volumes of methanol (800 μL) were added to 200 μL raw milk and the mixture was vigorously vortexed for 5 min, kept on ice for 20 min, and then centrifuged at 4ºC and 13,200 × g for 20 min. The clear, colorless supernatant was weighed, and aliquoted into 1.5-mL tubes, 100 μL each, and each was evaporated to dryness using a centrifugal evaporator (CVE-1000, EYELA, Tokyo, Japan) equipped with a liquid-nitrogen trap under reduced pressure. The dried samples were stored at −80ºC until analysis. Just before analysis, each tube was dissolved with 100 μL of distilled water.

(2) Seaweed samples

Seaweeds were frozen in liquid nitrogen, and the frozen sample was immediately crushed into fine powders using a blender. Then the powder (1−10 g) was weighed and dissolved in appropriate amount of distilled water: raw seaweed, 10 volumes; processed seaweed, from 5 to 10 volumes; dried seaweed, from 10 to 3000 volumes. Dilution ratios were adjusted based on the solution viscosity and the iodine levels in the samples. The mixtures were continuously stirred at 4ºC for 2 h and then centrifuged at 6610 ×g for 20 min. The supernatant was collected, measured, filtered through gauze bandage, and stored at −80ºC until analysis.

Liquid samples, such as ponzu, tsuyu, and different varieties of soy sauce (shoyu) were directly diluted with water.

3-2-5 Preparation of iodine working solution

An aliquot of iodine stock solution (100 mg/L iodine) was first 100-fold diluted with distilled water to obtain 1.00 mg/L iodine solution. as follows. First, pipette 1.00 mL of distilled water into a 1.5-mL Eppendorf tube and discard 10.0 μL from the tube. Then, 10.0 μL of 100 mg/L iodine solution was added to the tube, and mixed thoroughly by vortexing, resulting in 1.00 mg/L iodine solution. Then, this iodine solution was stepwise diluted to obtain 500, 250, 125, 62.5, 31.3, and 15.6 μg/L iodine solutions. All the working solutions were freshly prepared before each analysis.

3-2-5 Standard addition

In the present study, to obtain calibration curve under the background of sample matrices (sample calibration curve), the standard addition method was applied. Sample was 25 μL aliquoted into six 0.5-mL safe-lock tubes labeled S0 to S5. To S0 tube, 25 μL of distilled water

(0 ng iodine) was added. To S1 tube, 25 μL of 15.6 μg/L iodine solution (0.39 ng iodine) was added. To S2 tube, 25 μL of 31.3 μg/L iodine solution (0.783 ng iodine) was added. To S3 tube, 25 μL of 62.5 μg/L iodine solution (1.56 ng iodine) was added. To S4 tube, 25 μL of 125 μg/L iodine solution (3.13 ng iodine) was added. To S5 tube, 25 μL of 250 μg/L iodine solution (6.25 ng iodine) was added. All the mixtures were subjected to APS treatment.

To judge the presence and absence of the matrix effect on the S-K reaction, the same series of S0–S5 samples were prepared using 25 μL distilled water instead of sample solution, and were treated simultaneously with the standard-added sample series to obtain calibration curve without disturbance by sample matrix (water-control calibration curve).

3-2-6 APS treatment

To degrade organic substance containing iodine to release free iodine, and to degrade those disturbing the S-K reaction such as ascorbic acid, strong reducing agent, oxalate and citric acid, potent metal chelator, it is inevitable to perform APS treatment. The iodine standard added samples were treated with APS as follows.

APS solution (about 300 mg/mL) was prepared just before use by dissolving solid APS in distilled water. A 100-μL aliquot of APS solution was added to each tube containing 50 μL sample solution, a final volume of 150 μL. The tubes were securely capped, vortexed, and centrifuged using a tabletop centrifuge for a few seconds. The tubes were then placed in a home-made tube holder (Fig. 3-3) to press the tube during incubation to keep the tube tightly closed, and the cassette was set in a high-temperature chamber (ST-110, ESPEC) at 110°C for 1 h. After incubation, the cassette was removed from the heating chamber, and the samples were allowed to cool to room temperature. The cooled samples were vortex, briefly centrifuged, and placed in a refrigerated circulating bath (NESLAB, RTE-9) maintained at 25ºC.

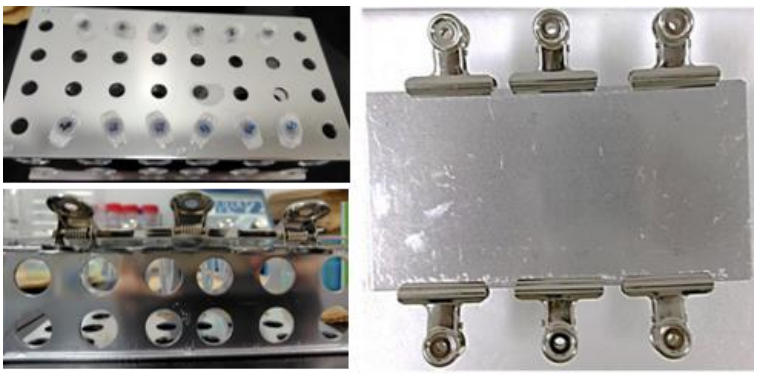

Figure 3-3. Home-made tube holder to prevent the tube lid from opening during incubation at 110ºC.

3-2-7 Measurement of the S-K reaction

The S-K reaction was performed in a semi-micro quartz cell as follows. An aliquot of each APS-treated sample (50 μL) was transferred into a 1.5-mL Eppendorf tube and mixed with 100 μL of AS solution. To this mixture, 50 μL of CE solution was added. After mixing using pipet, the mixture was immediately transferred into the cell, and the absorbance at 405 nm (A_{405}) was continuously recorded using a Shimadzu UV-Vis spectrophotometer (UV2550). The temperature of the cell was controlled at 25ºC using a cell holder in which 25ºC water was circulated by a refrigerated circulating bath (NESLAB, RTE-9) (Fig. 3-4).

After each analysis, the cell was washed at least three times with tap water, followed by distilled water to minimize cross-contamination, and dried completely by spraying nitrogen gas. S0 samples were measured twice for each analysis to evaluate reproducibility. Each raw data was transferred to Excel and further analyzed using in-house programs written in Visual Basic for Applications (Microsoft).

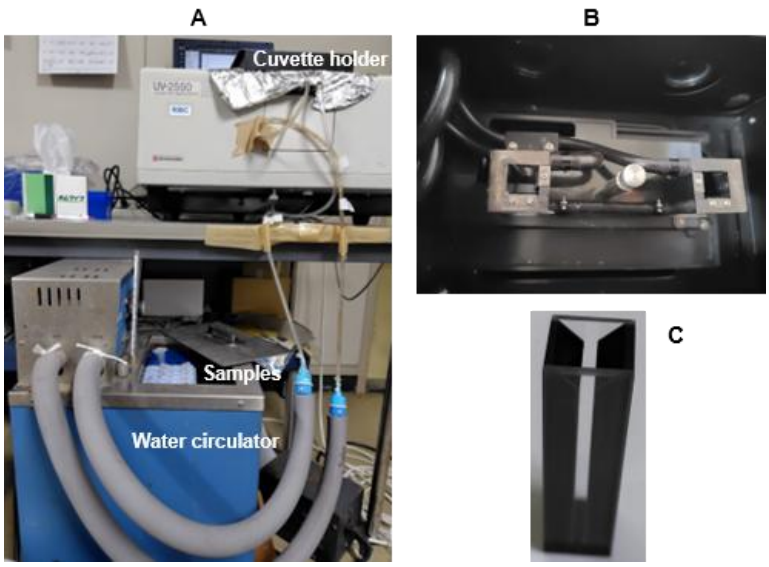

Figure 3-4. Refrigerated circulating bath (A), thermostatic cell holder (B), semi-micro quartz cell (C).

3-3 Results

3-3-1 Calibration curves

Figure 3-5 shows typical calibration curves obtained for raw milk samples.

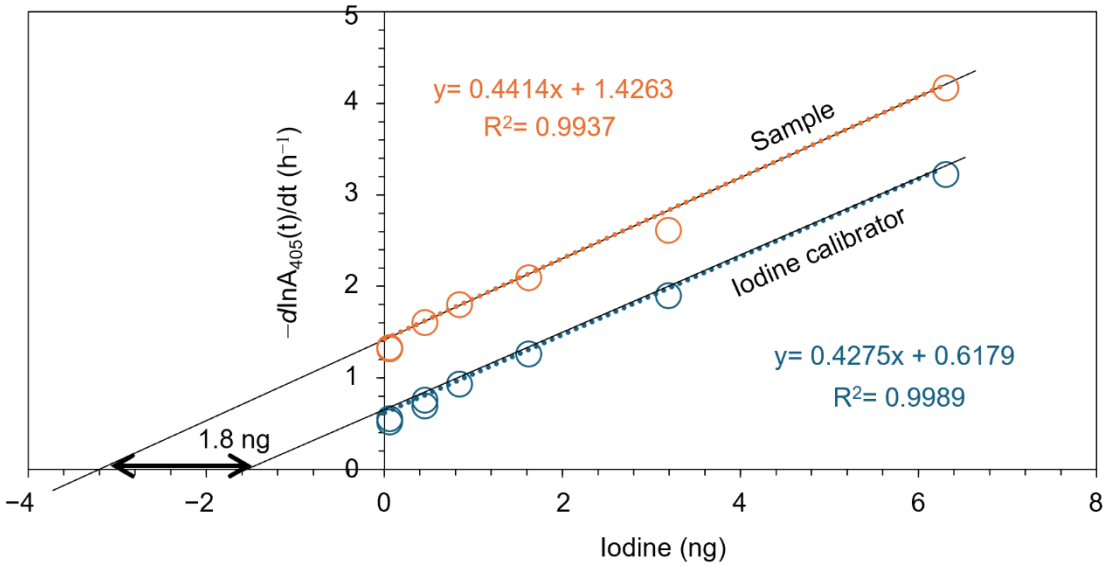

Figure 3-5. Typical calibration curve obtained for a milk sample (Meg milk, snow brand). ln $A_{405}(t)$ versus t plot was linear after the temperature equilibrium established, and from the slope of the plot $k[I]_0$ was obtained (Equation 4). The $k[I]_0$ value was plotted against the added amounts of iodine. The difference in the x-axis intercept between sample calibration curve (orange) and water calibration curve (blue) is equal to the amount of iodine present in 25 μL of milk sample, in this case 1.8 ng.

Both sample calibration curve and water calibration curve showed excellent linearity, and the slope of the calibration curves are nearly identical, indicating that there are no substantial levels of matrix effects. Therefore, in this case, the amount of iodine extracted from raw milk was obtained as the difference in the x-axis intercept between the two calibration curves.

Figure 3-6 shows typical calibration curves obtained for dry seaweed sample. In this case, iodine was extracted from the seaweed into distilled water. Both ample calibration curve and water calibration curve are linear, and the slope is nearly identical, indicating that S-K reaction disturbing substances were not extracted into water from the dried arame. From the difference in x-axis intercepts, the iodine content was determined to be 2.19 ng. in the sample.

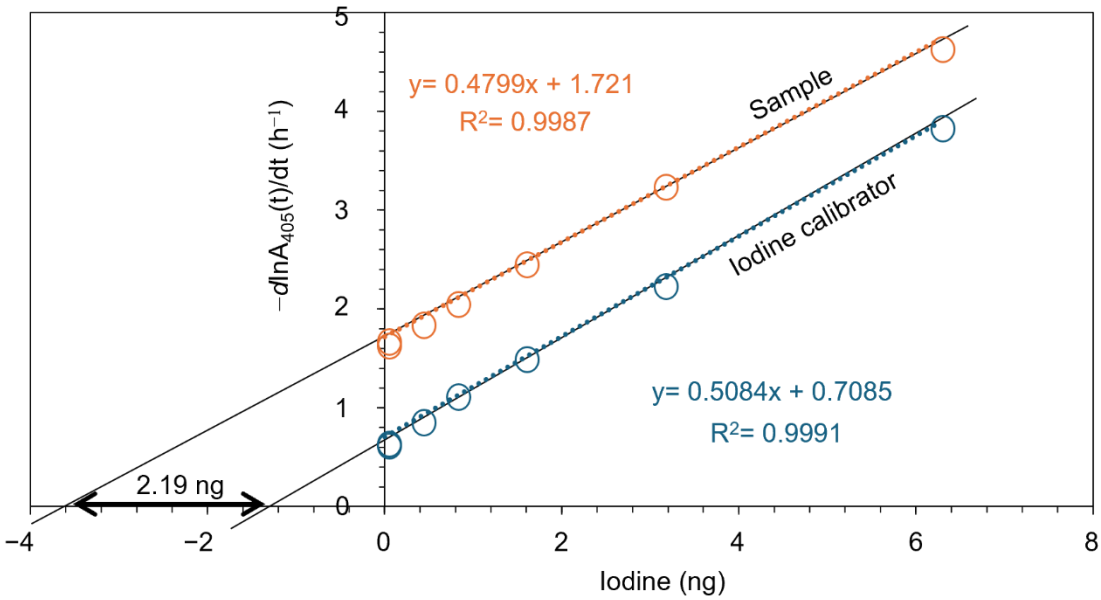

Figure 3-6. Typical calibration curve of 100-fold diluted water extract from kizami Arame sample.

3-3-2 Reproducibility of the present method

To examine inter-day variability, iodine content of the same sample was analyzed at least 10 times on different days. Figure 3-7 shows a typical result obtained for the methanol extracts from Meg milk. In this case, the coefficient of variation (CV) was calculated to be 8.7%.

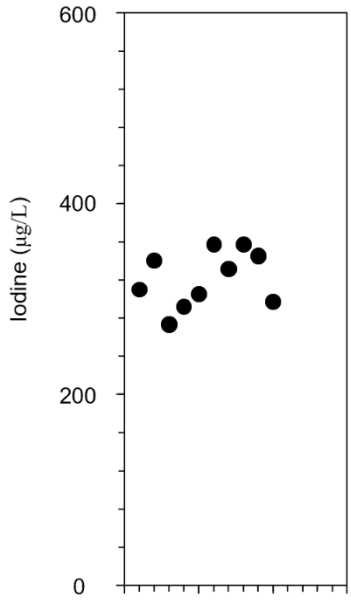

Figure 3-7. Inter-day variability in iodine concentration determined for the same milk sample**.**

Inter-day CV values for raw milk samples were in the range from 4.5 to 10%, indicating that the present method to measure iodine content of raw milk has satisfactory precision.

3-3-3 Some processed foods contain the S-K reaction disturbing substances difficult to remove

In the S-K method, it is essential that sample calibration curve has the slope identical with that of water calibration curve. If the slope of these two calibration curves differs, it is impossible to estimate the iodine-independent reaction rate for the sample solution. When the slope is same between the calibration curves, then the iodine-independent reaction rate for the sample solution can be estimated to be identical to that observed for distilled water.

Various compounds such as ascorbic acid, potassium thiocyanate, ferrous ammonium sulfate, and zinc are known to interfere with the S-K reaction (47). Figure 3-8 shows the calibration curve obtained for processed milk drinks. Although the sample calibration curve had good linearity, the slope of the curve was one third of that of water calibration curve, indicating the presence of substances that interfere with the S-K reaction.

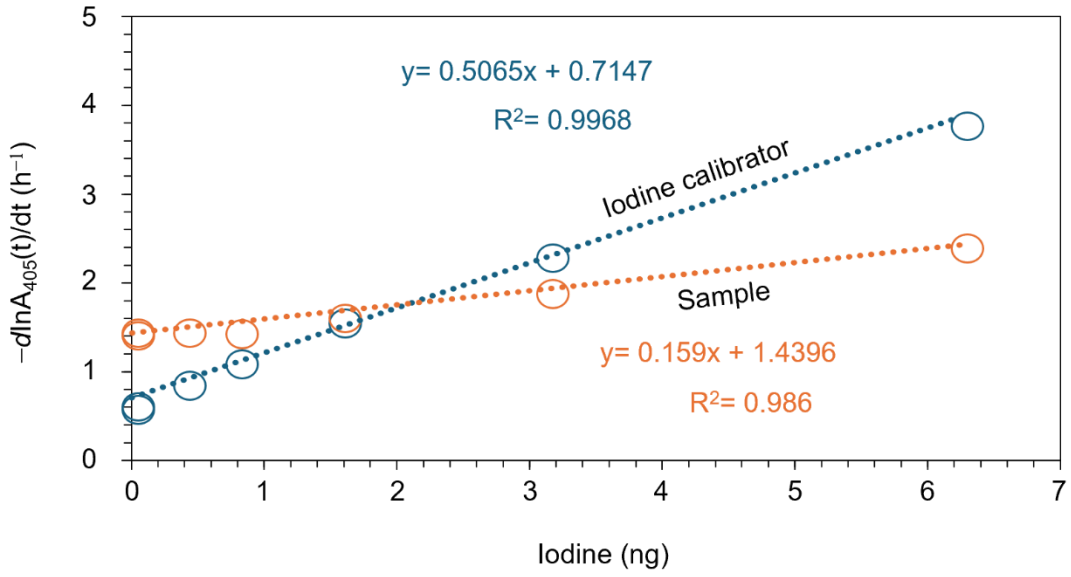

Figure 3-8. Calibration curve obtained for a processed milk drink.

As various kinds of ingredients including emulsifiers are added into processed milk drinks, iodine extracts from the milk drinks were further subjected to MonoSpin C18 (hydrophobic

extraction), MonoSpin SAX (strong cation exchanger), and MonoSpin NH2 (hydrophilic extraction). However, after these treatments, the slow of the sample calibration curve was much smaller compared to the water calibration curve, indicating that some substances still remained to disturb the S-K reaction.

In the case of processed or seaweed-extract products such as nori tsukudani, aosa nori tsukudani, kombu-dashi (Japanese soup stock made from kelp), and soy sauce (soy sauce that contains kelp extract), iodine extracts from these food products by distilled water contained substances that strongly interfere with the S-K reaction. Figure 3-9 shows the calibration curve obtained for nori tsukudani.

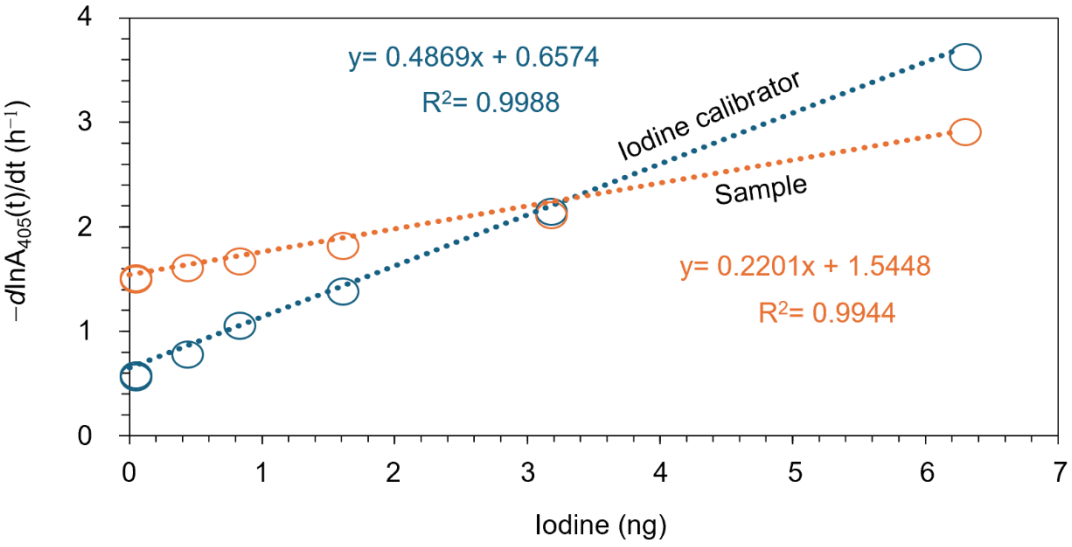

Figure 3-9. Calibration curve obtained for a nori tsukudani.

As in the case of processed milk drinks, the sample calibration curve was linear, but the slope was about half of that of the water calibration curve. I tried various methods to prevent interference: further dilution with distilled water; cleanup using solid-phase extraction using MonoSpin; extraction with ethanol, methanol, and acetonitrile. However, at present, it was not succeeded to obtain sample calibration curve parallel with the water calibration curve.

3-3-4 Iodine content in raw milk products

In the present study, iodine contents in 21 milk products from different varieties were successfully determined. The results are summarized in Table 3-1.

Table 3-1. Iodine content in milk products produced in various regions of Japan.

Trade name	Source	ID	Mean (μg/L)	SD	CV (%)
Megmilk snow brand	Sapporo	QC	321	28	8.7
Morinaga milk	Kobe	A	219	10	4.6
Meiji whole milk	Tokyo	B	166	9	5.4
A_2 farm milk	Kanazawa	C	186	17	9.1
Koiwai farm milk	Maruyachi, Iwate	D	148	15	10.0
Awajishima milk	Awajishima	E	195	14	7.2
A_2 Hiruzen Jersey	Maniwa, Okayama	F	321	27	8.4
JA kyoto	Natan, Kyoto	G	349	33	9.5
Meiji whole milk	Asahikawa, Hokkaido	H	130	7	5.4
Takanashi organic milk	Iwakura, Kanagawa	I	237	19	8.0
Sarobetsu milk	Toyotomi-cho, Hokkaido	J	194	14	7.2
Yotsuba milk	Tokachi, Hokkaido	K	203	15	7.4
Unadjusted milk	Ono city, Hyogo	L	201	9	4.5
Family mart milk	Ohayo dairy, Okayama	M	178	16	9.0
Unadjusted milk	Kanazawa	N	140	11	7.9
Dairy milk	Sakai city, Osaka	O	264	17	6.4
Kyoto agricultural	Furusato, Kyoto	P	217	17	7.8
Milk for bread	Sakai city, Osaka	Q	193	9	4.7
White rose milk-non-fat	Kotoura, Tottori	R	306	14	4.6
Mellow Pasteurized milk	Nankoku, Kochi	S	229	16	7.0
Kitsugi Pasteurized milk	Unnan city, Shimane	T	231	11	4.8

Source: Manufacturing location of the milk. ID: milk code. SD: standard deviation. CV (%): coefficient of variation in percentage.

The iodine content in milk samples varied from 130 μg/L to 349 μg/L. The mean iodine content was 220 ± 60 μg/L. According to the Japanese Food Composition Table (2024), regular raw milk contains 160 μg/kg milk, which is comparable to the value obtained in the present results. The present mean value of milk iodine content is also similar to that observed for whole pasteurized milk in the UK (230 μg/kg milk) (48), where milk is one of the major dietary source

of iodine. In the USA, milk has been reported to show large variation in iodine content, with an average iodine concentration of 340 µg/kg milk (49), which is slightly higher compared to those of Japan and UK. A meta-analysis reported that milk iodine concentrations around the world ranged from 55 to 499 µg/kg milk, high variability in iodine content of milk globally (50).

Although milk is widely consumed across all age groups, its iodine content is not routinely declared on food product labels, unlike other micronutrients. This lack of information creates uncertainty regarding the actual dietary intake of iodine from milk and dairy products. Therefore, it is recommended that the iodine content of milk and milk products be mandatorily included on the food product label.

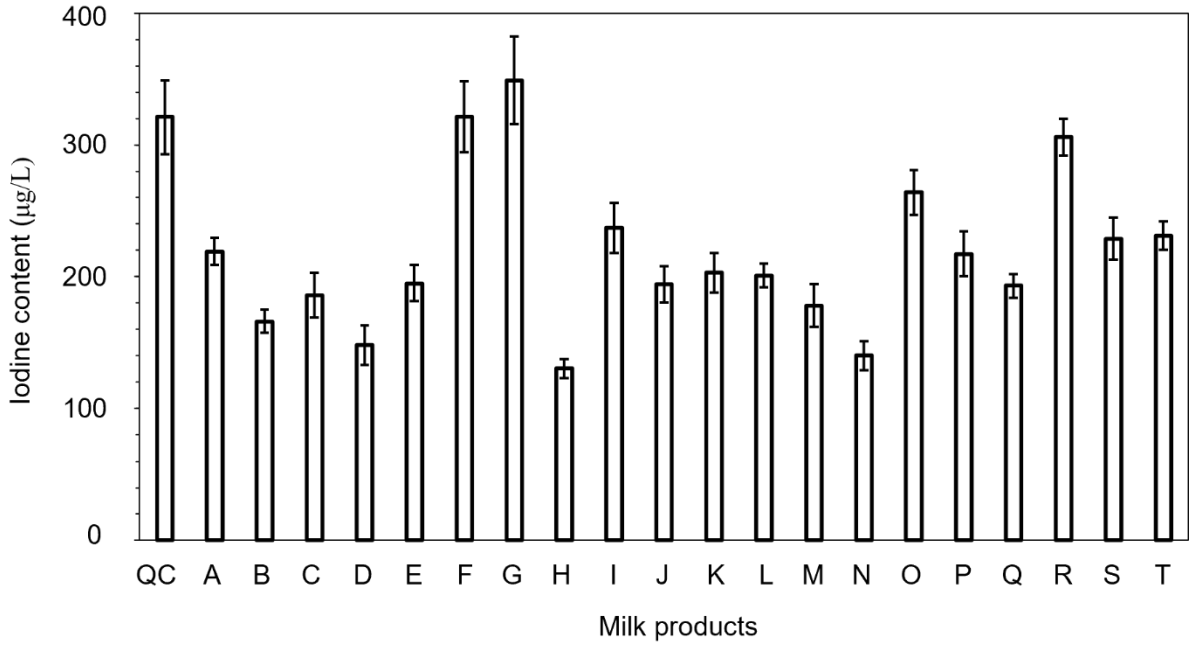

Figure 3-10. Iodine content in the milk samples. QC denotes quality control milk samples, and other alphabet A−T in the x-axis denotes the milk samples from various brands as shown in Table 3-1.. JA Kyoto milk (G) from Natan Kyoto contained the highest amounts of iodine (349 µg/L) among all the 21 milk samples and Meiji whole milk (H) from Asahikawa, Hokkaido, contained the lowest (130 µg/L) levels of iodine. The mean iodine content was 220 ± 60 µg/L.

3-3-4 Iodine content in seaweed

In the present study, iodine content of various seaweed products was determined. The results are summarized in Table 3-2.

Table 3-2. Iodine content in seaweed from various regions in Japan.

Name	Source	Mean	SD	CV (%)
Fresh seaweed (wet weight)		μg/100 g		
Hijiki	Ehime	316	26	8.2
Aosa	Matsusaka, Mie	135.4	5.1	3.8
Wakame	Osaka Bay	42.6	3.3	7.7
Mozuku	Okinawa	22.5	1.0	4.4
Dried seaweed (dry weight)		mg/100 g		
Kizami kombu	Hokkaido	210	10	4.8
Oboro kombu	Hokkaido	139.8	6.4	4.6
Furikake kombu	Himeji, Hyogo	128.2	15.7	12.2
Hijiki	Mie-gun, Mie	68.6	5.9	8.6
Kobucha	Southern Hokkaido	23.3	1.6	6.7
Kizami Arame	Ise city, Mie	5.79	0.24	4.1
Wakame	Ofunato city, Iwate	0.55	0.02	3.6
Kizami nori (A)	Ariake sea, Chiba	0.83	0.01	12
Kizami nori (B)	Chiba	0.33	0.02	6.1
Others		mg/100 g or mL		
Kombu dashi	Hokkaido	48.8	0.1	0.2
Dashi shoyu (A)	Hiroshima	27.92	0.86	3.1
Goma kombu	Hokkaido	23.98	0.02	0.08
Ponzu	Chiba	4.32	0.14	3.2
Tsuyu	Chiba	2.93	0.14	4.8
Dashi shoyu (B)	Hokkaido	1.44	0.06	4.2

Mean values are expressed in μg/100 g, mg/100 g or mL. SD: standard deviation. CV (%): coefficient of variation in percentage.

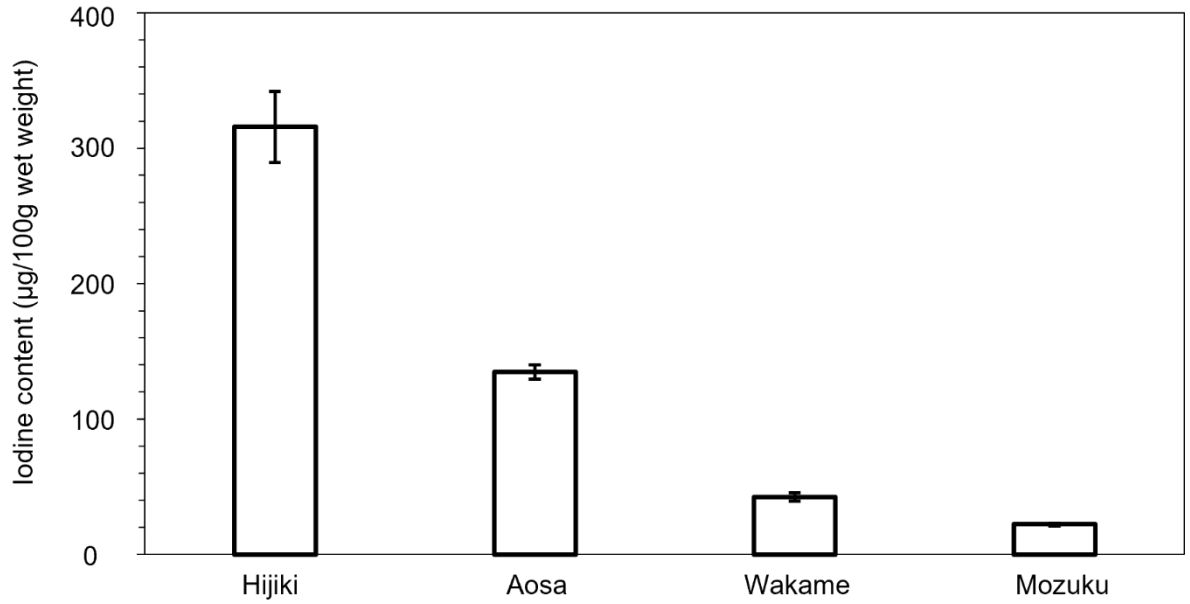

Figure 3-11. Iodine content in fresh seaweed.

Iodine contents of four most popular fresh seaweeds, hijiki, aosa, wakame, and mozuku, were determined (Fig. 3-11). Hijiki (*Hiziki*) contained 316 ± 26 μg/100 g wet weight, aosa (*Ulva* spp.) 135 ± 5 μg/100 g wet weight, wakame (Undaria pinnatifida) 42.6 ± 3.3 μg/100 g wet weight, and mozuku (Okinawan mozuku) 22.5 ± 1.0 μg/100 g wet weight.

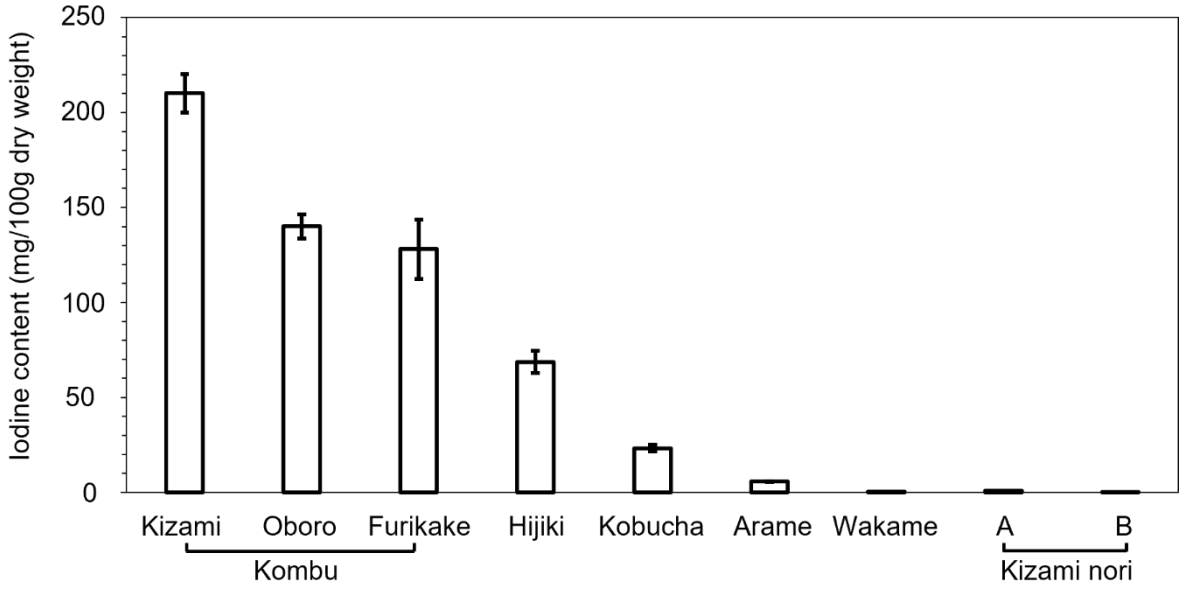

Figure 3-12. Iodine content in dried seaweed.

Figure 3-12 shows the iodine content in dried seaweed. Among the kombu (*Saccharina* spp.) varieties, dried kizami kombu contained the highest iodine content of 210 ± 10 mg/100 g dry weight, whereas kizami nori (*Pyropia* spp.) contained the lowest amount of iodine, 0.33 ± 0.02 mg/100 g dry weight.

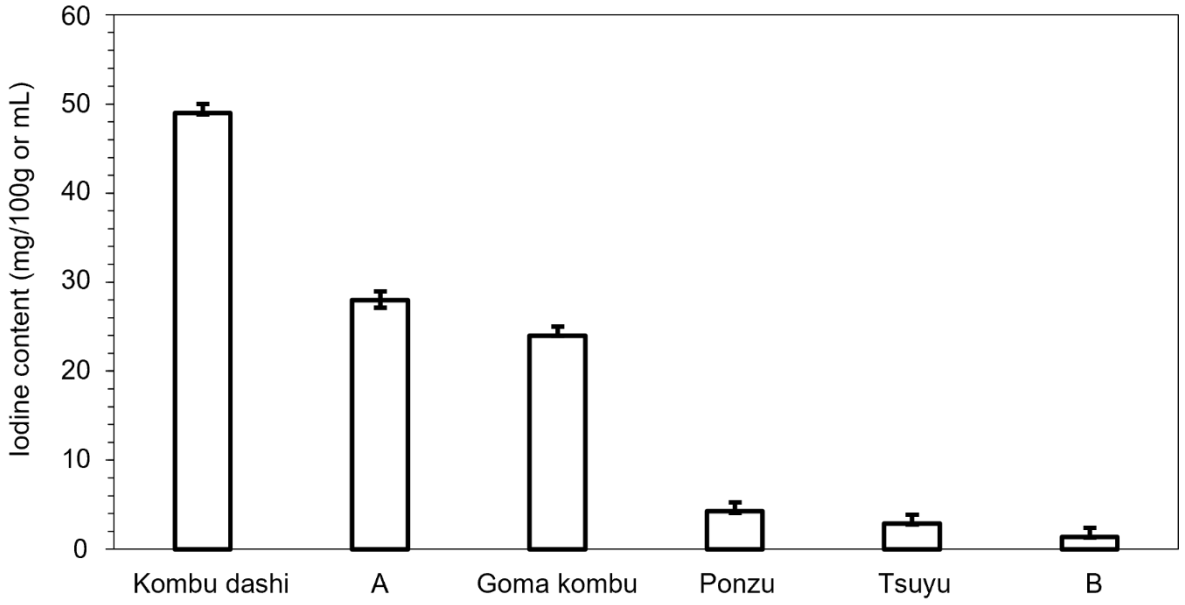

Figure 3-13. Iodine content in seaweed products.

Kelp-extracted products such as kombu dashi, dashi shoyu, ponzu, and tsuyu also contain significant amounts of iodine (Fig. 3-13).

3-4 Discussion

The present study has revealed that very large variation in iodine contents exists in the seaweed products consumed by Japanese individuals. A study conducted by Tsubota-Utsugi et al. reported that iodine intake among the participants exceeded the tolerable upper intake level intermittently (approximately once a week) rather than continuously (51). Low bioavailability of iodine from seaweed compared to iodine supplements (> 90%) (52), iodine losses that occur during cooking and preparation processes, as most iodine values for seaweed are calculated from raw weight (53). Furthermore, many Japanese dishes commonly combine seaweed with soy-based foods such as soy sauce, natto (fermented soybeans), tofu, miso (fermented soybean paste), which may interfere with iodine absorption, as soy products are considered goitrogenic

foods (54). These factors may contribute to the relatively lower incidence of health effects caused by high iodine intake in Japan compared to other developed countries.

Furthermore, seaweeds are not only rich in iodine but are also low in calories and packed with various nutrients such as dietary fibers, minerals, vitamins, bioactive compounds, peptides, and carotenoids (72). Because of these health benefits, the popularity of seaweed has expanded to many Western countries as well (53,55–57).

Although protein precipitation of milk samples by adding four volumes of MeOH, able to successfully reduce the sample matrix in regular milk. While milk drinks were unable to be analyzed by a similar procedure. The presence of emulsifiers and other ingredients in milk drinks might play an interfering role. Only precipitating with MeOH was not sufficient to reduce these interfering compounds.

Similarly, the iodine content of processed seaweed or kelp extract (dashi) such as nori tsukudani, aosa nori tsukudani, kombu-dashi (Japanese soup stock made from kelp), and soy sauce (soy sauce that contains kelp extract) could not be measured by the present method. Different separation columns, such as MonoSpin reversed phase column C18, ion exchange column SAX, HILIC NH2 column, were used to interfere with substances, but did not work. Likewise, the added ingredients present in the samples were checked for potential interfering compounds. Among the added ingredients tested, no matrix effects were observed for glucose, sucrose, oligosaccharides, and bonito flakes; however, a nonlinear curve was observed for mirin, which was present in the dashi samples. From the obtained result, it is conformed that additional ingredients present in the processed samples interfered with the sample matrix. Therefore, the present method is not suitable for samples that contain various added ingredients, such as an emulsifier or thickening agents.

In conclusion, milk and seaweed samples with minimal added chemical compounds are suitable by the present method and obtained results are reliable to the Japanese Food Composition Table. For the samples which contain additional substances, other cleanup and sample processing methods needed to remove the interfering compounds.

References

1. Arczewska K. D, and Piekielko-Witkowska A. (2025) The Influence of Micronutrients and Environmental Factors on Thyroid DNA Integrity. *Nutrients.*17:2065.
2. Luo Y., Kawashima A., Ishido Y., Yoshihara A., Oda K., Hiroi N., Ito T., Ishii N., and Suzuki K. (2014) odine excess as an environmental risk factor for autoimmune thyroid

disease. *Int J Mol Sci.* 15, 12895–12912.
3. Brent G. A. (2012) Mechanisms of thyroid hormone action. *J Clin Invest*. 122, 3035-3043.
4. Dietary Reference Intakes for Vitamin A, Vitamin K, Arsenic, Boron, Chromium, Copper, Iodine, Iron, Manganese, Molybdenum, Nickel, Silicon, Vanadium, and Zinc. (2000) Institute. of Medicine (US) Panel of Micronutrients, National Academies Press
5. Hatch-McChesney A., and Lieberman H. R. (2022) Iodine and iodine deficiency: a comprehensive review of a re-emerging issue. *Nutrients.* 14:3473
6. Watanabe N. (2025) A narrative review of long-term inorganic iodine monotherapy for Graves' disease with a historical relationship between iodine and thyroid. *Endocrinol. J.* 72, 23–36
7. Sorrenti S., Baldini E., Pironi D., Lauro A., D'Orazi V., Tartaglia F., Tripodi D., Lori E., Gagliardi F., Ptraticò M., Illuminati G., D'Andrea V., Palumbo P., and Ulisse S. (2021) Iodine: its role in thyroid hormone biosynthesis and beyond. *Nutrients*. 13:4469
8. WHO. Guideline: fortification of food-grade salt with iodine for the prevention and control of iodine deficiency disorders. (2014)
9. UNICEF Data: Monitoring the situation of children and women. (2023)
10. WHO, UNICEF, ICCIDD. Assessment of iodine deficiency disorders and monitoring their elimination: a guide for program managers. (2007)
11. Network IG. Global scorecard of iodine nutrition 2025 (2025)
12. Patriota E. S. O, Lima I. C. C., Nilson E. A. F., Franceschini S. C. C., Goncalves V. S. S., and Pizato N. (2022) Prevalence of insufficient iodine intake in pregnancy worldwide: a systematic review and meta-analysis. *Eur J Clin Nutr.* 76, 703–715.
13. Zimmermann M. B. (2023) The remarkable impact of iodisation programs on global public health. *Proc Nutr Soc*. 82, 113-119
14. Du Y., Liu P., Zhang W., Yao J., Meng F., Fan L., Liu L., Li, M., Lv C., Jiang W., and Sun D. (2023). Serum thyroglobulin as a biomarker of iodine excess and thyroid disease occurrence in adults. *J Trace Elem Med Biol.* 78:127172.
15. Network IG. Status of the Iodine Nutrition and Salt Iodization Program in Nepal Country Brief. 2023 (2023)
16. Population MoHa. Nepal DHS Summary Report. Kathamndu, Nepal; 2022. (2022)
17. Giri B., Pandey S., Shakya S., Neupane B. B., Kandel K. P., Yadav C .K., Neupane B. P., Rajendra Bahadur G. C., Saud P. S., and Yonjan M. (2022) Excessive iodine in iodized household salt in Nepal. *Ann N Y Acad Sci*. 1514, 166–173
18. Paudyal N., Chitekwe S., Rijal S., Parajuli K., Pandav C., Maharjan M., Houston R., and Gorstein J. (2022) The evolution, progress, and future direction of Nepal's universal salt iodization program. *Matern Child Nutr*. 18 (S1):e12945.

19. Population MoHa, ERA N, UNICEF, EU, USAID, CDC. Nepal National Micronutrient Status Survey, 2016. Kathmandu, Nepal; 2018.
20. Tamang M. K., Gelal B., Tamang B., Lamsal M., Brodie D., and Baral N. (2019) Excess urinary iodine concentration and thyroid dysfunction among school age children of eastern Nepal: a matter of concern. *BMC Res Notes*. 12:294.
21. Heydon E. E., Thomson C. D., Mann J., Williams S. M., Skeaff S. A., Sherpa K. T., and Heydon J. L. (2009) Iodine status in a Sherpa community in a village of the Khumbu region of Nepal. *Public Health Nutrition*. 12, 1431-1436.
22. Farebrother J., Zimmermann M. B., Andersson M. (2019) Excess iodine intake: sources, assessment, and effects on thyroid function. *Ann N Y Acad Sci.* 1446, 44-65.
23. Teti C., Panciroli M., Nazzari E., Pesce G., Mariotti S., Olivieri A., and Bagnasco M. (2021) Iodoprophylaxis and thyroid autoimmunity: an update. *Immunol Res*. 69, 129–138.
24. Joshi A., and Yonzon P. (2018) Community based study of thyroid disorder prevalence in *Nepal Endocrine Abstracts*. 63:776.
25. Lamichhane S., Acharya S. K., and Lamichhane P. (2022) Iodine deficiency and thyroid dysfunction: current scenario in Nepal. *Ann. Med. Surg. (Lond)* 82:104673
26. Fuse Y., Tsukada N., Urakawa Y., Yokoyama J., Matsuzaki M., Shishiba Y., and Irie M. (2022) Studies on urinary excretion and variability of dietary iodine in healthy Japanese adults. *Endocr. J.* 69, 427-440
27. Zava T. T., and Zava D. T. (2011) Assessment of Japanese iodine intake based on seaweed consumption in Japan: a literature-based analysis. *Thyroid. Res*. 4:14.
28. Kishida R., Yamagishi K., Muraki I., Sata M., Tamakoshi A., and Iso H. (2020) Frequency of seaweed intake and its association with cardiovascular disease mortality: the JACC study. *J. Atheroscler. Thromb*. 27, 1340–1347
29. Ministry of Health LaW. Dietary reference intakes for Japanese (2020)
30. Unosawa K., Aita T., and Hamaguchi S. (2024) Hypothyroidism due to seaweed overconsumption. *Cureus* 16:e55231.
31. Michikawa T., Inoue M., Shimazu T., Sawada N., Iwasaki M., Sasazuki S., Yamaji T., Tsugane S. (2012) Seaweed consumption and the risk of thyroid cancer in women: the Japan Public Health Center-based Prospective Study. *Eur. J. Cancer Prev*. 21, 254–260.
32. Akamizu T., Nakamura Y., Tamaoki A., Inaba Y., Amino N., and Seino Y. (2003) Prevalence and clinico-epidemiology of familial Graves' disease in Japan based on nationwide epidemiologic survey in 2001. *Endocr. J.* 50, 429–436.
33. GOV.UK. National Diet and Nutrition Survey 2019 to 2023: report. 2025
34. Katagiri R., Asakura K., Uechi K., Masayasu S., and Sasaki S. (2015) Adequacy of iodine intake in three different Japanese adult dietary patterns: a nationwide study. *Nutr. J.* 14:129
35. Murakami K., Livingstone M. B. E., and Sasaki S. (2018) Thirteen-Year Trends in Dietary Patterns among Japanese Adults in the National Health and Nutrition Survey 2003(-)2015:

continuous Westernization of the Japanese diet. *Nutrients*. 10:994.
36. Hisada A., Takatani R., Yamamoto M., Nakaoka H., Sakurai K., Mori C., and JECS group. (2022) Maternal iodine intake and neurodevelopment of offspring: the Japan Environment and Children's Study. *Nutrients.* 14:1826.
37. Smyth P. P. A. (2021) Iodine, seaweed, and the thyroid. *Eur. Thyroid J*. 10, 101–108.
38. van der Reijden O. L., Zimmermann M. B., and Galetti V. (2017) Iodine in dairy milk: sources, concentrations and importance to human health. *Best Pract .Res. Clin. Endocrinol. Metab*. 31, 385–395.
39. Nicol K., Nugent A. P., Woodside J. V., Hart K. H., and Bath S. C. (2024) The impact of replacing milk with plant-based alternatives on iodine intake: a dietary modelling study. *Eur. J. Nutr.* 63, 599–611
40. Fecher P. A., Goldmann I., and Nagengast A. (1988) Determination of iodine in food samples by inductively coupled plasma mass spectrometry after alkaline extraction. *J. Anal. At. Spectrom.* 13, 977–982.
41. Nitschke U., and Stengel D. B. (2015) A new HPLC method for the detection of iodine applied to natural samples of edible seaweeds and commercial seaweed food products. *Food Chem.* 172, 326–334
42. Bichsel Y., and von Gunten U. (1999) Determination of iodide and iodate by ion chromatography with postcolumn reaction and UV/Visible detection. *Anal. Chem*. 71, 34–38.
43. Srivorakul T., Varanusupakul P., and Alahmad W. (2020) Development of a sample treatment method for a flow injection determination of iodine in eggs: a comparison study. *Anal. Sci.* 36, 491–495
44. Sandell E. B., and Kolthoff I. M. (19134) Chronometric catalytic method for the determination of micro-quantities of iodine. *J. Am. Chem. Soc*. 56, 1426.
45. Jooste P. L., and Strydom E. (2010) Methods for determination of iodine in urine and salt. *Best Pract. Res. Clin. Endocrinol. Meta*b. 24, 77–88.
46. Pino S., Fang S. L., and Braverman L. E. (1998) Ammonium persulfate: a new and safe method for measuring urinary iodine by ammonium persulfate oxidation. *Exp. Clin. Endocrinol. Diabetes.* 106, S22-S27.
47. Ohashi T., Yamaki M., Pandav C. S., Karmarkar M. G., and Irie M. (2000) Simple microplate method for determination of urinary iodine. *Clin. Chem*. 46, 529−536
48. GOV.UK. Nutrient analysis of cows' milk: sampling and analytical report 2025
49. Roseland J. M., Phillips K. M., Vinyard B. T., Todorov T., Ershow A. G., and Pehrsson P. R. (2023) Large Iodine Variability in Retail Cows' Milk in the U.S.: A Follow-Up Study among Different Retail Outlets. *Nutrients* 15:3077
50. Tattersall J. K., Peiris M. S., Arai M., McCully K., Pearce N., Rayman M. P., Stergiadis S., and Bath S. C. (2024) Variation in milk-iodine concentration around the world: a systematic

review and meta-analysis of the difference between season and dairy-production system. *Food Chem*. 459:140388.

51. Tsubota-Utsugi M., Imai E., Nakade M., Matsumoto T., Tsuboyama-Kasaoka N., Nishi N., and Tsubono Y. (2013) Evaluation of the prevalence of iodine intakes above the tolerable upper intake level from four 3-day dietary records in a Japanese population. *J. Nutr. Sci. Vitaminol. (Tokyo)*. 59, 310-316.
52. Aquaron R., Delange F., Marchal P., Lognone V., and Ninane L. (2002) Bioavailability of seaweed iodine in human beings. *Cell Mol. Biol. (Noisy-le-grand)*. 48, 563–569
53. Blikra M. J., Henjum S., and Aakre I. (2022) Iodine from brown algae in human nutrition, with an emphasis on bioaccessibility, bioavailability, chemistry, and effects of processing: A systematic review. *Comp.r Rev. Food Sc.i Food Saf.* 21,1517–1536
54. Yoshida M., Mukama A., Hosomi R., and Fukunaga K. (2017) Soybean Meal Reduces Tissue Iodine Concentration in Rats Administered Kombu. *Biochem. Res. on Trace Elem*. 28, 28–34.
55. Young M., Paul N., Birch D., and Swanepoel L. (2022) Factors Influencing the Consumption of Seaweed amongst Young Adults. *Foods* 11:3052
56. Palmieri N., and Forleo M. (2020) The potential of edible seaweed within the western diet. A segmentation of Italian consumers. *Int. J. Gastron. Food Sci.* 20:100202.
57. Vellinga R. E., Sam M., Verhagen H., Jakobsen L. S., Ravn-Haren G., Sugimoto M., Torres D., Katagiri R., Thu B. J., Granby K., Hoekstra J., and Temme E. H. M. (2021) Increasing Seaweed Consumption in the Netherlands and Portugal and the Consequences for the Intake of Iodine, Sodium, and Exposure to Chemical Contaminants: A Risk-Benefit Study. *Front Nutr*. 8:792923.

Chapter IV

Effects of long-term intake of moderate excess iodine on major metabolism and cognitive function of mice

4-1 Introduction

In nature, iodine is found in several forms, generally classified as organic and inorganic. Iodide (I^-) is the most common inorganic form of iodine, followed by iodate (IO_3^-) (1). Iodized salt or iodine-fortified foods contain iodine in the form of potassium iodide (KI^-) or potassium iodate (KIO_3^-) (2). Iodide is rapidly and almost completely absorbed in the stomach or duodenum, whereas IO_3^- is first reduced in the gut and then absorbed as I^-. Thyroid gland takes up iodide from the plasma to synthesize thyroid hormones and most of the remaining iodine is excreted into urine. Iodine is also accumulated in the mammary gland of lactating woman and excreted into breast milk for the baby. Small amounts of iodine are also taken up by salivary glands, gastric mucosa, and choroidal plexuses (3).

When iodine intake is sufficient, uptake by the thyroid gland may be less than 10%, whereas in chronic deficiencies it can exceed 80% (4). Generally, people living in iodine-sufficient areas with normal thyroid function have been shown to tolerate excess iodine up to 1–3 mg/day without clinical symptoms (5). High concentrations of iodine exert an acute inhibitory effect on thyroid hormone production by temporarily inhibiting iodine organification and thyroid hormone synthesis, a phenomenon known as the Wolff-Chaikoff effect (6). This protective mechanism reduces thyroid hormone production after the consumption of excessive iodine. Failure to escape from the Wolff-Chaikoff effects may result in iodine-induced autoimmunity, which can be transient or permanent in susceptible individuals with pre-existing thyroid disease (7).

Thyroid hormones regulate the body's metabolism and play an important role in regulating carbohydrate, lipid, and protein metabolism. Consequently, thyroid dysfunction not only causes autoimmune thyroiditis, goiter, and thyroid nodules, but is also associated with elevated blood glucose, increased blood pressure, and altered blood lipid levels, leading to increased cardiometabolic risk (8). While long-term health effects of iodine deficiency are widely recognized, the consequences of excess iodine intake, particularly from iodine-fortified supplements such as iodized salt are less studied. As discussed in Chapters I and III, populations from previously iodine-deficient regions, including the Nepalese population, are more susceptible to excess iodine than populations with good access to dietary iodine, such as the

Japanese. Unfortunately, there are no long-term human studies performed in such regions where iodine supplementation exceeds recommended levels.

Excess iodine intake has been shown to negatively impact immune health and alter gut microbiota via non-thyroidal mechanism. Because gut microbiota influence intestinal iodine absorption, various animal studies reported different responses in gut microbiota composition and thyroid hormone secretion with the same dose of iodine intake among obese versus healthy, male versus female, and mice with thyroid disease (9–11). These findings indicate that iodine exerts diverse metabolic effects even when administered at equivalent doses. Therefore, further research is warranted to elucidate the effects of excess iodine intake on major organs, including the liver, heart, kidneys, salivary glands, and gastrointestinal tract.

4-1-1 Purpose of the mouse study

The minimum iodine requirement of mouse feed is reported to be 0.15 μg/g feed (12). However, in most of the excess iodine intake animal model studies, much higher doses of iodine are given through drinking water (13–17). In addition, there are limited studies on the long-term effects of moderate levels of excess iodine administration through feed. Therefore, to address this gap, in the present pilot study, I gave mice special feed containing 17 μg iodine/g feed as KIO_3 to mirror the excess iodine intake in Nepal.

4-1-2 Mouse study plan

Figure shows my mouse experiment design to examine effects of long-term intake of moderately excess iodine.

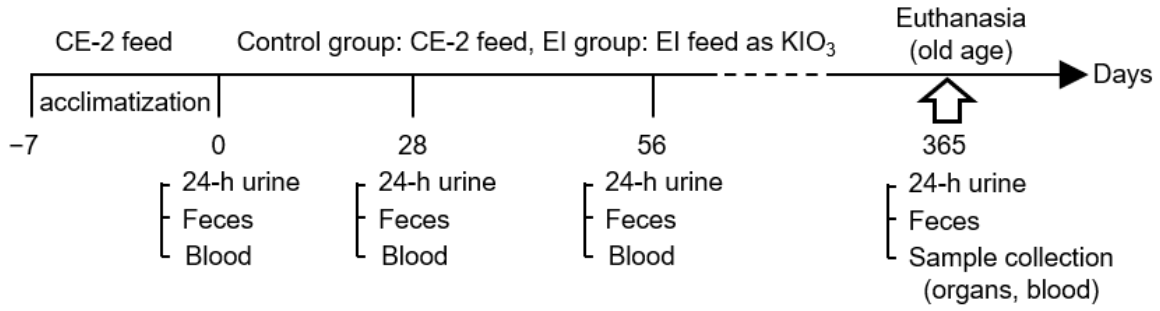

Figure 4-1. Schematic illustration of experimental design.

In this experiment, after one week of acclimatization, mice are divided into excess iodine (EI)

group and control group. The control group mice eat CE-2 feed (1.7 μg iodine/g feed), and the EI group mice eat iodine-fortified CE-2 feed (17 μg iodine/g feed). Both feeds are available from CLEA Inc. (Japan), and they contain iodine as KIO_3, as the same iodine species as used for iodized salt in Nepal. Feed and water intake will be measured twice a week, body weight will be measured once a week, and blood, 24-h urine, and feces samples will be collected once a month until euthanasia. Immediately after euthanasia, blood and major organs, including the thyroid gland, salivary gland, liver, and kidneys, will be collected.

In the present study, to test various devices to be use and to master necessary skills, I performed a pilot study using 6 mice.

4-2 Materials and Methods

4-2-1 Reagents

Formalin neutral buffer solution (10%, pH 7.4) was purchased from FUJIFILM Wako Pure Chemical Corporation (Osaka, Japan). All the reagents used were the same as those described in Chapters II and III.

4-2-2 Equipment

(1) Feed box

To measure individual iodine intake accurately from the feed amounts taken, it is necessary to know the exact amounts of feed taken by individual mouse. Therefore, I tried powder form of feed and a specially designed feed box for powdered feed (Fig. 4-2).

Figure 4-2. Feed box used in the present study.

(2) Water bottle

For easy access to tap water, an automatic sipper-tube water bottle (CLEA) was used (Fig. 4--3).

Figure 4-3. Water bottle equipped with a stainless-steel sipper tube (no ball valve type).

(3) Metabolic cage

Metabolic cages are necessary to collect 24-h urine and feces. Two types of metabolic cages (SN-783-0 and 3600M021) were tested to collect 24-h urine and feces collection. Figures 4-4A and 4-4B show SN-783-0 and 3600M021, respectively.

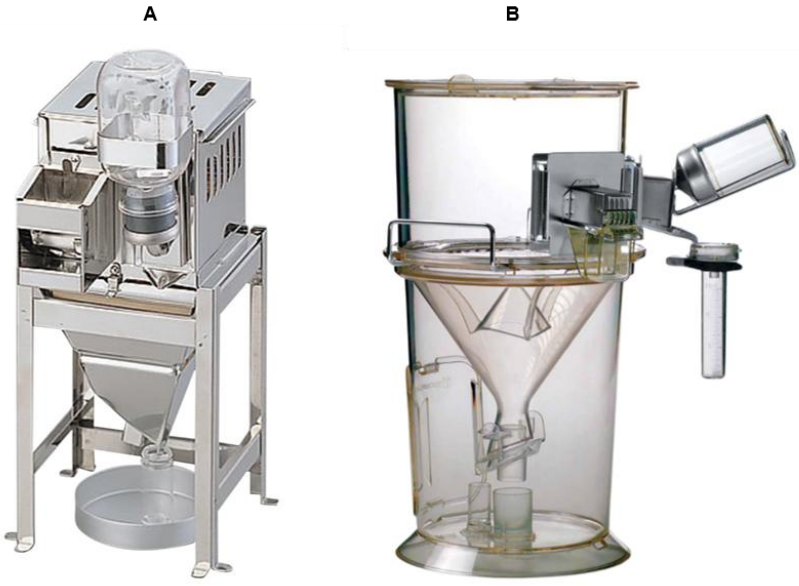

Figure 4-4. Metabolic cages tested for 24-h urine and feces collection. **(**A) Shinano, SN-783-0, all stainless steel. (B) Tecniplast, 3600M021, mostly plastic.

(4) Restrainer device for blood collection from mouse tail vein

In the present study, I tried to obtain about 10 μL of blood from the tail vein of mouse at least once per two weeks to follow time-dependent changes in metabolites in plasma such as blood glucose. The following restrainer (Fig. 4-5) was tested to restrain mouse movement during blood collection.

Figure 4-5. A mouse restrainer (CL-4903) tested for the blood collection from tail vein.

4-2-3 Confirmation of iodine content in control and iodine-fortified feed, and tap water

Both CE-2 and iodine-fortified CE-2 feeds were obtained from CLEA. According to data provided by CLEA, CE-2 feed contains approximately 1.7 μg iodine/g feed in the form of KIO_3. The major nutrient composition of the feed is in the supporting Table S4-1. For t iodine-fortified CE-2 feed (EI feed), we ordered the manufacturer to add 10 times more KIO_3 to CE-2 feed.

Using the method described in Chapter III, the iodine content of CE-2 feed, EI feed, and the tap water used as drinking water were measured. Feeds were dissolved in 10 volumes of distilled water, vortexed, and centrifuged as described for seaweed iodine measurement. The supernatant of CE-2 feed was analyzed without further dilution, whereas the supernatant from the EI feed was further diluted 20-fold with distilled water.

Calibration curves obtained are shown in Figures 4-6A and 4-6B, respectively. CE-2 feed contained 0.8 μg iodine/g feed, lower than the content the manufacturer determined for CE-2 feed different from the present lot. EI feed contained 16 μg/g feed, which is almost identical with the ordered amounts of 17 μg/g feed. Therefore, in the present study, EI group mice were given feed containing 20-fold higher amounts of iodine compared to the control group mice.

Figure 4-6C shows the calibration curve obtained for the tap water.

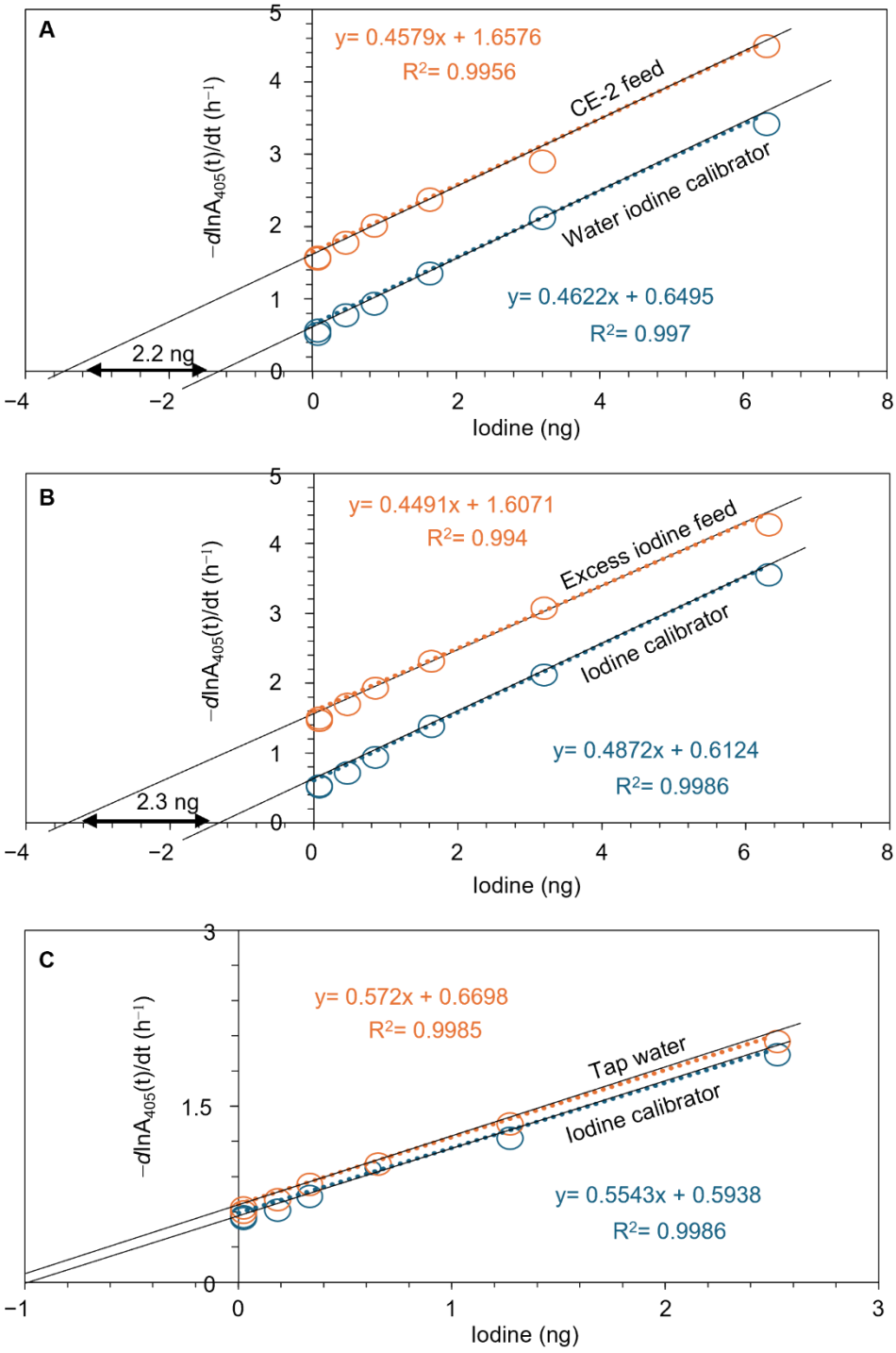

Figure 4-6. Calibration curves for CE-2 (A), EI feed (B), and tap water (C).

The iodine content of the tap water was 4 µg/L, which is considerably low. As individual mouse drinks about 5 mL/day, iodine intake through the tap water is only 0.02 µg, negligible compared to iodine intake through the feed.

4-2-4 Animals

Because C57BL/6J mice have been used as aging model and rich data relating to aging are accumulated, C57BL/6J mice were selected. Six adult, pathogen-free, eight-week-old female mice (C57BL/6J, weight 18–19.5 g) were purchased from Kiwa Laboratory Animals Research Institute Ltd. (Osaka, Japan). The mice were housed individually and acclimatized for three weeks before being introduced to EI feed, under standard room temperature (22 ± 2ºC) with a 12/12 h light/dark cycle (dark 20:00−8:00), and mice were allowed ad libitum access to feeds and water.

4-2-5 Experiment design

Figure 4-7 shows the present experiment design.

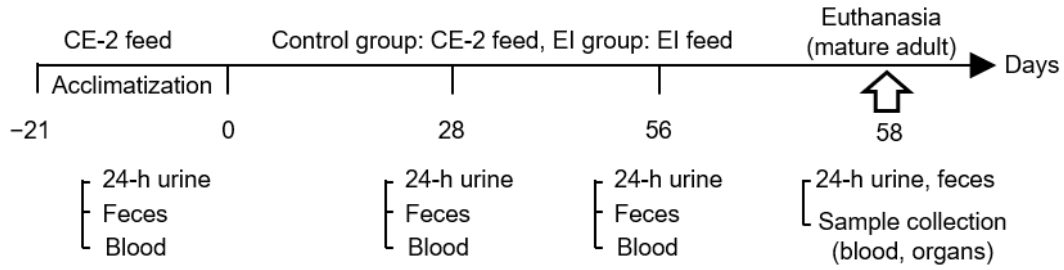

Figure 4-7. Design of the present pilot mouse study. The control group (n = 3) eat CE-2 feed and the EI group mice (n = 3) take iodine fortified CE-2 feed. The blood, 24-h urine, and feces samples were collected once a month until euthanasia. Immediately after euthanasia, blood and major organs, including the thyroid gland, salivary gland, liver, and kidneys, are collected.

During the acclimatization period, all mice were fed CE-2 feed. Feed and water were replaced twice a week. The weight of feed box and water box were measured before and after intake, and the amount of feed and water intake were calculated as difference in the respective weight. Body weight was measured once a week. Before the start of EI feed, 24-h urine and feces were collected. After that, mice were assigned to two groups: the control group (n = 3, CE-2 feed) and the EI group (n = 3, EI feed). Every month, approximately 10 μL of blood, as well as 24-h urine and feces, were tried to collect. To minimize stress, blood and 24-h urine collections were performed on different days.

4-2-6 Collection of 24-h urine and feces

All the mice (n = 6) were housed individually in metabolic cages (SN-783-0 or 3600M021) (Fig. 4-4) for 24-h, during which mice were allowed access to feed and water ad libitum. After 24-h, the collected urine was centrifuged at 13,200 × g for 20 min, the total volume was measured, and the samples were transferred into Eppendorf tubes. Urine samples were stored at −80ºC until analysis. Collected feces were stored at −80ºC.

4-2-7 Blood collection

Blood was collected from the tail vein without anticoagulant by using a mouse-specific restrainer or home-made restrainer, and serum was separated from the blood after coagulation by centrifuging at 4670 × g for 2 min and −80ºC until analysis.

4-2-7 Organ collection

After 56 days of EI feeding, mice were anesthetized using isoflurane inhalation and then euthanized by cervical dislocation. Blood was immediately collected from abdominal aorta, followed by collection of thyroid gland and other organs, including salivary gland, brain, adrenal glands, kidney, pancreas, spleen, heart, liver, lungs, and ovaries. The organs were weighed, and half portion of each organ was immediately frozen in liquid nitrogen and stored at −80ºC. The remaining halves were fixed with 1.5 mL of 10% neutral buffered formalin. Blood sample was left at room temperature to coagulate, and then serum was collected by centrifugation at 4670 × g for 1 min and stored at −80ºC until analysis.

4-3 Results

4-3-1 Body weight

Figure 4-8 shows the change in body weight during the experiment. There was no apparent difference in the body weight between the CE-2 feed group: the mean body weight at the end of the experiment was same between the two groups, 22.4 g. During the entire experiment, average weight gain was 3.6 g for the control mice and 3.5 g for the EI mice. The weight gain and body weight results are consistent with data from CLEA, which shows body weight of 19-weeks C57BL/6J female mice was 21.6 g (at the end of the experiment, the mice were 19 weeks old).

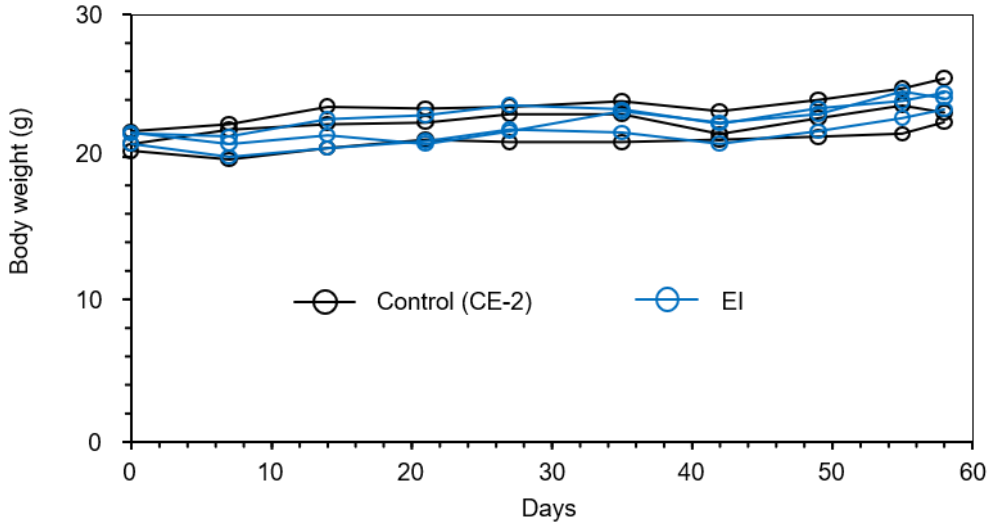

Figure 4-8. Change in body weight during experiments. Blue circle, EI group. Black circle, control group.

4-3-2 Feed and water intake

Figures 4-9 shows feed intake.

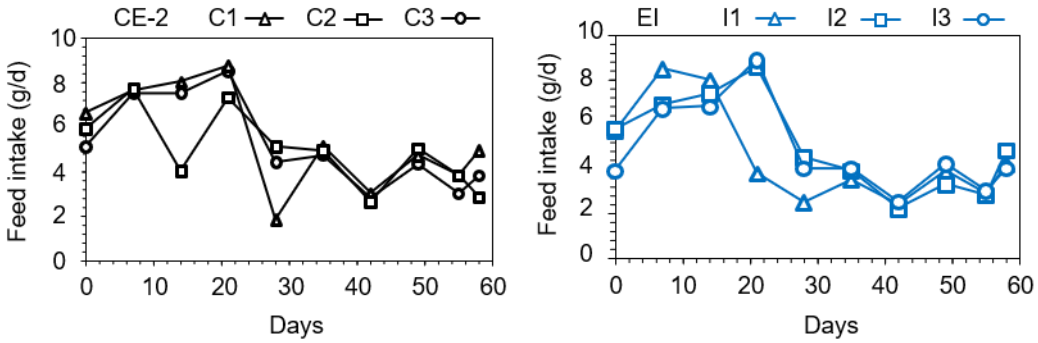

Figure 4-9. Feed intake in control group (black) and EI group (blue). y-axis, the average daily feed intake in grams. x-axis, day after the start of EI feed.

Feed intake abruptly decreased by about 3 g on day 30. This is due to the following reason. Because the female mice were small, they entered the empty space of the plastic tunnel of the feed box (Fig. 4-2) easily and contaminated the feed in the container with urine and feces, resulting in apparently high feed intake. To restrict free moving in the tube, we attached a plastic cap to the end of the tube as shown in Figure 4-10.

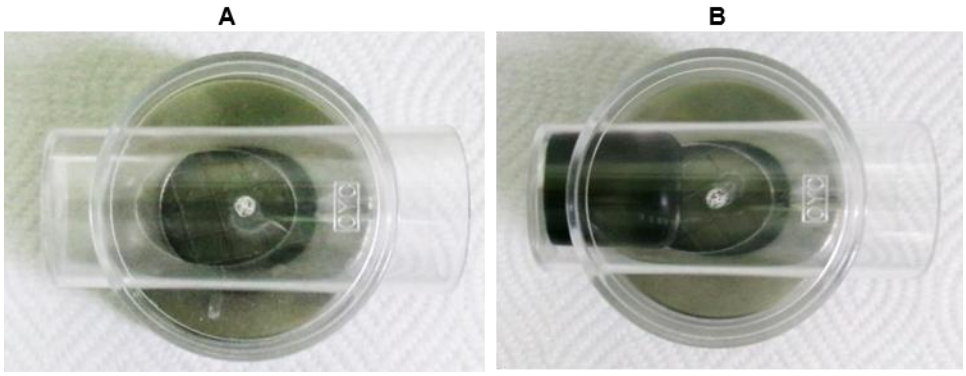

Figure 4-10. Attachment of a plastic cap to the end of the tube of the feed box. (A), before. (B), after. The cap effectively restricted the mouse from free moving in the tube.

After this improvement of the feed box to reduce the empty space (day 30), feed contamination with urine and feces were prevented significantly. The average daily feed intake of control group was slightly higher than that of EI group.

Figures 4-11 shows water intake. On day 58, mice were in the metabolic cages to collect

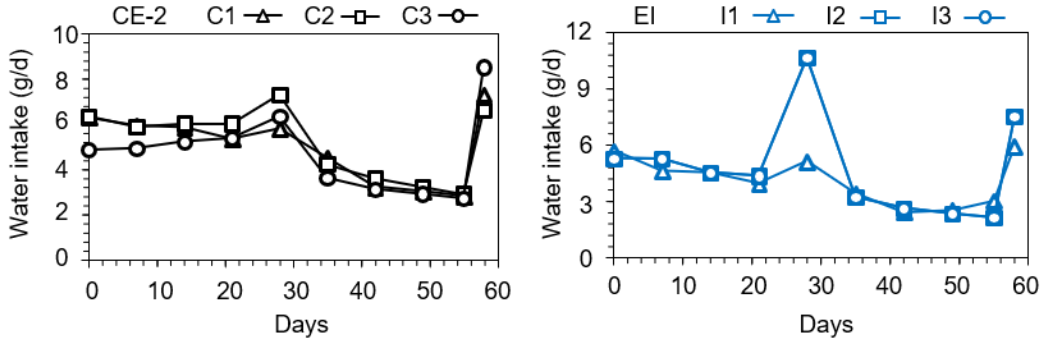

Figure 4-11. Water intake in the control and EI groups. y-axis, the average daily water intake. x-axis, day after the start of EI feed. I

24-urine and feces. The large value on this day seems to be due to some technical problems. The high value for I2 mouse on day 28 was also due to technical mistakes. The water intake was same between the two groups. Importantly, the water intake showed gradual decrease from 5 mL/day to 3 mL/day. It is unclear why this decrease occurred.

4-3-3 Iodine content of 24-h urine

When iodine is sufficient, more than 90% of dietary iodine is excreted in the urine, making urine iodine content one of the best biomarkers of recent iodine intake. Urine samples from CE-2 fed mice were diluted 40-fold with distilled water, whereas those from EI fed mice were 400–500 folds diluted. Then, 25 μL of the diluted samples were aliquoted and subjected to iodine determination (see Chapter III). The results are summarized in Table 4-1.

Table 4-1. Mouse urine output and iodine intake per 24 hours. Urine output, 24-h urine amount in g. Total urinary I, total amount of iodine in 24-h urine in μg.

	CE-2 feed				EI feed		
	C1	C2	C3	C4	I1	I2	I3
Day 0 (n = 6)							
Urine output (g/d)	2.2	1.2	1.4	1.8			
Total urinary I (μg/d)	4.18	4.78	6.02	6.12			
Day 28 (n = 6)							
Urine output (g/d)		0.79	1.33		1.37	2.49	1.17
Total urinary I (μg/d)		2.83	3.55		30.7	59.0	48.8
Day 56 (n = 6)							
Urine output (g/d)	1.18	1.96	1.25		0.94	1.74	1.44
Total urinary I (μg/d)	1.53	4.04	3.13		34.6	52.6	52.9

Urine samples C5 and C6 collected on Day 0, and C1 collected on Day 28, were excluded because of contamination.

Due to the contamination with feed powders and feces, two urine samples were excluded from the analysis. To reduce the accidental entering of feed powders and feces into urine-collection tube, the tube position and the amount of feed in the feed box of the metabolic cage were adjusted. CE-2 (0.8 μg/g feed) was given to control group mice and EI feed (16 μg/g feed) was given to EI group mice. The mean urinary iodine output on Day 0 of control group was 5.28 ± 0.82 μg/day, 3.19 ± 0.36 μg/day on Day 28, 2.90 ± 1.04 μg/d on Day 56. On the other hand, the mean urinary iodine output of EI group was 46.2 ± 11.7 μg/day on Day 28 and 46.7 ± 8.6 μg/day on Day 56. The volume of 24-h urine was same between the two groups. Figure 4-12 showed these results using bar graph.

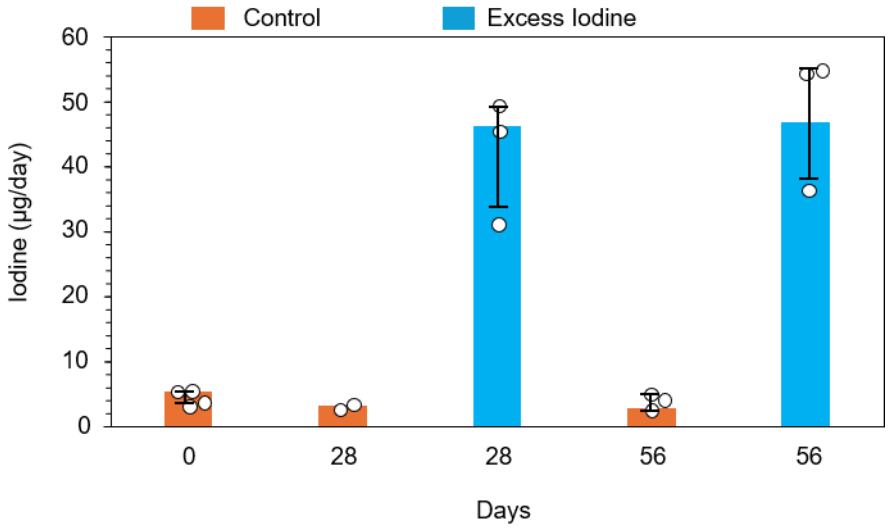

Figure 4-12. Iodine output into 24-h urine.

Table 4-2 summarizes the amount of iodine taken by feed and that excreted into urine, iodine balance, for control and EI groups.

Table 4-2. Summary of iodine balance in control and EI group mice.

	Feed intake	Water intake	Iodine intake	Urine output	Urinary iodine excretion
	(g/d)	(g/d)	(μg/d)	(g/d)	(μg/d)
Control (n=3)	5.2 ± 1.9	5.0 ± 1.6	8.8	1.4 ± 0.5	4.02 ± 1.4
EI (n=3)	4.8 ± 2.0	4.7 ± 2.2	77	1.5 ± 0.4	46.4 ± 10.3

The data is shown as mean ± SD

Control group mice took 8.8 μg iodine per day, and EI group mice 77 μg iodine per day through feed. In the case of control group, 46% of iodine taken from CE-2 feed was excreted into urine. On the other hand, 60% of iodine taken from EI feed was excreted into urine. As for the amount of feed intake and urine volume, there was no apparent difference between the two groups.

4-3-4 Content of proline and 4-hydroxyproline in CE-2 and EI feed

To evaluate the intake of free proline and 4-hydroxyproline through feed, the total amounts of these two secondary amino acids were measured using the method described in Chapter II. Fifty milligrams of CE-2 and EI feed was mixed with 1 mL distilled water, vortexed, and centrifuged. The resultant supernatant was analyzed without further dilution or after further 10-fold dilution with distilled water. Figure 4-13 shows total ion chromatograms obtained for CE-2 and EI feed.

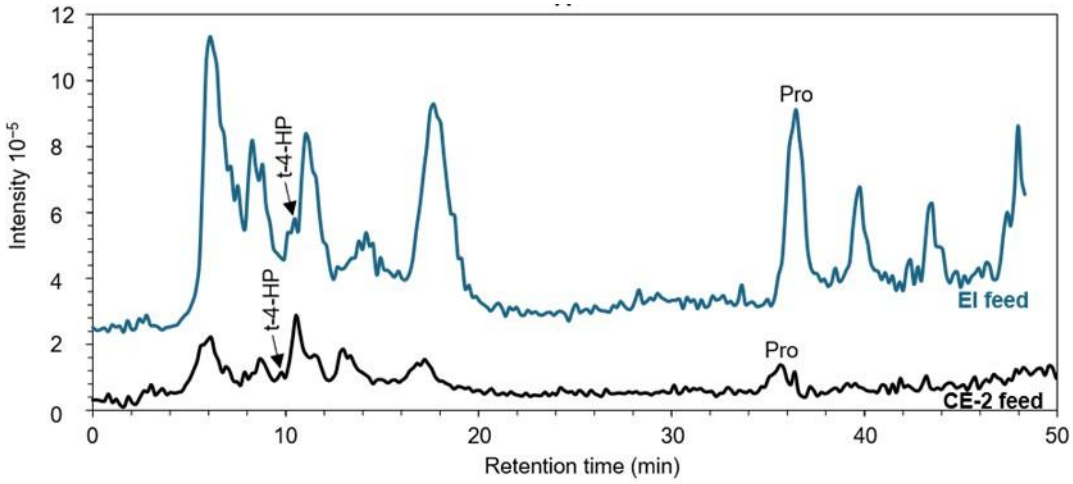

Figure 4-13. Total ion chromatograms of S0 sample from CE-2 and EI feed.

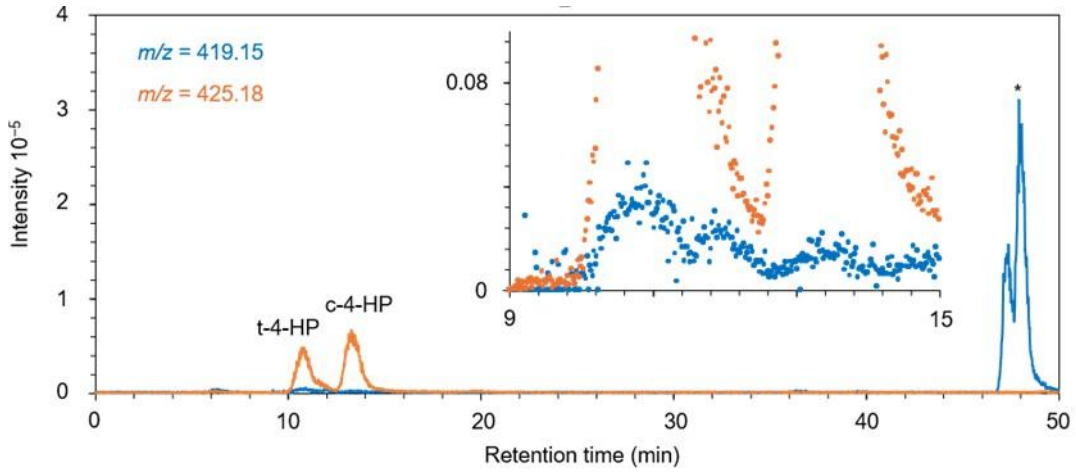

Figure 4-14. Extracted chromatograms of *m*/*z* 419.15 and 425.18 ions obtained for S0 sample from CE-2 feed. The inset is enlargement of the region around the $^{13}C_6$-dabsyl t-4-HP and c-4-HP peaks. Water extract from CE-2 feed was 10-fold diluted and analyzed.

Figure 4-14 shows the extracted chromatograms of *m/z* 419.15 (blue in the figure) and 425.18 ions (orange in the figure) obtained for S0 sample from CE-2 feed. There is a blue peak overlapping with $^{13}C_6$-dabsyl t-4-HP peak. However, this blue peak eluted slightly faster compared to $^{13}C_6$-dabsyl t-4-HP, indicating that the blue peak is not ^{12}C-dabsyl t-4-HP because the latter should migrate slightly more slowly compared to $^{13}C_6$-dabsyl t-4-HP due to isotope effects. Figure 4-15 shows the corresponding extracted chromatograms obtained for EI feed.

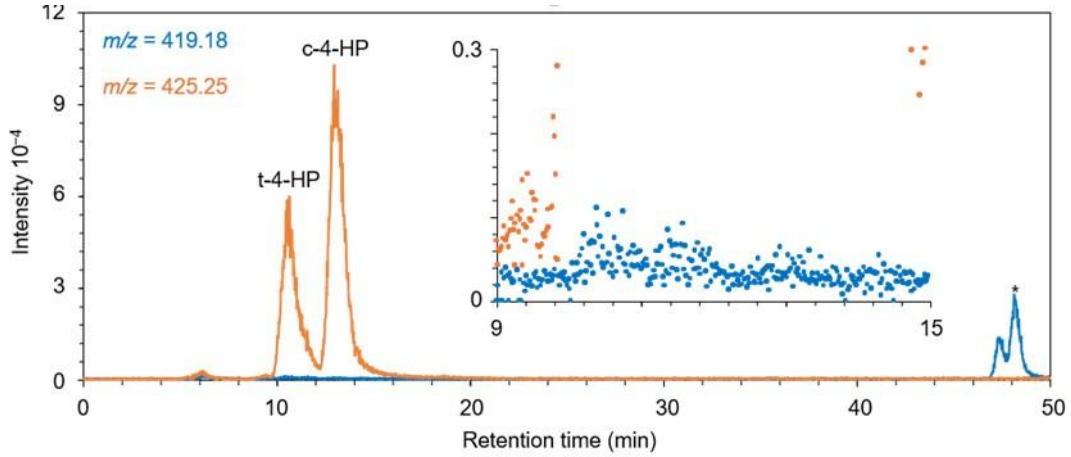

Figure 4-15. Extracted chromatograms of *m/z* 419.15 and 425.18 ions obtained for S0 sample from EI feed. The inset is enlargement of the region around the $^{13}C_6$-dabsyl t-4-HP and c-4-HP peaks. Water extracts from EI feed were used without dilution.

No ^{12}C-dabsyl t-4-HP and c-4-HP peaks were detected for EI feed. From these results, it is found that both CE-2 and EI feed do not contain detectable levels of 4-hydroxyproline.

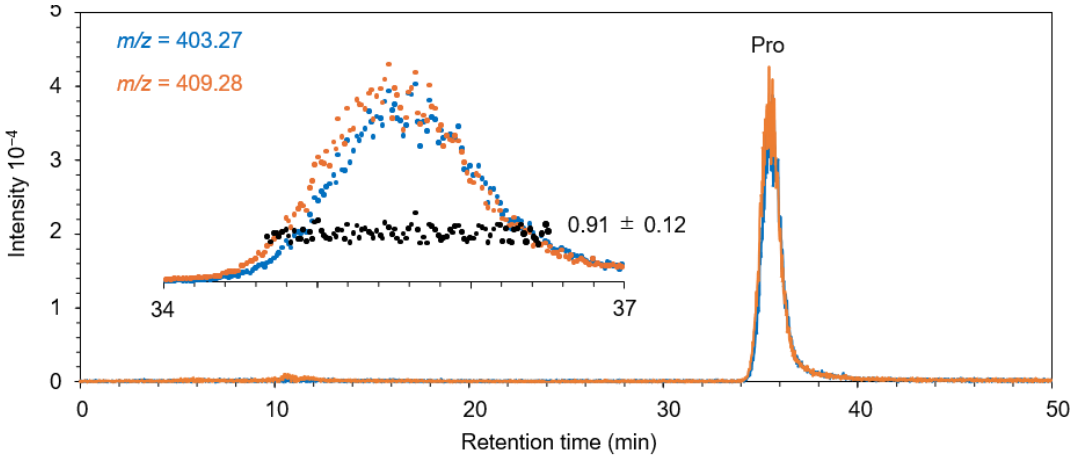

Figure 4-16. Extracted chromatograms of *m/z* 403.25 and 409.23 ions obtained for S0 sample from CE-2 feed. The region around the $^{13}C_6$-dabsyl Pro is enlarged.

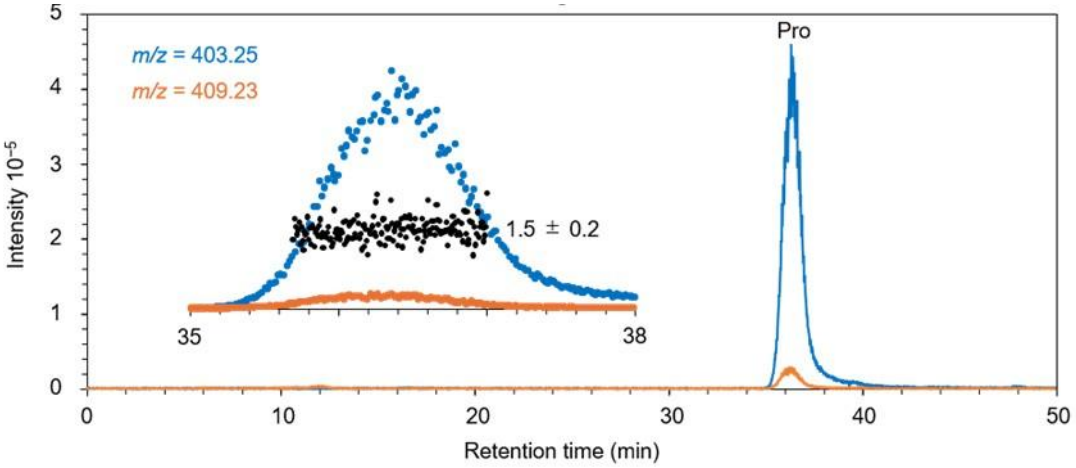

Figure 4-17. Extracted chromatograms of *m*/*z* 403.25 and 409.23 ions obtained for S0 sample from EI feed. The region around the $^{13}C_6$-dabsyl Pro is enlarged.

Figures 4-16 and 4-17 show the extracted chromatograms of *m*/*z* 403.25 (blue in the figure) and 409.23 ions (orange in the figure) obtained for S0 sample from CE-2 and EI feed, respectively. In both chromatograms, protonated ^{12}C-dabsyl proline (*m*/*z* 403.25 ion) was detected clearly as a large peak.

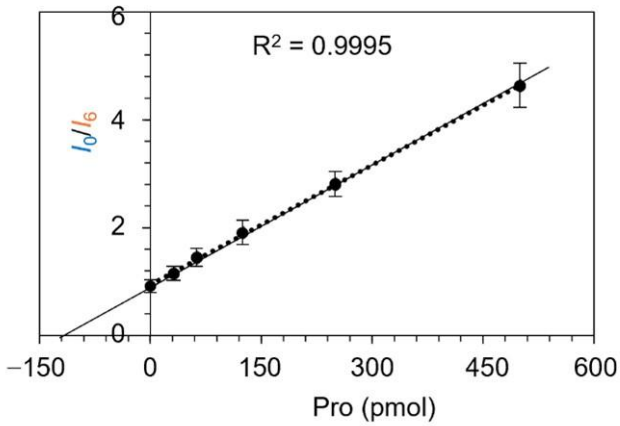

Figure 4-18. Calibration curve obtained for Pro from CE-2 feed. I_0/I_6, intensity ratio between *m*/*z* 403.25 ion and *m*/*z* 409.23 ion. x-axis, the amounts of Pro added to the water extracts from CE-2 feed. The content of Pro was obtained as 128.4 ± 2.5 pmol from the x-axis intercept.

Figure 4-18 shows calibration curve obtained for the water extract from CE-2 feed. The

total content of Pro in CE-2 was found to be 2.17 ± 0.04 μmol/g feed from the x-axis intercept of this calibration curve. In the case of EI feed, the total content of Pro was 2.69 ± 0.52 μmol/g feed.

4-3-5 Total content of proline and *trans*-4-hydroxyproline in urine

Total amounts of Pro and 4-HP in 24-h urine samples were determined using the method described in Chapter II. Urine samples were diluted 10-fold with distilled water, and the diluted sample was subjected to analysis. The results are summarized in Table 4-3.

Table 4-3. Total amounts of proline and *trans*-4-hydroxyproline in 24-h urine**.** C1, C2, C3, control group mice. I1, I2, I3, EI group mice.

Mouse	Day 0 (n = 3)		Day 28 (n = 2)		Day 56 (n = 6)	
	proline	t-4-HP	proline	t-4-HP	proline	t-4-HP
	(nmol)	(nmol)	(nmol)	(nmol)	(nmol)	(nmol)
C1	153 ± 7	162 ± 5			28.3 ± 1.6	15.3 ± 1.3
C2	102 ± 6	184 ± 7			131 ± 15	96.6 ± 3.7
C3	143 ± 4	179 ± 18	105 ± 5	67.4 ± 2.4	79.6 ± 2.0	51.6 ± 3.6
I1			67.0 ± 2.3	52.6 ± 2.7	37.3 ± 1.6	17.6 ± 1.3
I2					108 ± 3	110 ± 2
I3					77.6 ± 2.6	64.8 ± 2.4

All values are presented as mean ± SD. All the values are presented in nmol.

All the 24-h urine examined contained substantial amounts of Pro and t-4-HP. Interestingly, in all the 24-urine collected on Day 0 from control mice, the total amounts of t-4-HP was higher than those of Pro by 1.1–1.8 fold. The determination of respective amount of D- and L-enantiomers is underway.

4-3-6 Thyroid gland

Figure 4-19 shows the thyroid gland.

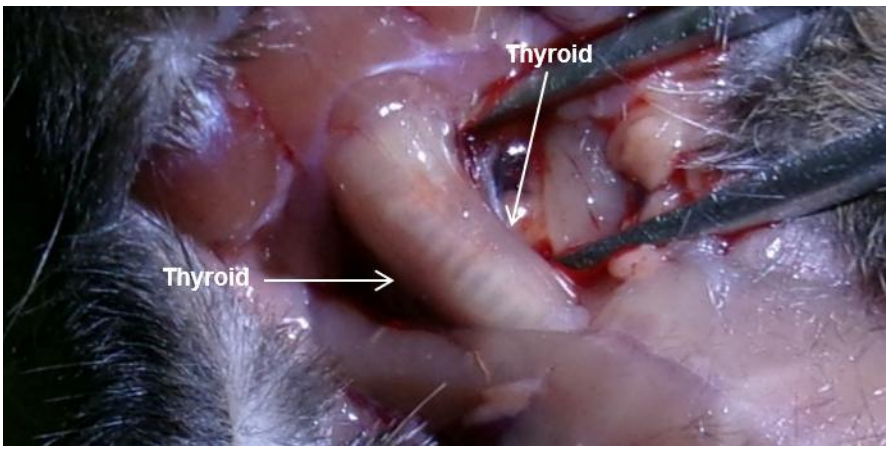

Figure 4-19. Mouse thyroid gland. Arrows indicate left and right lobe of the thyroid gland (reddish thin leaf-like appearance).

As the thyroid gland was very thin and attached with trachea, it was difficult to separate the gland from the trachea. There was no apparent difference in the size and shape of the thyroid gland between control and EI groups. Histological examination of thyroid glands is underway.

4-3-7 Comparison of performance between two types of metabolic cage

It is essential to quantitatively determine the amount of analyte of interest such as iodine excreted into 24-h urine. Figure 4-20 shows the outlet portion of the metabolic cages.

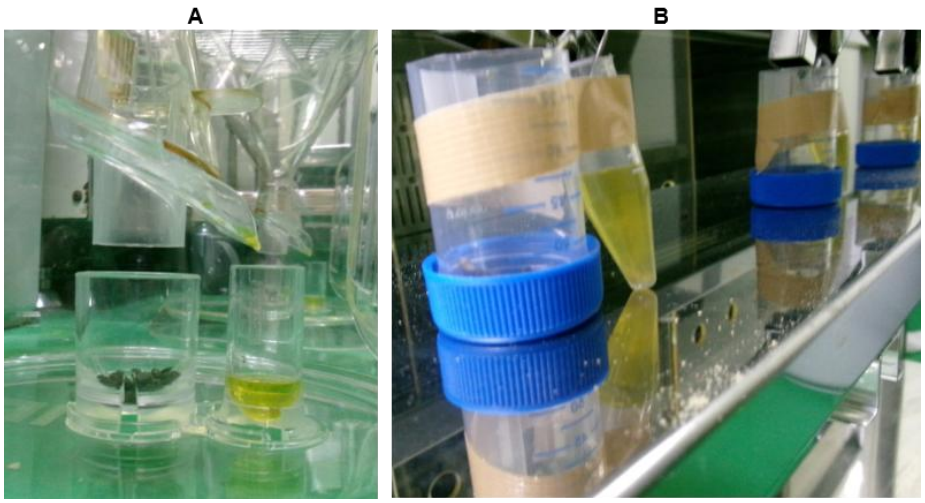

Figure 4-20. Urine and feces collection using plastic (A) and stainless-steel cage (B)**.**

In the case of stainless-steel cages, substantial amounts of feed powder entered into urine collection tube (Fig. 4-20B). To prevent this contamination, normal feed boxes were changed to those for powder feed. However, it was still difficult to reduce feed contamination to allowable levels. On the other hand, in the case of plastic metabolic cages, accidental entering of food powder into urine was successfully reduced to minimum levels by reducing the feed amount in the feed box. In addition, the plastic metabolic cages were much easy to handle compared to the stainless-steel metabolic cages.

4-4 Discussions

From the present pilot study, many important problems to address before starting of full animal studies have been revealed. First, taking 10-μL of blood from mouse tail vein with giving mouse as small stress as possible was found to be quite difficult. Further improvement of devices and the technique to handle them. Second, removement of thyroid gland to measure correctly its weight seemed to be impossible because the gland was too thin and invisible without blood in the gland, although other organs could be easily removed. Third, as a large water bottle attached with outlet tube having no stop ball, it was difficult to obtain reliable water intake for each mouse. It is recommended to use 50–100-mL bottle attached with tube with two balls.

In this pilot study, excess iodine was given to mice through powder form feed fortified with iodate. By improving the feed box (Fig. 4-10), the dispersal of feed from the feed box was minimized and the urination and defecation in the box was perfectly inhibited, enabling the estimation of exact amount of iodine intake. In the case of EI group mice, 60% of iodine ingested was excreted into urine. It is important to measure iodine content of 24-h feces to further evaluate the iodine balance per day. I am now trying to develop a method to measure iodine in mouse feces.

In this pilot study, it was confirmed that not only Pro but also t-4-HP exists in substantial amounts in urine. As CE-2 and EI feed contained no detectable levels of t-4-HP, the observed t-4-HP in the urine was derived from metabolic activities of mouse and/or gut microbes. It is essential to determine the D- and L-enantiomer ratio of Pro and t-4-HP to estimate the contribution of gut microbes to urine t-4-HP. The determination of the enantiomer ratio is now underway using the method developed in Chapter II.

References

1. Blikra M. J., Henjum S., and Aakre I. (2022) Iodine from brown algae in human nutrition, with an emphasis on bioaccessibility, bioavailability, chemistry, and effects of processing: A systematic review. *Compr. Rev. Food Sci. Food Saf*. 21, 517–536.
2. Sorrenti S., Baldini E., Pironi D., Lauro A., D'Orazi V, Tartaglia F., Tripodi, D., Lori E., Gagliardi F., Praticò M., Illuminati G., D'Andrea V., Palumbo, P., and Ulisse S. (2021) Iodine: Its Role in Thyroid Hormone Biosynthesis and Beyond. *Nutrients* 13:4469
3. Institute. of Medicine (US) Panel of Micronutrients. (2001) Dietary reference intakes for vitamin A, vitamin K, arsenic, boron, chromium, copper, iodine, iron, manganese, molybdenum, nickel, silicon, vanadium, and zinc. National Academies Press (US)
4. Hatch-McChesney A., and Lieberman H. R. (2022) Iodine and iodine deficiency: a comprehensive review of a re-emerging issue. *Nutrients* 14:3473
5. Watanabe N. (2025) A narrative review of long-term inorganic iodine monotherapy for Graves' disease with a historical relationship between iodine and thyroid. *Endocr. J.* 202, 23-36.
6. Wolff J., and Chaikoff I. L. (1948) Plasma inorganic iodide as a homeostatic regulator of thyroid function. *J. Biol. Chem*. 174, 555–564.
7. Leung A. M., and Braverman L. E. (2012) Iodine-induced thyroid dysfunction. *Curr. Opin. Endocrinol. Diabetes Obes.* 19, 414–419
8. Pingitore A., Gaggini M., Mastorci F., Sabatino L., Cordiviola L., and Vassalle C. (2024) Metabolic syndrome, thyroid dysfunction, and cardiovascular risk: the Triptych of Evil. I*nt J Mol Sci.* 25:10628
9. Shen H., Han J., Li Y., Lu C., Zhou J., Li Y., and Su X. (2019) Different host-specific responses in thyroid function and gut microbiota modulation between diet-induced obese and normal mice given the same dose of iodine. *Appl. Microbiol. Biotechnol*. 103, 3537–3547.
10. Gong B., Meng F., Wang X., Han Y., Yang W., Wang C., and Shan Z. (2047) Effects of iodine intake on gut microbiota and gut metabolites in Hashimoto thyroiditis-diseased humans and mice. *Commun Biol.* 7:136.
11. Shen H., Xu J., Lu C., Han J., Zhou J., Ming T., et al. Effects of the sex factor on mouse iodine intake: interactions between the gut microbiota composition and metabolic syndromes. *ACS Omega* 6, 28569-28578.
12. National Research Council (US) Subcommittee on Laboratory Animal Nutrition. (1995) Nutrient Requirements of Laboratory Animals: Fourth Revised Edition, National Academies Press (US).
13. Chen X. Y., Lin C. H., Yang L. H., Li W. G., Zhang J. W., Zheng W-W., Wang X., Qian J.,

Huang J-I, and Lei Y-X. (2016) The Effect on sodium/iodide symporter and pendrin in thyroid colloid retention developed by excess iodide intake. *Biol. Trace Elem. Res.* 172, 193–200.
14. Ismail H. T. H. (2022) The impact of iodine exposure in excess on hormonal aspects and hemato-biochemical profile in rats. *Biol. Trace Elem. Res*. 200, 706–719.
15. Guo Y., Hu C., Xia B., Zhou X., Luo S., Gan R., Duan P., and Tan Y. (2022) Iodine excess induces hepatic, renal and pancreatic injury in female mice as determined by attenuated total reflection Fourier-transform infrared spectrometry. *J. Appl. Toxicol.* 42, 600–616.
16. Cui Y., Zhang B., Zhang Z., Nie J., and Liu H. (2021) Long-term repetitive exposure to excess iodine induces mitochondrial apoptosis, and alters monoamine neurotransmitters in hippocampus of rats of different genders. *Toxicol. Res. (Camb).* 10, 975-982.
17. Amano I., Ninomiya A., Yajima H., Suda-Yajima M., Kokubo M., Khairinisa M. A., Haraguchi S., Haijima A., and Koibuchi N. (2025) Effects of excessive iodine intake during the perinatal period on thyroid function and higher brain functions in mouse offspring. *Endocr. J.* 72, 999–1010
18. Laboratory J. When are mice considered old? : The Jackson Laboratory; 2017

Acknowledgement

First of all, I would like to express my sincere gratitude towards Koshien-Gakuen Educational Institution chief director Tomoko Kume for giving me a precious chance to perform PhD study at Koshien University. I would also like to express my sincere gratitude to all the teachers and staff members of Koshien University, for their kindness, love, and support.

I would like to acknowledge my supervisor, Professor Dr. Tetsuo Ishida, for his invaluable guidance, support, and encouragement throughout this journey. It would not have been possible to complete this work on time without his constant support and help.

I gratefully acknowledge the Rotary Club of Kyoto-Southwest for the financial support (scholarship) and for various Japanese cultural experiences and hiking activities.

I express my sincere gratitude to Mrs. Astuta Noriko (a former student of Koshien University) for helping me enroll at this beautiful university. I will always be indebted to her. I also extend my sincere thanks to Prof. Dr. Jayalaxmi Pradhan, Campus Chief Chairperson of Padma Kanya Multiple Campus, for her recommendation of my academic pursuit in Japan.

Finally, I dedicate this research work to my family for their sacrifices, love, unwavering support, and for everything they have done, which gave me the strength to keep going.

Supporting Information

(1) Chapter II

Figure S2-1. Photographs of samples used for evaluation of the method developed to analyze the stereoisomers of proline and 4-hydroxyproline.

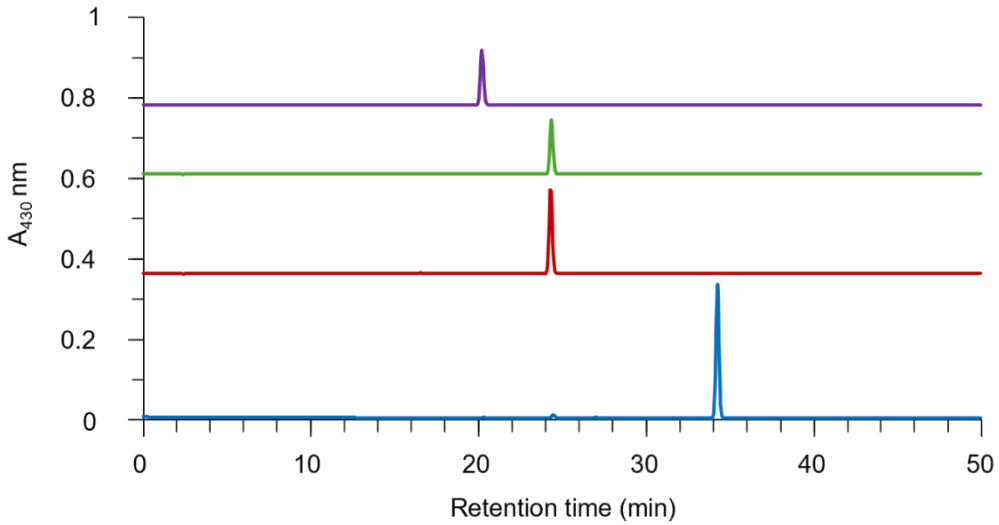

Figure S2-2. Chromatograms of dabsyl t-4-HP_L (purple), c-4-HP_L (green), c-4-HP_D (red), and DL-Pro (blue). An Inertsil ODS-3 column (3 μm, 1.5 mm × 150 mm) was used. A_{430}, absorbance at 430 nm.

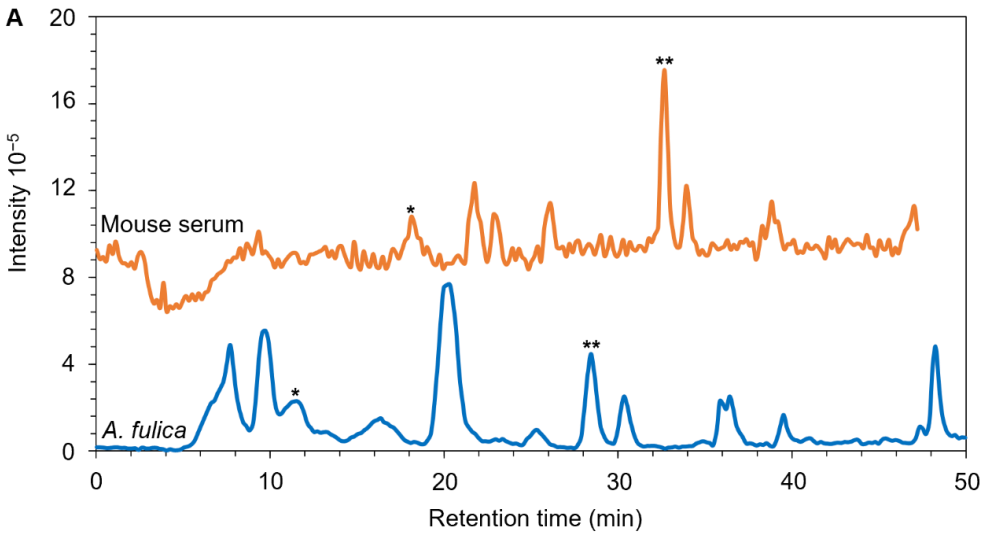

Figure S2-3. Total ion chromatograms obtained for S0 sample of mouse serum and *A. fulica* hemolymph. Peak labeled with *, dabsyl t-4-HP. Peak labeled with **, dabsyl Pro.

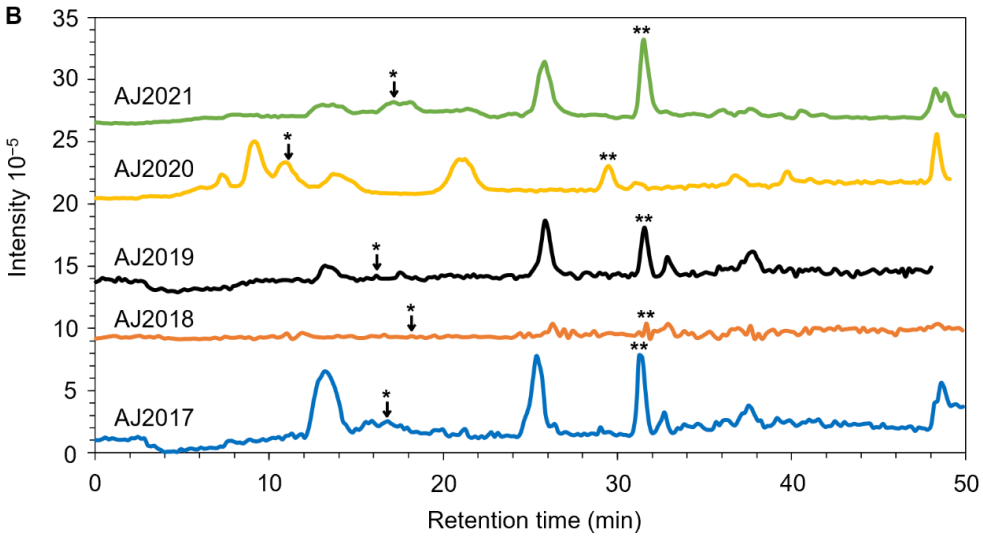

Figure S2-4. Total ion chromatograms obtained for S0 sample of aronia juice harvested in indicated year. Peak labeled with *, dabsyl t-4-HP. Peak labeled with **, dabsyl Pro.

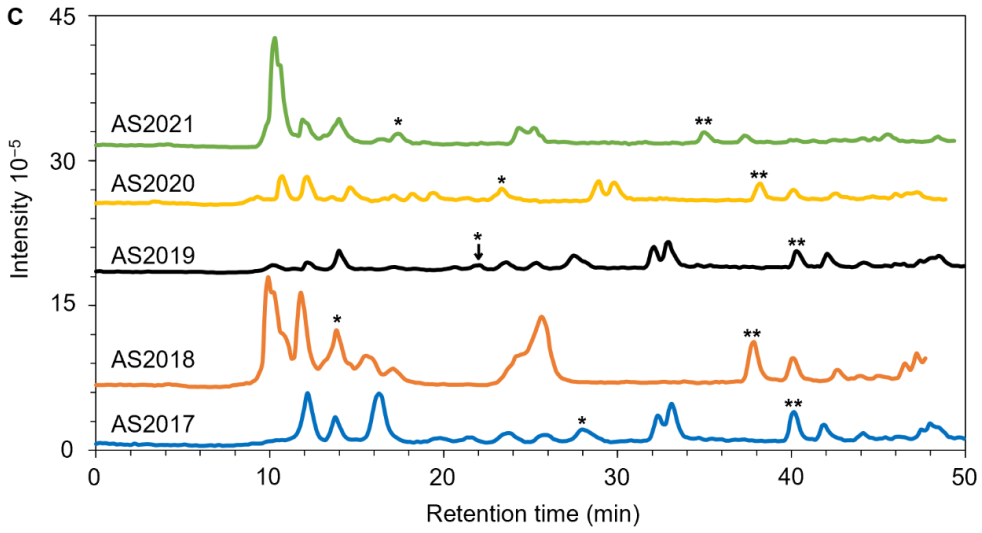

Figure S2-5. Total ion chromatograms obtained for S0 sample of aronia seeds harvested in indicated year. Peak labeled with *, dabsyl t-4-HP. Peak labeled with **, dabsyl Pro.

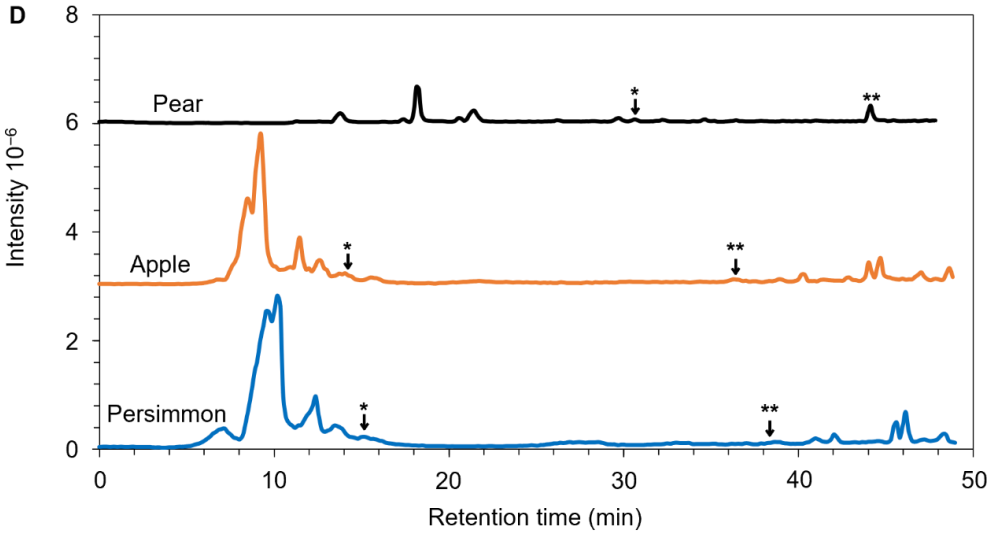

Figure S2-6. Total ion chromatograms obtained for S0 sample of pear, apple, and persimmon juice. Peak labeled with *, dabsyl t-4-HP. Peak labeled with **, dabsyl Pro.

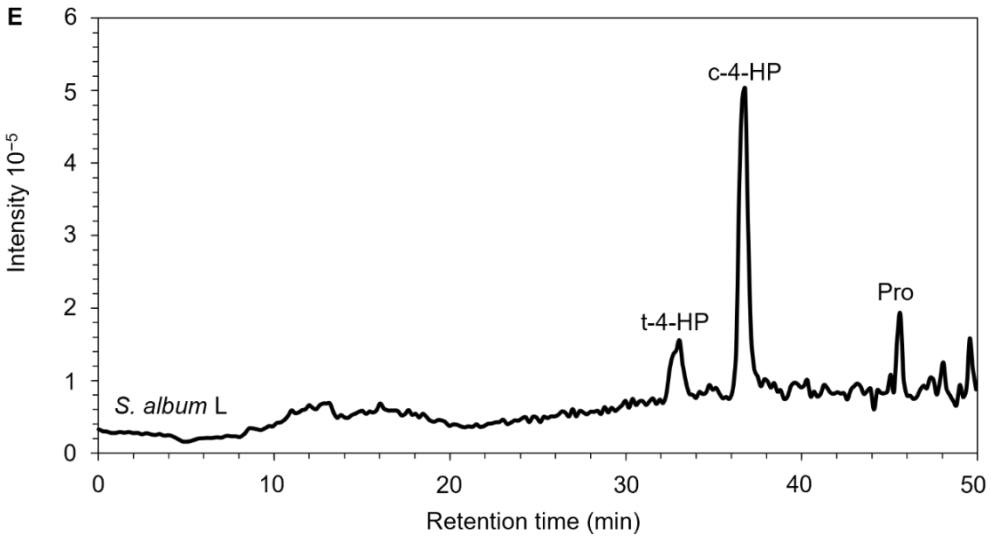

Figure S2-7. Total ion chromatograms obtained for S0 sample of *S. album* wood powder.

Table S2-1. Total amounts of Pro, t-4-HP, and the enantiomer ratio ($r_{D/L}$) in aronia juice and seeds harvested in 2017–2021. Values are the mean ± standard deviation.

Samples	Total Pro	Total t-4-HP	Pro ($r_{D/L}$) ratio		
	(μmol/L)	(μmol/L)	$r_{D/L}$	L	D
			$\times(10^{-2})$	(μmol/L)	(μmol/L)
AJ 2017	303 ± 20	74 ± 5	2.26 ± 0.22	296 ± 19	7.0 ± 0.7
AJ 2018	148 ± 8	76 ± 5	6.78 ± 0.82	139 ± 7	9.4 ± 1.3
AJ 2019	218 ±7	92 ± 3	3.22 ± 0.22	211 ± 6	6.8 ± 0.5
AJ 2020	164 ± 6	63 ± 3	6.21 ± 0.13	154 ± 5	10.0 ± 0.4
AJ 2021	129± 6	46 ± 1	11.6 ± 1.3	116 ± 6	13.4 ± 1.7
AS 2017	230 ± 21	30 ± 2	1.64×10^{-3}	229.6	0.4
AS 2018	304 ± 23	41 ± 3	1.23×10^{-3}	303.6	0.4
AS 2019	98 ± 7	19 ± 3	2.82×10^{-3}	97.4	0.3
AS 2020	139 ± 5	22.3 ± 0.6	1.55×10^{-3}	138.8	0.2
AS 2021	45 ± 2	8.6 ± 1.0	1.25×10^{-3}	44.8	0.06

The data are presented as mean ± SD. Total c-4-HP and t-4-HP_D were not detected in any of the samples. AJ: Aronia juice, AS: Aronia seeds.

(2) Chapter III

1. Calibration curves obtained for 20 different raw milk products.

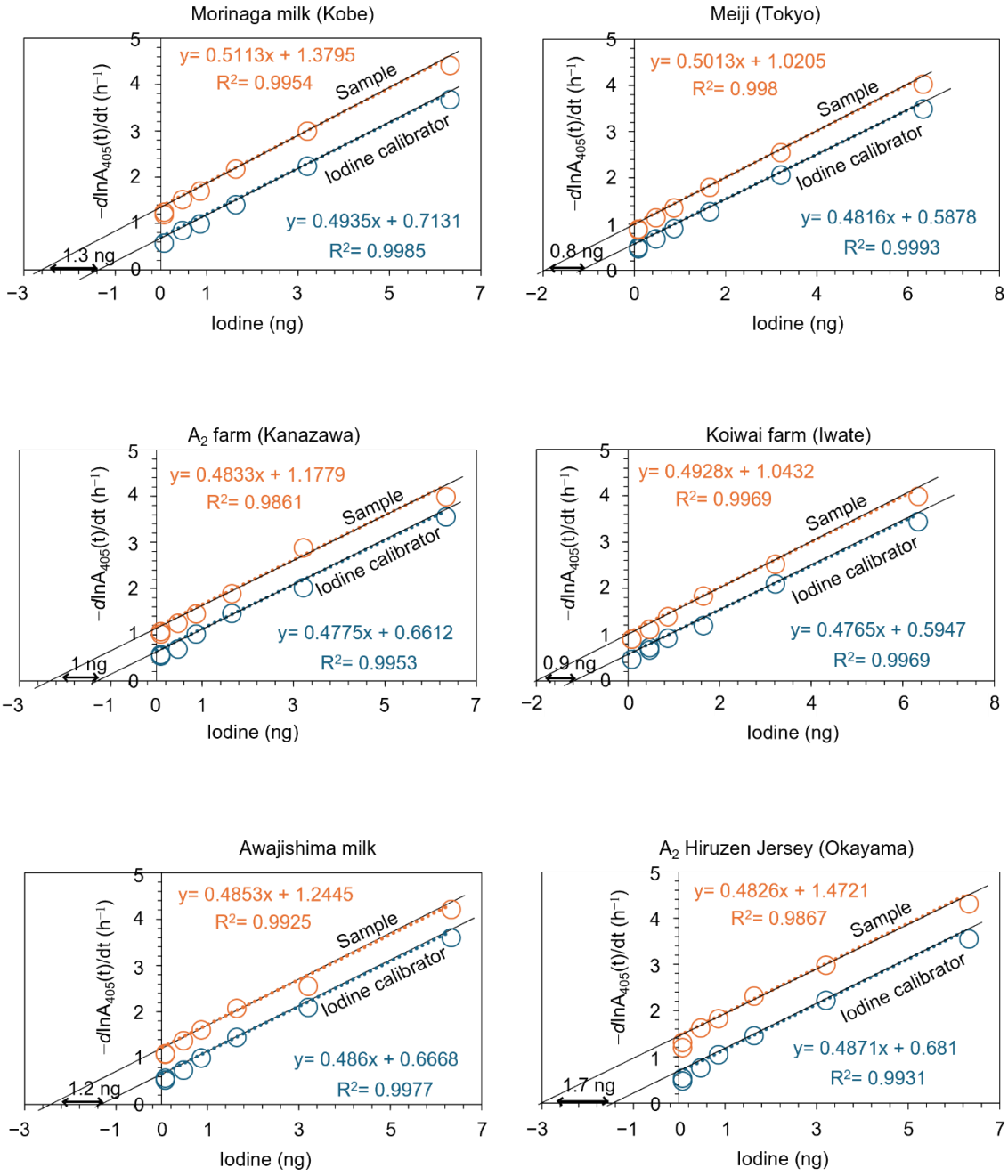

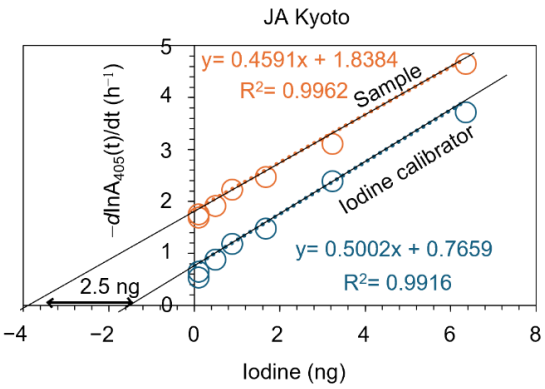
JA Kyoto
y= 0.4591x + 1.8384
R²= 0.9962
Sample
Iodine calibrator
y= 0.5002x + 0.7659
R²= 0.9916
2.5 ng
−dlnA405(t)/dt (h−1)
Iodine (ng)

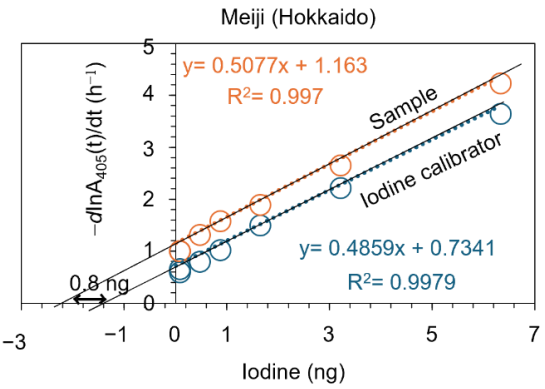
Meiji (Hokkaido)
y= 0.5077x + 1.163
R²= 0.997
Sample
Iodine calibrator
y= 0.4859x + 0.7341
R²= 0.9979
0.8 ng
−dlnA405(t)/dt (h−1)
Iodine (ng)

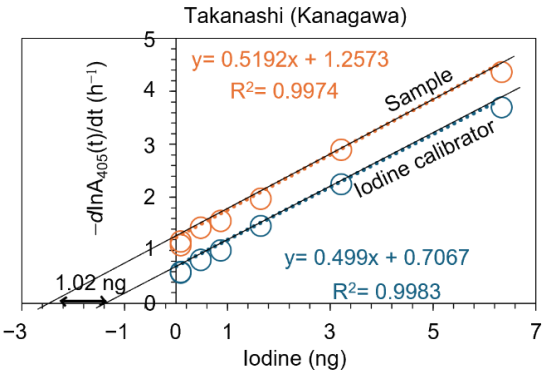
Takanashi (Kanagawa)
y= 0.5192x + 1.2573
R²= 0.9974
Sample
Iodine calibrator
y= 0.499x + 0.7067
R²= 0.9983
1.02 ng
−dlnA405(t)/dt (h−1)
Iodine (ng)

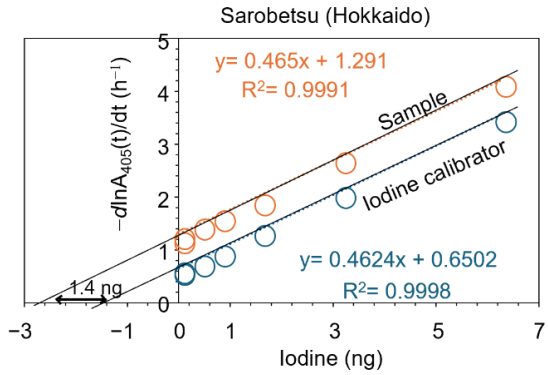
Sarobetsu (Hokkaido)
y= 0.465x + 1.291
R²= 0.9991
Sample
Iodine calibrator
y= 0.4624x + 0.6502
R²= 0.9998
1.4 ng
−dlnA405(t)/dt (h−1)
Iodine (ng)

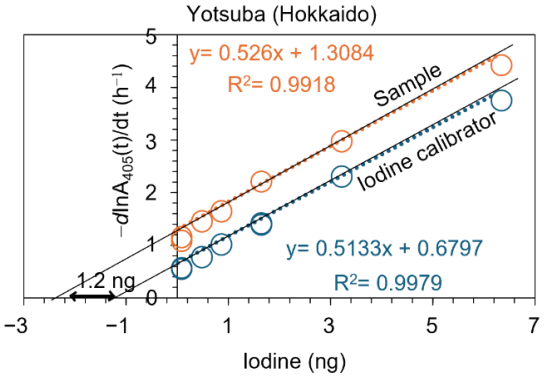
Yotsuba (Hokkaido)
y= 0.526x + 1.3084
R²= 0.9918
Sample
Iodine calibrator
y= 0.5133x + 0.6797
R²= 0.9979
1.2 ng
−dlnA405(t)/dt (h−1)
Iodine (ng)

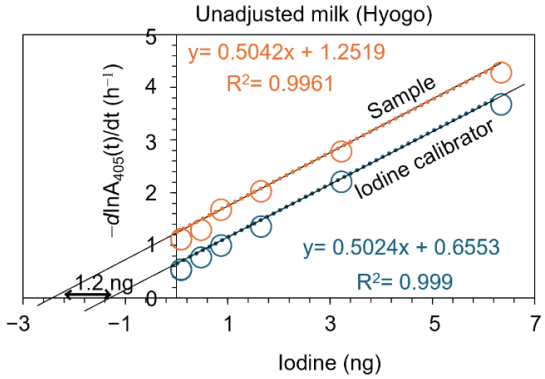
Unadjusted milk (Hyogo)
y= 0.5042x + 1.2519
R²= 0.9961
Sample
Iodine calibrator
y= 0.5024x + 0.6553
R²= 0.999
1.2 ng
−dlnA405(t)/dt (h−1)
Iodine (ng)

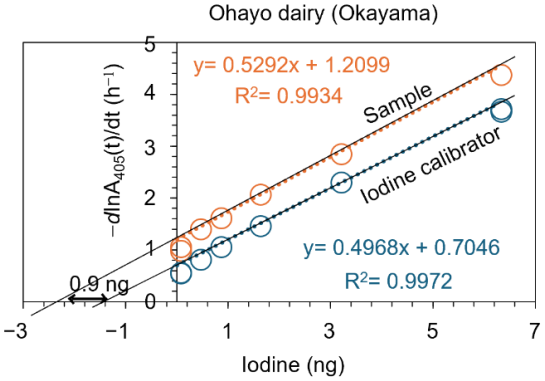
Ohayo dairy (Okayama)
y= 0.5292x + 1.2099
R²= 0.9934
Sample
Iodine calibrator
y= 0.4968x + 0.7046
R²= 0.9972
0.9 ng
−dlnA405(t)/dt (h−1)
Iodine (ng)

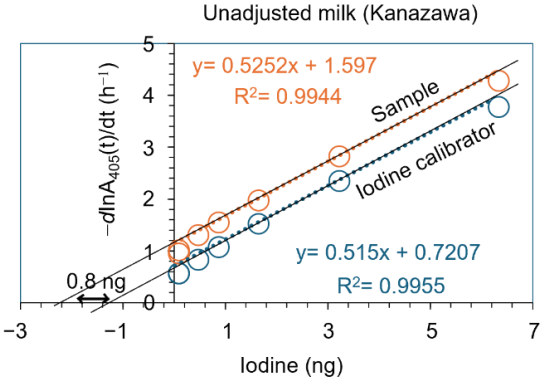
Unadjusted milk (Kanazawa)
y= 0.5252x + 1.597
R²= 0.9944
Sample
Iodine calibrator
y= 0.515x + 0.7207
R²= 0.9955
0.8 ng
−dlnA405(t)/dt (h−1)
Iodine (ng)

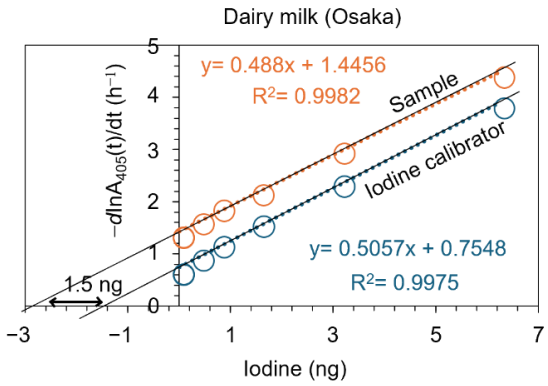
Dairy milk (Osaka)
y= 0.488x + 1.4456
R²= 0.9982
Sample
Iodine calibrator
y= 0.5057x + 0.7548
R²= 0.9975
1.5 ng
−dlnA405(t)/dt (h−1)
Iodine (ng)

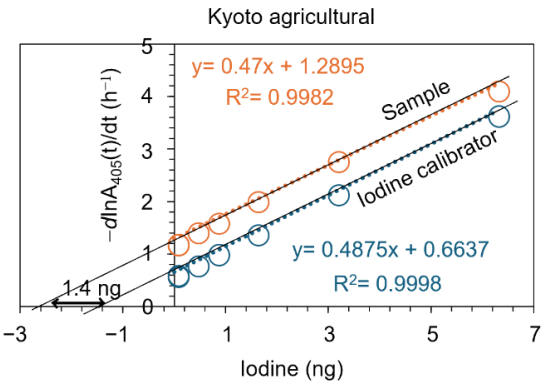
Kyoto agricultural
y= 0.47x + 1.2895
R²= 0.9982
Sample
Iodine calibrator
y= 0.4875x + 0.6637
R²= 0.9998
1.4 ng
−dlnA405(t)/dt (h−1)
Iodine (ng)

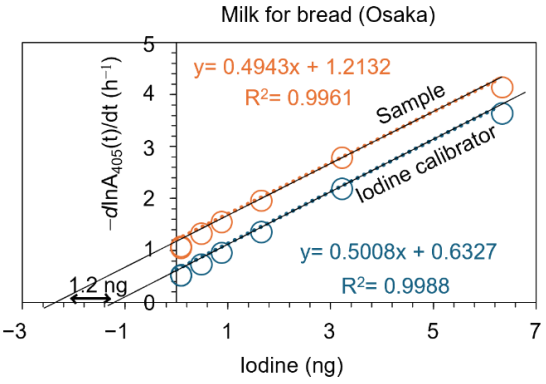
Milk for bread (Osaka)
y= 0.4943x + 1.2132
R²= 0.9961
Sample
Iodine calibrator
y= 0.5008x + 0.6327
R²= 0.9988
1.2 ng
−dlnA405(t)/dt (h−1)
Iodine (ng)

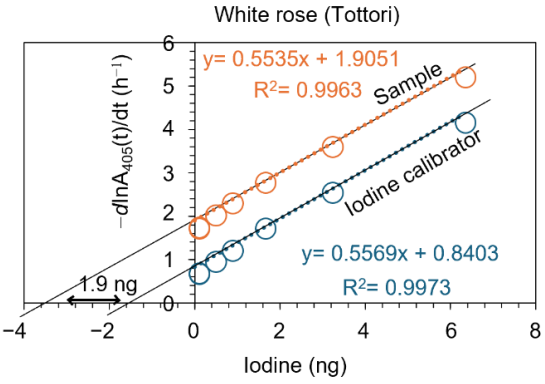
White rose (Tottori)
y= 0.5535x + 1.9051
R²= 0.9963
Sample
Iodine calibrator
y= 0.5569x + 0.8403
R²= 0.9973
1.9 ng
−dlnA405(t)/dt (h−1)
Iodine (ng)

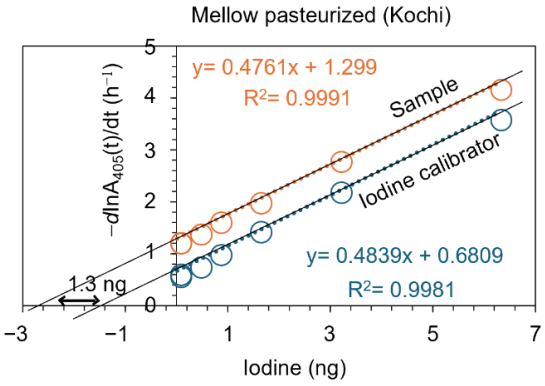
Mellow pasteurized (Kochi)
y= 0.4761x + 1.299
R²= 0.9991
Sample
Iodine calibrator
y= 0.4839x + 0.6809
R²= 0.9981
1.3 ng
−dlnA405(t)/dt (h−1)
Iodine (ng)

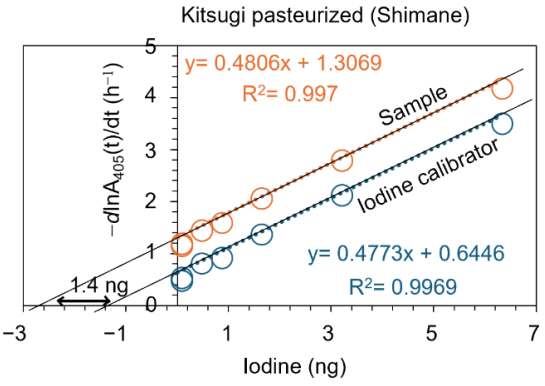
Kitsugi pasteurized (Shimane)
y= 0.4806x + 1.3069
R²= 0.997
Sample
Iodine calibrator
y= 0.4773x + 0.6446
R²= 0.9969
1.4 ng
−dlnA405(t)/dt (h−1)
Iodine (ng)

2. **Calibration curves obtained for 18 different seaweed products.**

Fresh seaweed

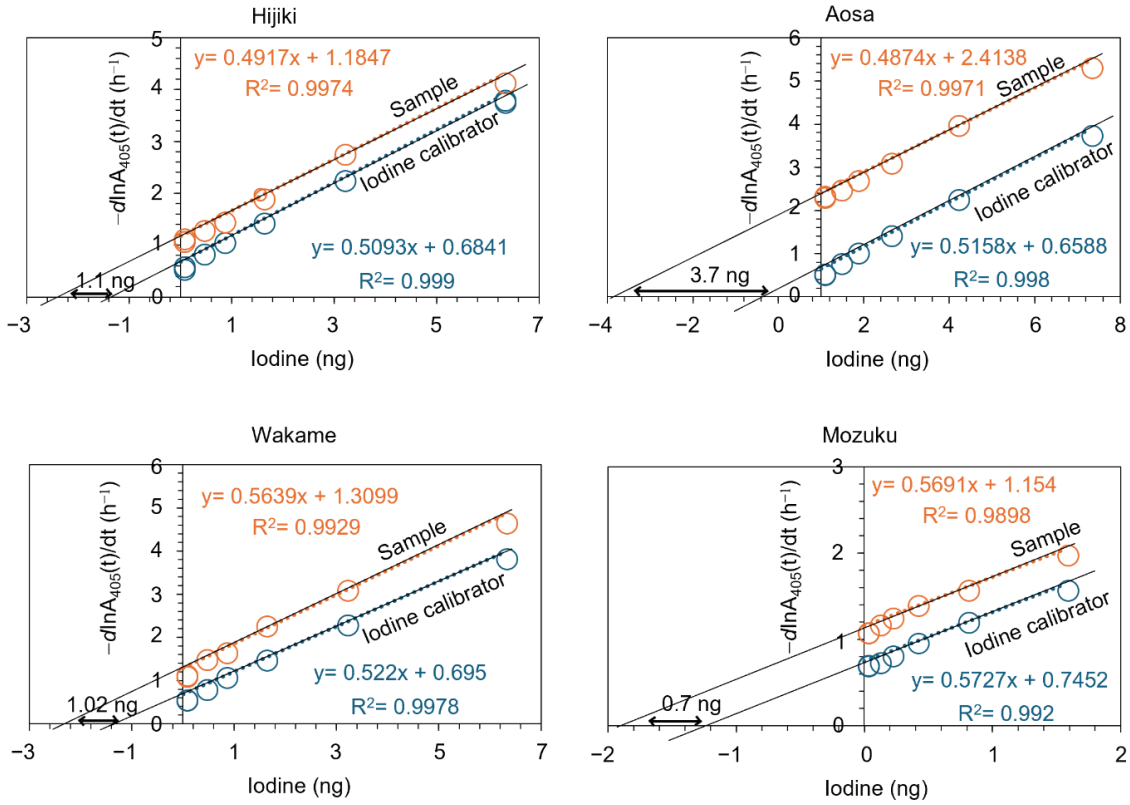

Dried seaweed

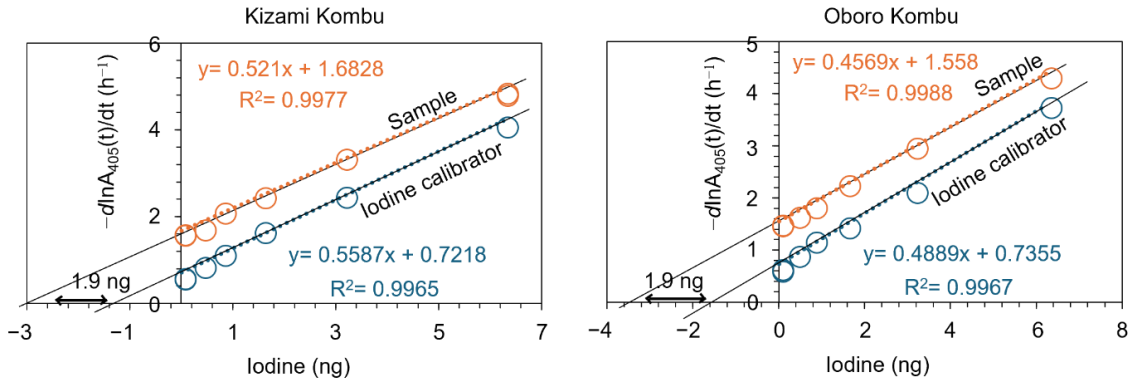

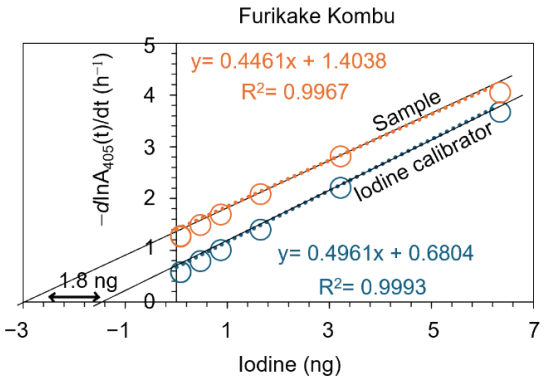
Furikake Kombu
y= 0.4461x + 1.4038
R²= 0.9967
Sample
Iodine calibrator
y= 0.4961x + 0.6804
R²= 0.9993
1.8 ng
−dlnA405(t)/dt (h−1)
Iodine (ng)

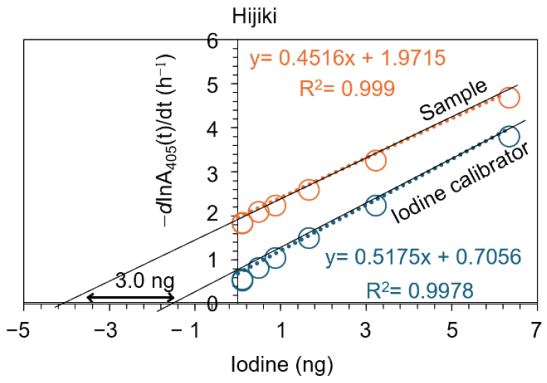
Hijiki
y= 0.4516x + 1.9715
R²= 0.999
Sample
Iodine calibrator
y= 0.5175x + 0.7056
R²= 0.9978
3.0 ng
−dlnA405(t)/dt (h−1)
Iodine (ng)

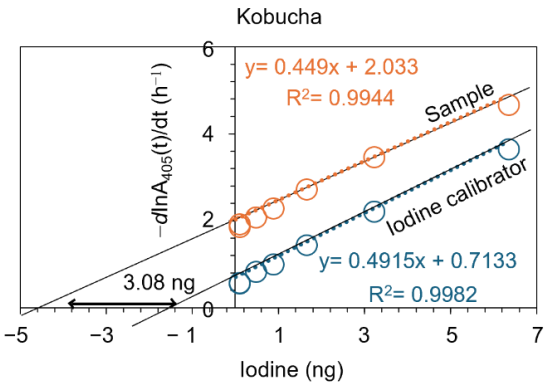
Kobucha
y= 0.449x + 2.033
R²= 0.9944
Sample
Iodine calibrator
y= 0.4915x + 0.7133
R²= 0.9982
3.08 ng
−dlnA405(t)/dt (h−1)
Iodine (ng)

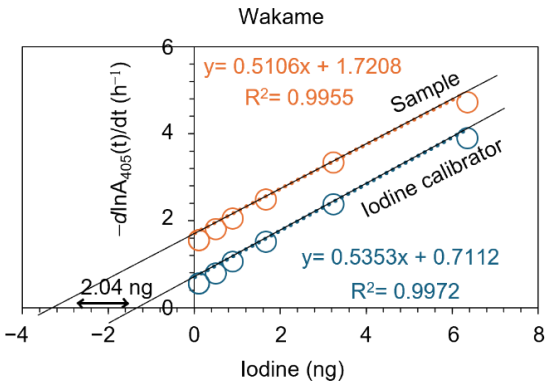
Wakame
y= 0.5106x + 1.7208
R²= 0.9955
Sample
Iodine calibrator
y= 0.5353x + 0.7112
R²= 0.9972
2.04 ng
−dlnA405(t)/dt (h−1)
Iodine (ng)

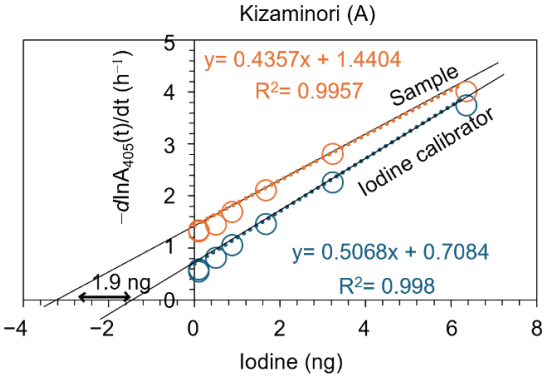
Kizaminori (A)
y= 0.4357x + 1.4404
R²= 0.9957
Sample
Iodine calibrator
y= 0.5068x + 0.7084
R²= 0.998
1.9 ng
−dlnA405(t)/dt (h−1)
Iodine (ng)

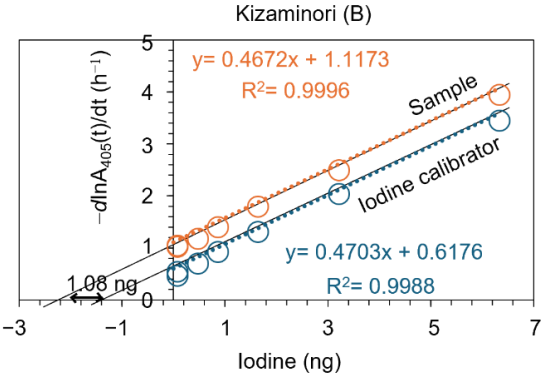
Kizaminori (B)
y= 0.4672x + 1.1173
R²= 0.9996
Sample
Iodine calibrator
y= 0.4703x + 0.6176
R²= 0.9988
1.08 ng
−dlnA405(t)/dt (h−1)
Iodine (ng)

Products containing kombu and/or extracts from kombu

Kombu dashi | Dashi shoyu (A) | Goma kombu

Ponzu | Tsuyu | Dashi shoyu (B)

Figure S3-1. Labels on the products subjected to iodine analysis.

Calibration curves

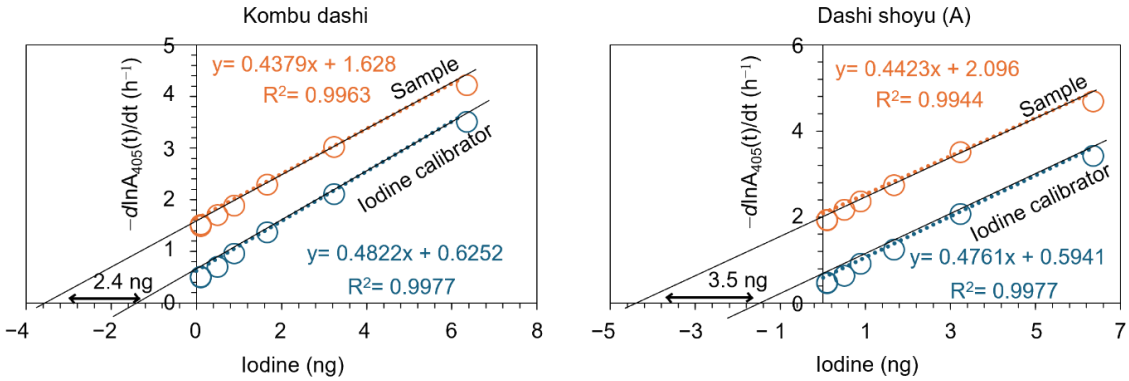

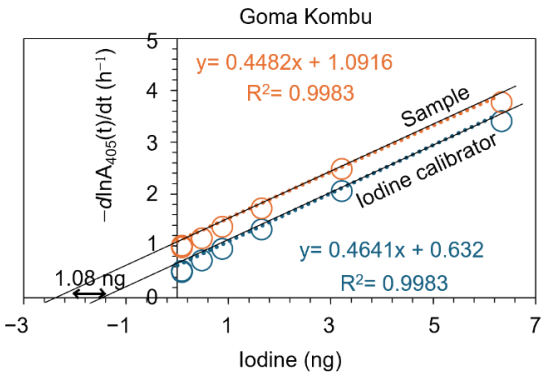
Goma Kombu
y= 0.4482x + 1.0916
R²= 0.9983
Sample
Iodine calibrator
y= 0.4641x + 0.632
R²= 0.9983
1.08 ng
−dlnA405(t)/dt (h−1)
Iodine (ng)

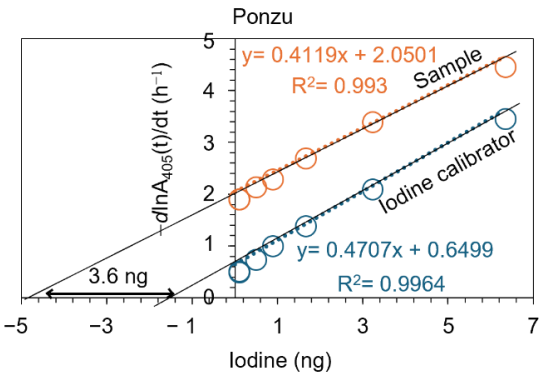
Ponzu
y= 0.4119x + 2.0501
R²= 0.993
Sample
Iodine calibrator
y= 0.4707x + 0.6499
R²= 0.9964
3.6 ng
dlnA405(t)/dt (h−1)
Iodine (ng)

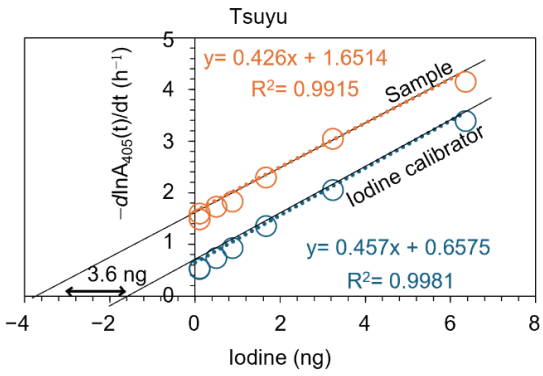
Tsuyu
y= 0.426x + 1.6514
R²= 0.9915
Sample
Iodine calibrator
y= 0.457x + 0.6575
R²= 0.9981
3.6 ng
−dlnA405(t)/dt (h−1)
Iodine (ng)

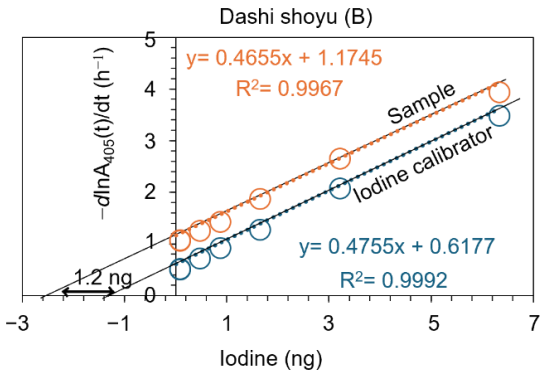
Dashi shoyu (B)
y= 0.4655x + 1.1745
R²= 0.9967
Sample
Iodine calibrator
y= 0.4755x + 0.6177
R²= 0.9992
1.2 ng
−dlnA405(t)/dt (h−1)
Iodine (ng)

3. Intra-assay precision of milk samples (10 times replicates)

Raw milk products

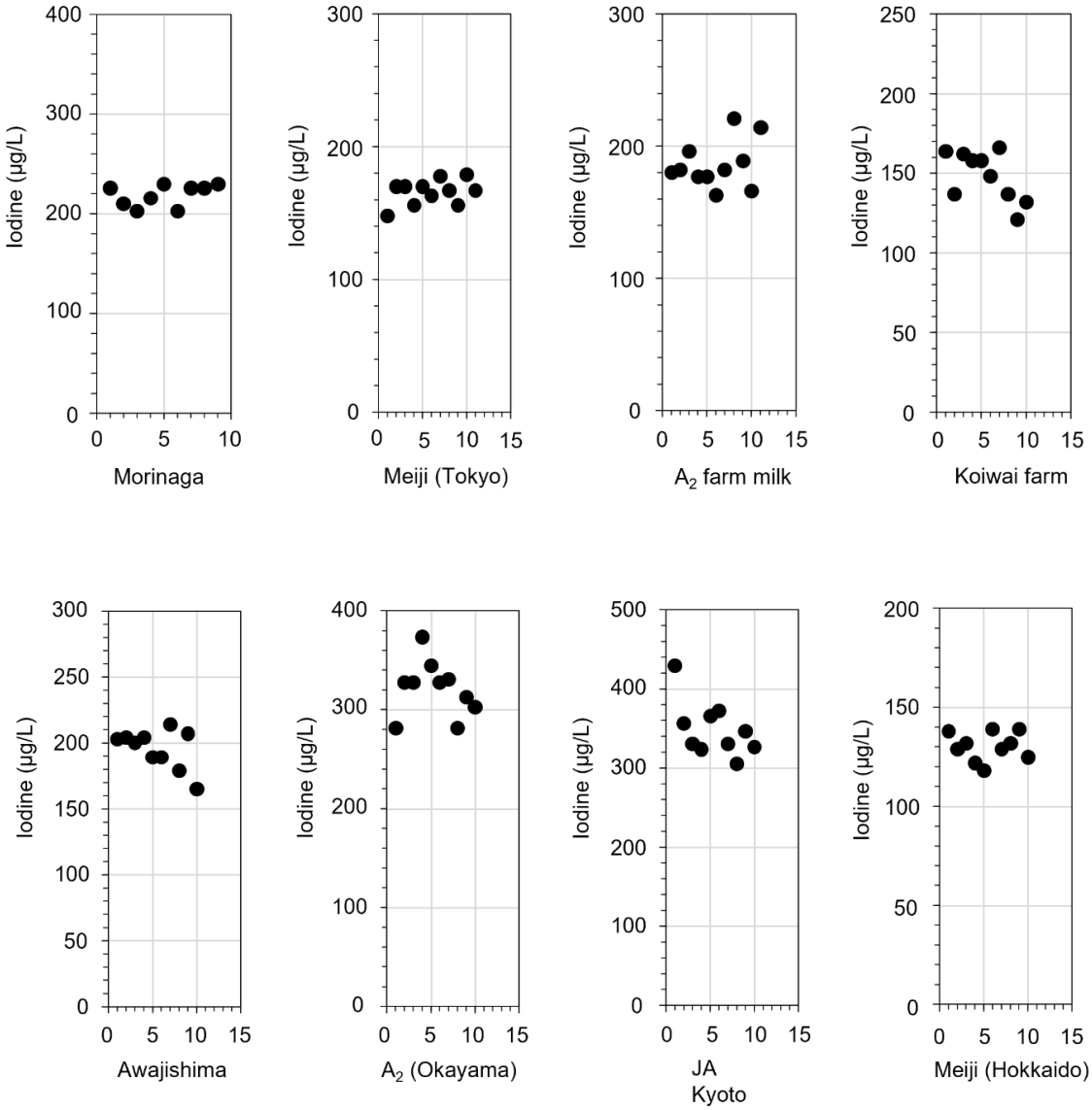

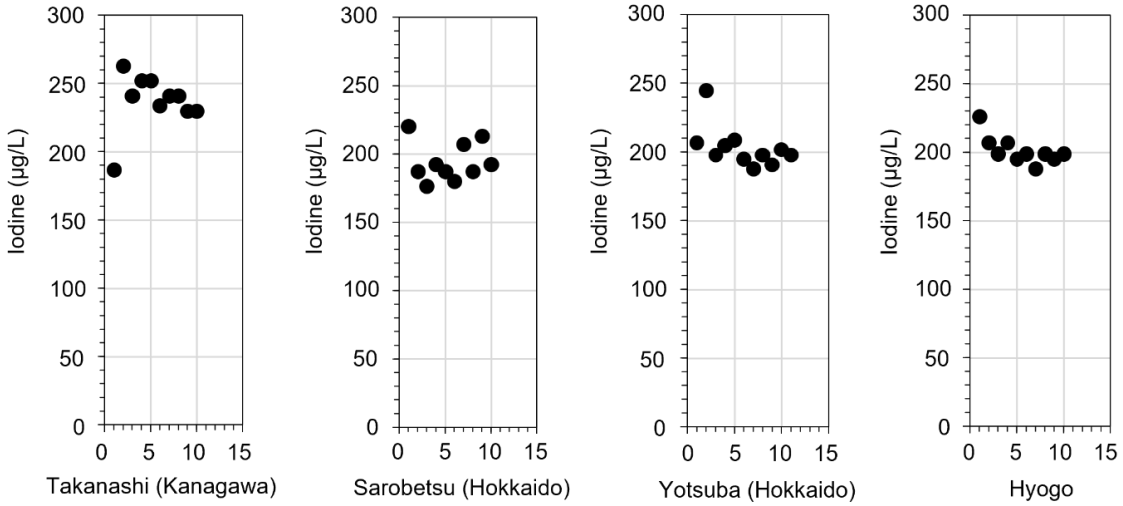
Iodine (μg/L)
Takanashi (Kanagawa)
Sarobetsu (Hokkaido)
Yotsuba (Hokkaido)
Hyogo

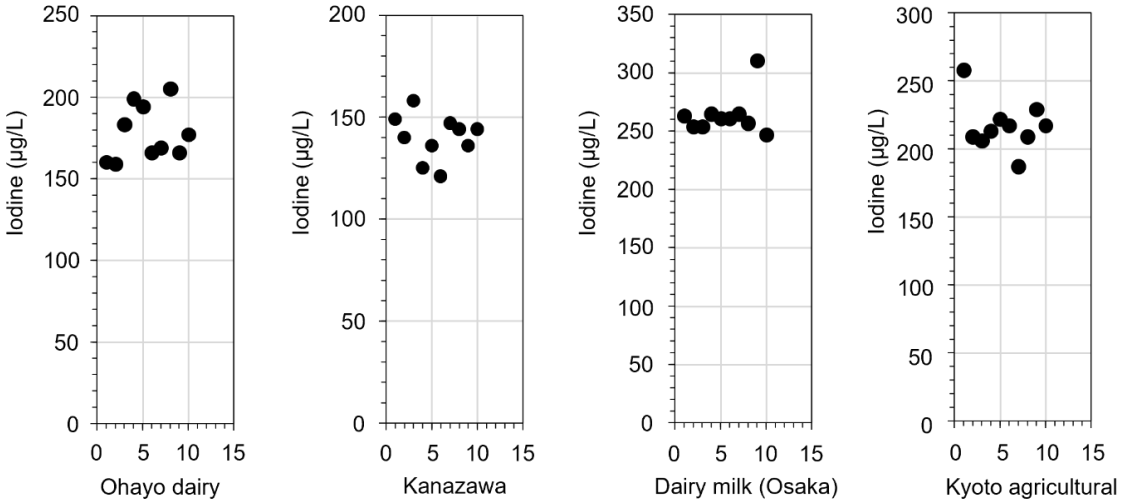
Iodine (μg/L)
Ohayo dairy
Kanazawa
Dairy milk (Osaka)
Kyoto agricultural

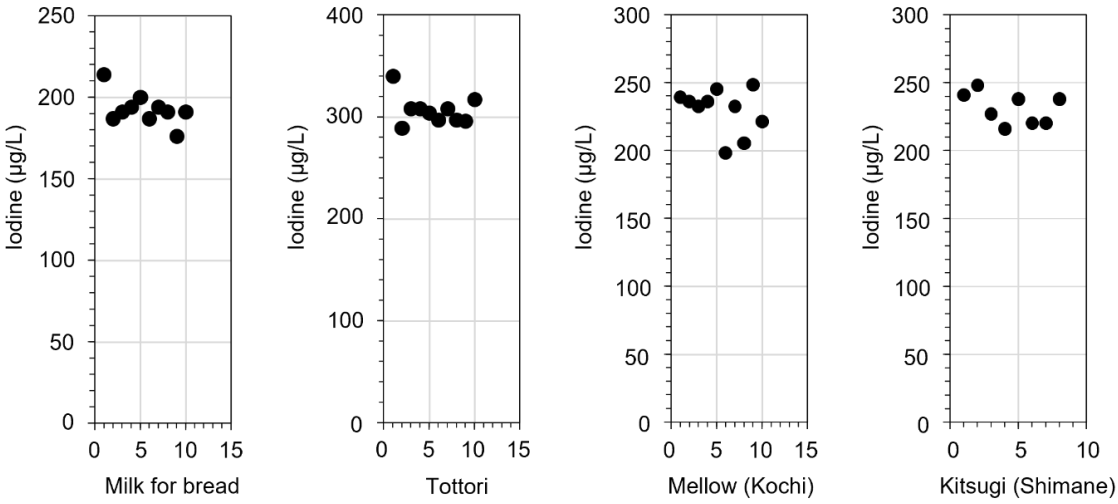
Iodine (μg/L)
Milk for bread
Tottori
Mellow (Kochi)
Kitsugi (Shimane)

Seaweed samples

Fresh seaweed

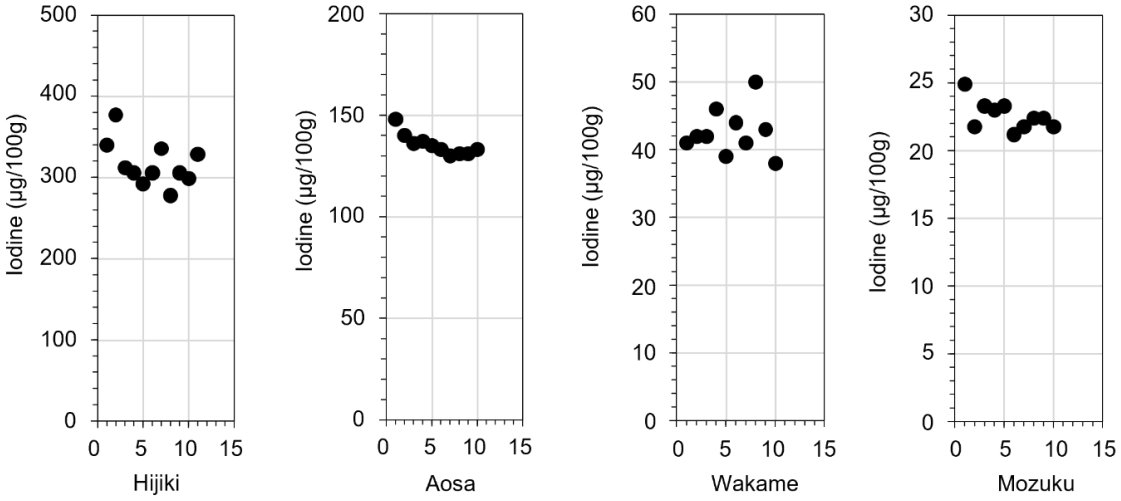

Dried seaweed

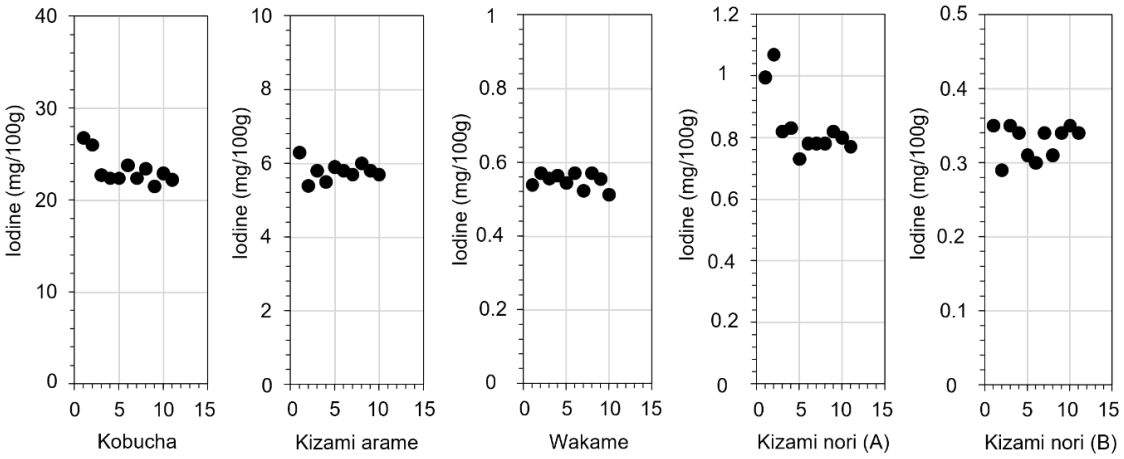

(3) Chapter IV

1. Iodine calibration curves obtained for 24-u urine samples

Day 0 urine

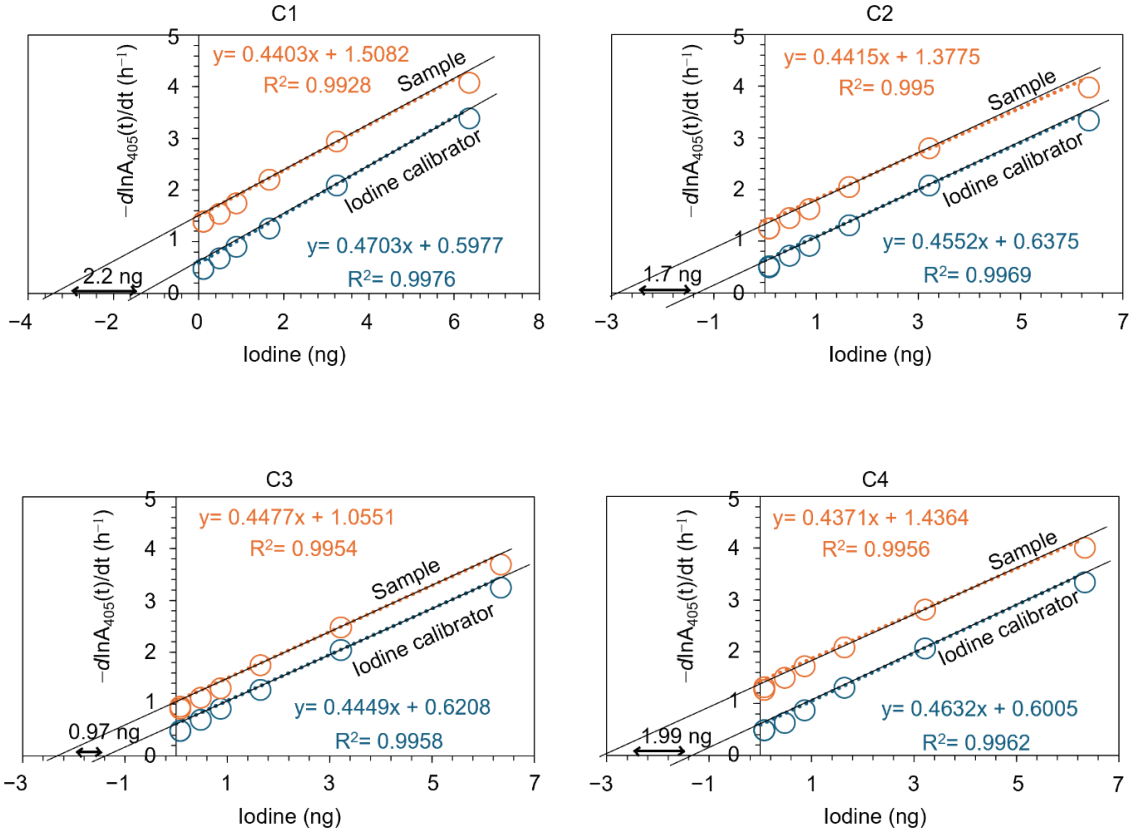

Day 28 urine

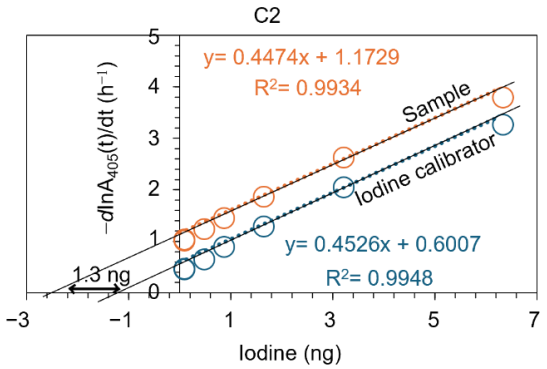
C2
y= 0.4474x + 1.1729
R²= 0.9934
Sample
Iodine calibrator
y= 0.4526x + 0.6007
R²= 0.9948
1.3 ng
−dlnA405(t)/dt (h−1)
Iodine (ng)

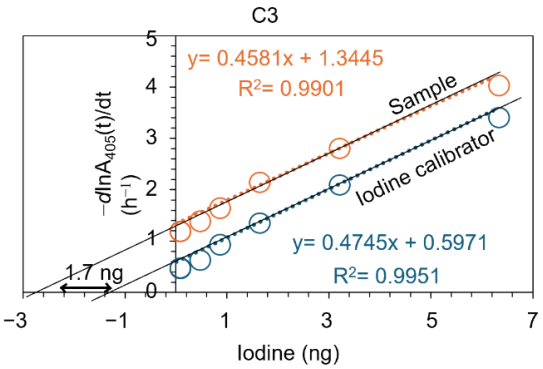
C3
y= 0.4581x + 1.3445
R²= 0.9901
Sample
Iodine calibrator
y= 0.4745x + 0.5971
R²= 0.9951
1.7 ng
−dlnA405(t)/dt (h−1)
Iodine (ng)

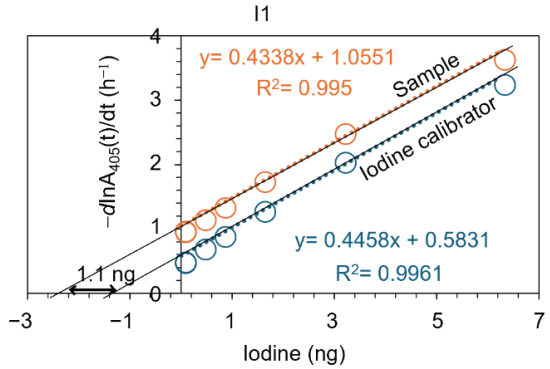
I1
y= 0.4338x + 1.0551
R²= 0.995
Sample
Iodine calibrator
y= 0.4458x + 0.5831
R²= 0.9961
1.1 ng
−dlnA405(t)/dt (h−1)
Iodine (ng)

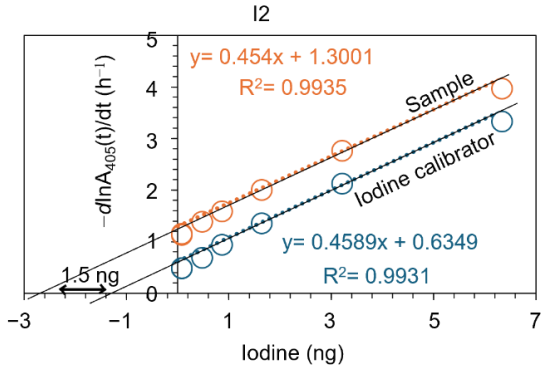
I2
y= 0.454x + 1.3001
R²= 0.9935
Sample
Iodine calibrator
y= 0.4589x + 0.6349
R²= 0.9931
1.5 ng
−dlnA405(t)/dt (h−1)
Iodine (ng)

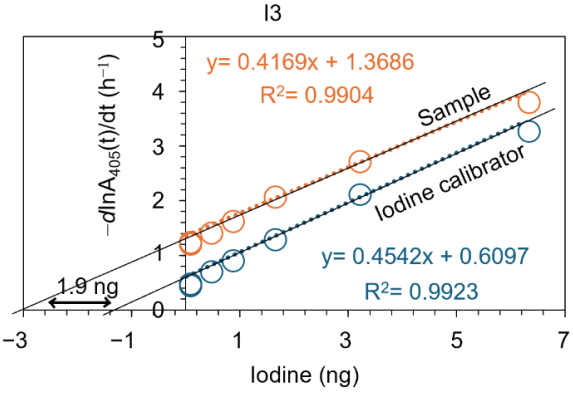
I3
y= 0.4169x + 1.3686
R²= 0.9904
Sample
Iodine calibrator
y= 0.4542x + 0.6097
R²= 0.9923
1.9 ng
−dlnA405(t)/dt (h−1)
Iodine (ng)

Day 56 urine

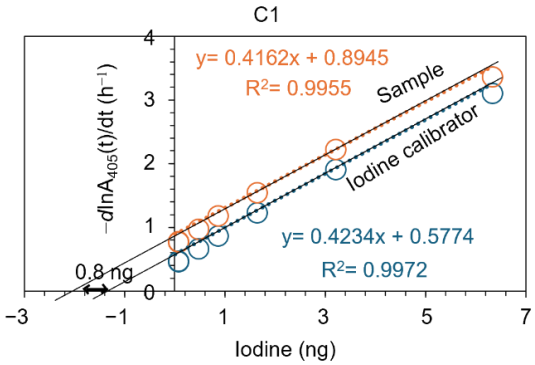
C1
y= 0.4162x + 0.8945
R²= 0.9955
Sample
Iodine calibrator
y= 0.4234x + 0.5774
R²= 0.9972
0.8 ng
−dlnA405(t)/dt (h−1)
Iodine (ng)

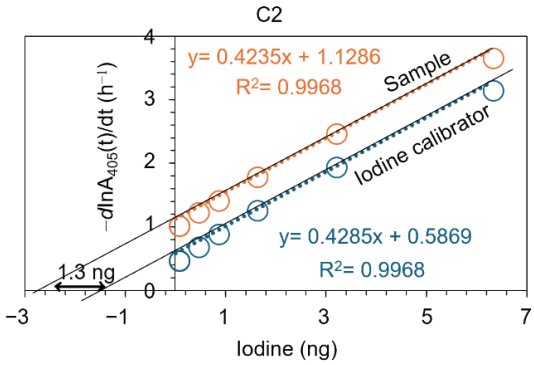
C2
y= 0.4235x + 1.1286
R²= 0.9968
Sample
Iodine calibrator
y= 0.4285x + 0.5869
R²= 0.9968
1.3 ng
−dlnA405(t)/dt (h−1)
Iodine (ng)

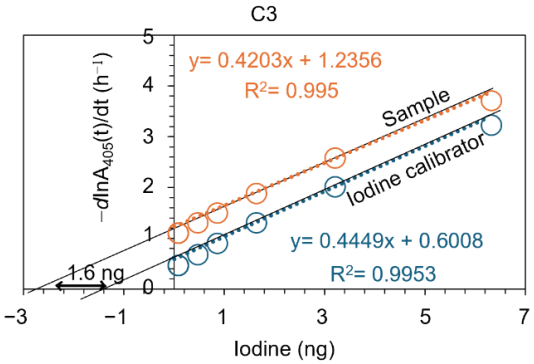
C3
y= 0.4203x + 1.2356
R²= 0.995
Sample
Iodine calibrator
y= 0.4449x + 0.6008
R²= 0.9953
1.6 ng
−dlnA405(t)/dt (h−1)
Iodine (ng)

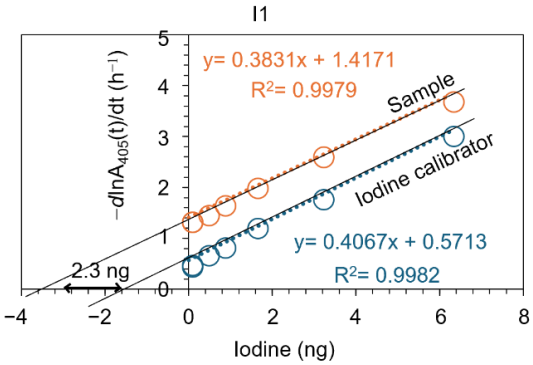
I1
y= 0.3831x + 1.4171
R²= 0.9979
Sample
Iodine calibrator
y= 0.4067x + 0.5713
R²= 0.9982
2.3 ng
−dlnA405(t)/dt (h−1)
Iodine (ng)

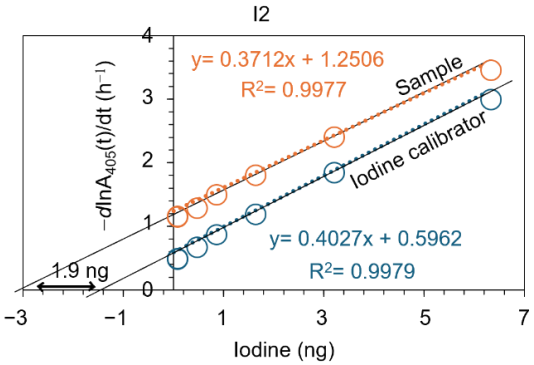
I2
y= 0.3712x + 1.2506
R²= 0.9977
Sample
Iodine calibrator
y= 0.4027x + 0.5962
R²= 0.9979
1.9 ng
−dlnA405(t)/dt (h−1)
Iodine (ng)

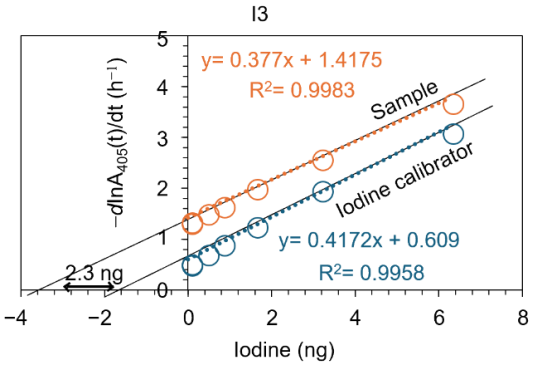
I3
y= 0.377x + 1.4175
R²= 0.9983
Sample
Iodine calibrator
y= 0.4172x + 0.609
R²= 0.9958
2.3 ng
−dlnA405(t)/dt (h−1)
Iodine (ng)

2. Determination of total amounts of proline, t-4-HP and c-4-HP in urine samples

Total ion chromatograms

Day 0 urine

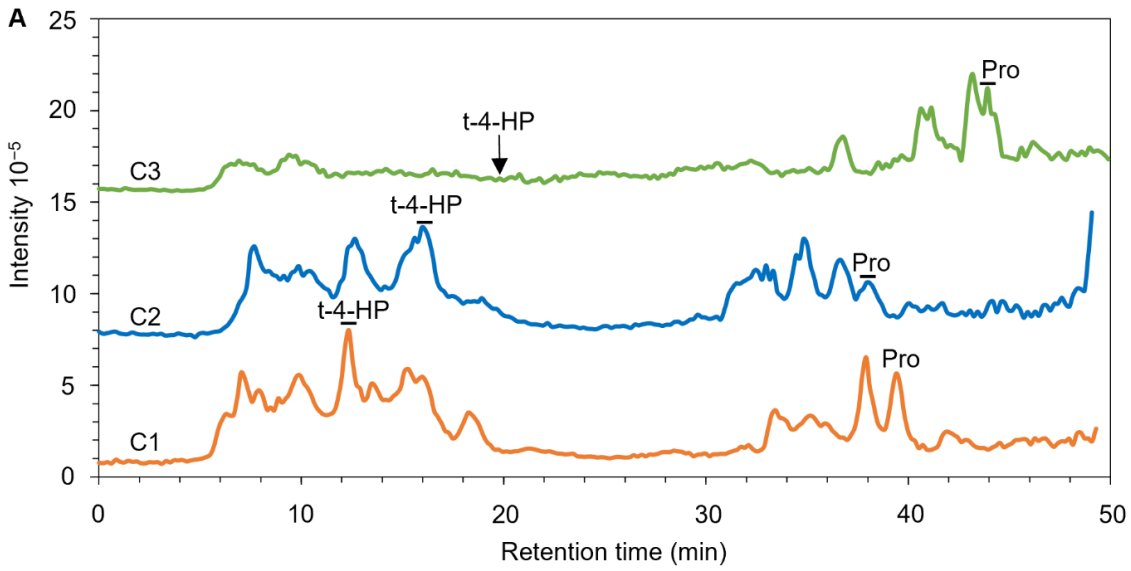

Day 28 urine

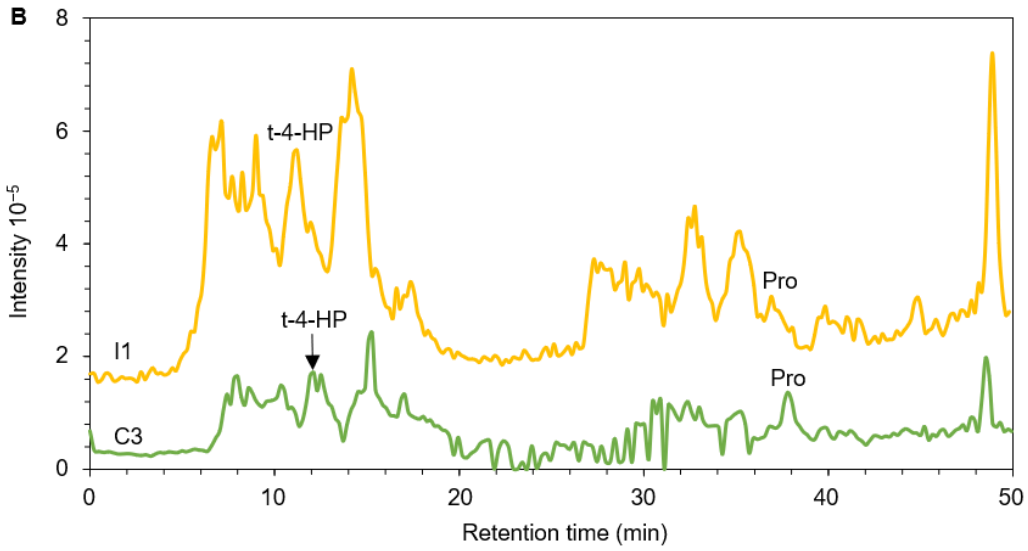

Day 56 urine

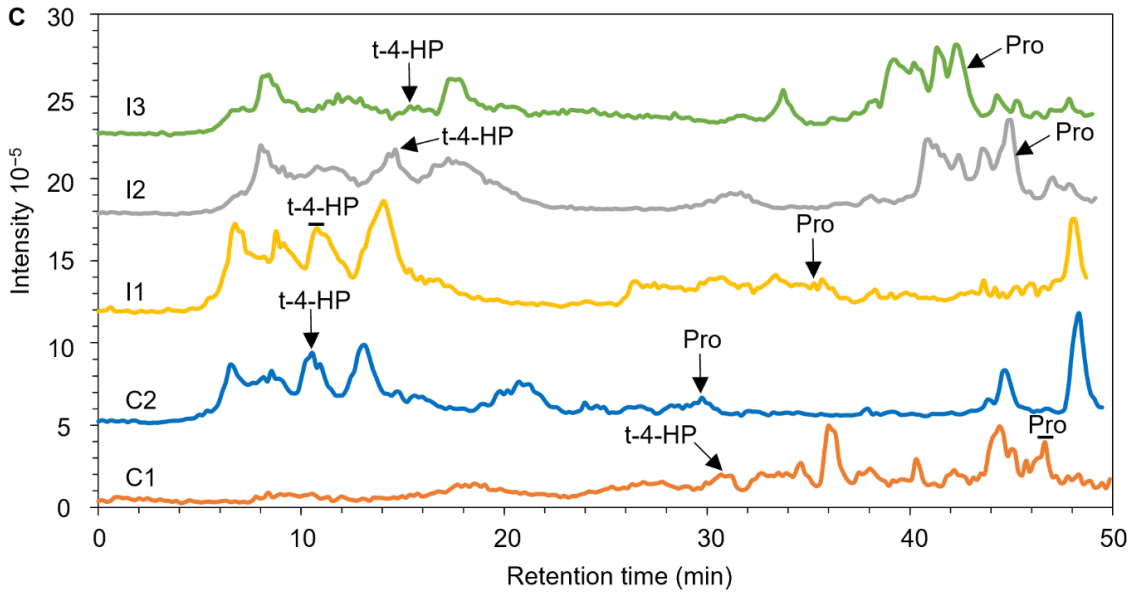
C
Intensity 10⁻⁵
Retention time (min)
I3
I2
I1
C2
C1
t-4-HP
Pro
0
5
10
15
20
25
30
40
50

Extracted chromatograms

Day 56 urine

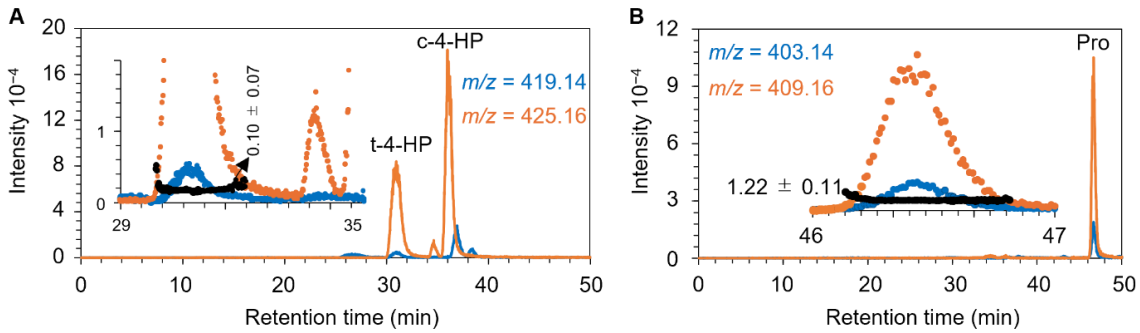

C1 mouse

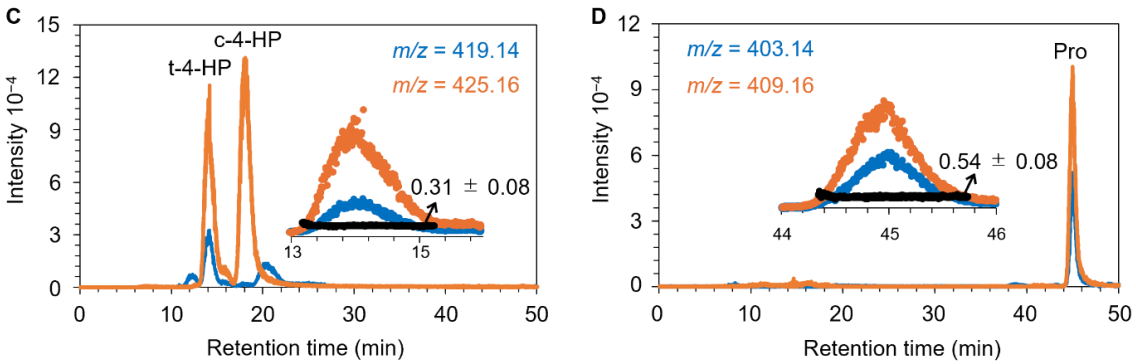

I2 mouse

Calibration curves for t-4-HP and Pro (I2 mouse)